

ORIGINAL ARTICLE

## Injectable Extracellular Matrix Hydrogels as Scaffolds for Spinal Cord Injury Repair

Dmitry Tukmachev, MD,<sup>1,2</sup> Serhiy Forostyak, MD, PhD,<sup>1,2</sup> Zuzana Koci, MS,<sup>1,2</sup> Kristyna Zaviskova, MS,<sup>1,2</sup> Irena Vackova, PhD,<sup>1</sup> Karel Vyborny, MS,<sup>1,2</sup> Ioanna Sandvig, PhD,<sup>3,4</sup> Axel Sandvig, MD, PhD,<sup>3,5</sup> Christopher J. Medberry, PhD,<sup>6</sup> Stephen F. Badylak, DVM, PhD, MD,<sup>6</sup> Eva Sykova, MD, DSc,<sup>1,2</sup> and Sarka Kubinova, PharmD, PhD<sup>1</sup>

Restoration of lost neuronal function after spinal cord injury (SCI) still remains a big challenge for current medicine. One important repair strategy is bridging the SCI lesion with a supportive and stimulatory milieu that would enable axonal rewiring. Injectable extracellular matrix (ECM)-derived hydrogels have been recently reported to have neurotrophic potential *in vitro*. In this study, we evaluated the presumed neuroregenerative properties of ECM hydrogels *in vivo* in the acute model of SCI. ECM hydrogels were prepared by decellularization of porcine spinal cord (SC) or porcine urinary bladder (UB), and injected into a spinal cord hemisection cavity. Histological analysis and real-time qPCR were performed at 2, 4, and 8 weeks postinjection. Both types of hydrogels integrated into the lesion and stimulated neovascularization and axonal ingrowth into the lesion. On the other hand, massive infiltration of macrophages into the lesion and rapid hydrogel degradation did not prevent cyst formation, which progressively developed over 8 weeks. No significant differences were found between SC-ECM and UB-ECM. Gene expression analysis revealed significant downregulation of genes related to immune response and inflammation in both hydrogel types at 2 weeks post SCI. A combination of human mesenchymal stem cells with SC-ECM did not further promote ingrowth of axons and blood vessels into the lesion, when compared with the SC-ECM hydrogel alone. In conclusion, both ECM hydrogels bridged the lesion cavity, modulated the innate immune response, and provided the benefit of a stimulatory substrate for *in vivo* neural tissue regeneration. However, fast hydrogel degradation might be a limiting factor for the use of native ECM hydrogels in the treatment of acute SCI.

### Introduction

**S**PINAL CORD INJURY (SCI) is a devastating disorder that often results in permanent motor and sensory dysfunctions due to the inability of axons to regenerate in the hostile environment of the lesion.<sup>1</sup> Current therapeutic approaches are being combined to activate the intrinsic neuronal regeneration capacity, such as blocking axon growth-inhibitory factors, reducing excitotoxicity and the inflammatory response, administration of neurotrophic factors, or using various types of stem and progenitor cells.<sup>2,3</sup> In addition to these approaches, tissue-engineered scaffolds play an important role in providing supportive substrates that contribute to replacing lost tissue and re-establishing damaged connections after SCI.<sup>4-7</sup>

In terms of SCI repair, biomaterials, with their own intrinsic biological activity that would encourage endoge-

nous tissue repair without the need for additional bioactive molecules such as exogenous growth factors or peptides, may provide high treatment effectivity together with relative ease of application and scalable manufacturing potential.<sup>8</sup>

In contrast to artificial tissue-engineered materials that fail to mimic the complex structure and chemistry of the extracellular microenvironment seen *in vivo*, biological scaffolds composed of native extracellular matrix (ECM) represent structures very similar to those of the uninjured host tissue with advantages, such as a natural three-dimensional (3D) structure, biological activity promoting cell adhesion and proliferation, and biodegradability.<sup>9</sup> The general concept of ECM scaffolds is based on the constructive remodeling process, in which a degradable biomaterial serves as a temporary inductive niche that is completely degraded and gradually

<sup>1</sup>Institute of Experimental Medicine AS CR, Prague, Czech Republic.

<sup>2</sup>2nd Medical Faculty, Charles University, Prague, Czech Republic.

<sup>3</sup>Department of Neuroscience, Norwegian University of Science and Technology, Trondheim, Norway.

<sup>4</sup>John Van Geest Centre for Brain Repair, School of Clinical Neurosciences, University of Cambridge, Cambridge, United Kingdom.

<sup>5</sup>Division of Pharmacology and Clinical Neuroscience, Department of Neurosurgery, Umeå University, Umeå, Sweden.

<sup>6</sup>McGowan Institute for Regenerative Medicine, Pittsburgh, Pennsylvania.

replaced by anatomically appropriate and functional tissue as opposed to scar tissue.<sup>10,11</sup>

Acellular tissue matrices have revealed an intrinsic ability to guide cells to differentiate into tissue-appropriate structures and phenotypes, and are also associated with positive *in vivo* host tissue remodeling and regeneration,<sup>12,13</sup> degradation of ECM-evoked recruitment of endogenous stem and progenitor cells, and modulation of the innate immune response.<sup>14,15</sup> After removal of cellular antigens, ECM scaffolds are considered biocompatible and nonimmunogenic even in allogeneic and xenogeneic settings. Currently, ECM scaffolds are being widely used for various tissue reconstructions, including heart valves, blood vessels, skin, bone, cartilage, trachea, lung, or peripheral nerves. A number of ECM scaffolds derived from a range of source species and tissues have also been approved by the FDA and commercially available for clinical use, for example, in wound healing, soft tissue repair, or heart valve replacement.<sup>10,11</sup>

In contrast to the extensive research on ECM scaffolds used for the reconstruction of various tissues, there are only a few studies addressing biological scaffolds for the repair of SCI based on an acellular muscle scaffold,<sup>16</sup> acellular sciatic nerve,<sup>17</sup> or acellular spinal cord scaffolds.<sup>18</sup> Nevertheless, the shape and conformation of such acellular scaffolds might be restrictive for bridging a chronic spinal cord lesion with an irregular cavity. Thus, in terms of suitability for clinical application, injectable *in situ* gelling hydrogels are more appropriate as these materials can easily conform to the lesion irregularity with minimal tissue damage during delivery.

To meet such requirements, tissue-specific injectable ECM hydrogels, prepared by decellularization of porcine brain, spinal cord (SC-ECM), and porcine urinary bladder (UB-ECM), have been recently described in terms of their composition, biomechanical properties, and neurotrophic properties.<sup>19,20</sup> These materials proved to be advantageous for providing a supportive environment for the *in vitro* neural cell growth. However, experimentally, it is unknown whether these materials can be successfully used for SCI repair, either alone or in combination with various types of cells.

To evaluate the potential neuroregenerative properties of the central nervous system (CNS) and non-CNS-derived materials *in vivo*, this study examined the effects of ECM hydrogels based on SC-ECM and UB-ECM in the model of SCI.

The *in vitro* cell-adhesive properties and neurotrophic potential of the ECM hydrogels were studied on human mesenchymal stem cells derived from Wharton's jelly (hWJ-MSCs) and on dorsal root ganglia (DRG) explant culture, respectively. To evaluate the *in vivo* tissue compatibility, the ECM hydrogels were injected into the spinal cord hemisection in rats and histologically evaluated. The tissue-scaffold interactions were further investigated using real-time qPCR to determine changes in the messenger RNA (mRNA) expression of genes related to the inflammation and immune response, secretion of neurotrophic and growth factors, and astrogliosis.

## Materials and Methods

### Preparation of ECM hydrogels

The preparation of the ECM hydrogels was based on a previously described procedure.<sup>9,19,21</sup> ECM samples were solubilized with 1.0 mg/mL pepsin in 0.01 N HCl (Sigma-

Aldrich, Steinheim, Germany) at a concentration of 10 mg ECM/mL and stirred at room temperature for 48 h to form a pregel solution (pH ~2). The pepsin-HCl ECM solution was neutralized to pH 7.4 with 0.1 N NaOH, isotonicity balanced with 10× phosphate-buffered saline (PBS), and diluted with 1× PBS to the concentration of 8 mg/mL. To form the hydrogel, the neutralized pregel was placed at 37°C for 45 min. The composition and biomechanical properties of the ECM hydrogels have been described in detail in Crapo *et al.*,<sup>9</sup> Medberry *et al.*,<sup>19</sup> and Wolf *et al.*<sup>21</sup>

### Cell culture

Fresh human umbilical cord samples were collected from healthy full-term neonates after spontaneous delivery with the informed consent of the donors using the guidelines approved by the Institutional Ethics Committee at University Hospitals (Pilsen and Prague, Czech Republic). About 10–15 cm per umbilical cord were aseptically transported into sterile PBS (IKEM, Prague, Czech Republic) with antibiotic-antimycotic solution (Sigma-Aldrich) at 4°C.

After removal of blood vessels, the remaining tissue was chopped into small pieces (1–2 mm<sup>3</sup>) and transferred to 10-cm Nunc culture dishes (Schoeller, Prague, Czech Republic) containing the complete Alpha-Minimum Essential Medium (East Port, Prague, Czech Republic) supplemented with 5% platelet lysate (IKEM) and gentamicin 10 µg/mL (Sandoz, Prague, Czech Republic), and cultivated at 37°C and 5% CO<sub>2</sub> in a humidified atmosphere.

On day 10, the explants were removed from the culture dishes and the remaining adherent cells were cultured for 3 weeks or until 90% confluence. The medium was changed two times a week. Cells of the third passage were identified by flow cytometry (FACSARIA™; Becton Dickinson, San Jose, CA) to confirm their purity. The following antibodies against human antigens were used: CD34, CD45, CD105 (Exbio, Vestec, Czech Republic); CD29, CD73, CD90, CD271, CD31, HLA-ABC, and CD235a (BD Pharmingen, San Jose, CA); CD133 (Miltenyi Biotec, Bergisch Gladbach, Germany). Data analysis was performed using BD FACSDiva software.

### In vitro cell growth and viability

*In vitro* cell growth on the surface of hydrogels was characterized using hWJ-MSCs cultures. Cell viability was determined after 1, 3, 7, and 14 days in culture using WST-1 reagent (Roche, Mannheim, Germany). Cells were cultured in 96-well plates (5000 cells/per well) coated with either UB-ECM or SC-ECM hydrogels (90 µL/well) before cell seeding. At the measured time points, 10 µL of WST-1 reagent was added to each well with 100 µL culture media and the plates were incubated for 2 h at 37°C. The absorbance was measured using a Tecan Spectra ELISA plate reader (Tecan Trading, Mannedorf, Switzerland) at 450 nm. Each type of hydrogel was seeded in triplicate; 14 independent experiments in three hydrogel batches were performed for each hydrogel type. Cell viability on the culture plastic was used as a control.

In 3D culture, cells were seeded within the hydrogels by adding concentrated cell suspension in PBS to neutralized liquid pregel solution for a final cell concentration of  $2.5 \times 10^6$  cells/mL. Cells were thoroughly mixed in the pregel and 200 µL of the suspension was transferred inside the seeding

rings with a diameter of 0.8 cm (Scaffdex, Tampere, Finland) placed in the 24-well plates, and transferred at 37°C for 45 min to form a hydrogel around the cells. Following this, the seeding rings were removed, 1 mL of media was added, and the hydrogel discs were imaged after 4 h, 24 h, 4 days, and 7 days in culture to quantify gel contraction (more details in the Supplementary Data; Supplementary Data are available online at [www.liebertpub.com/tea](http://www.liebertpub.com/tea)). The cell-seeded hydrogels used for *in vivo* experiments were placed into PBS and incubated at 37°C and 5% CO<sub>2</sub> in a humidified atmosphere for ~4 h before their implantation into the hemisection cavity.

The morphology of the cells on the hydrogels was examined by immunofluorescence staining for actin filaments. After fixation in 4% paraformaldehyde in 0.1 M PBS for 15 min, the cells were washed with 0.1 M PBS and stained with AlexaFluor 568 phalloidin (1:300); the nuclei were visualized using 4',6-diamidino-2-phenylindole (DAPI) fluorescent dye (all from Invitrogen, Paisley, United Kingdom).

#### DRG explant culture

Wistar rats (Velaz, Unetice, Czech Republic), aged 3–5 days, were used for DRG extraction. Briefly, their spinal cords were dissected and DRGs from low thoracic and lumbar parts were isolated, placed in cold Hank's Balanced Salt Solution without Ca<sup>2+</sup>/Mg<sup>2+</sup> solution (Invitrogen, Waltham, MA), and cleaned of peripheral nerve processes.

DRG explants were then placed on SC-ECM ( $n=5$ ) or UB-ECM ( $n=4$ ) hydrogels in 24-well plates and cultured in Neurobasal medium (Invitrogen) supplemented with 2% B27 (Life Technologies, Carlsbad, CA), 2 mM L-glutamine (Invitrogen), 0.5% NGF (50 ng/mL; PeproTech, Prague, Czech Republic), uridine (17.5 µg/mL; Sigma-Aldrich), and primocin (PeproTech) in humidified atmosphere at 37°C and 5% CO<sub>2</sub>. The medium was changed every 3 days.

After 7 days of culture, DRGs were fixed with 4% paraformaldehyde in 0.1 M PBS for 10 min and subjected to immunocytochemical staining for neurofilaments (NF160, 1:200; Abcam, Cambridge, United Kingdom) and cell nuclei (DAPI, 1:1000). Imaging was performed using a Leica fluorescent microscope (Leica DMI 6000B) and TissueGnostics software (TissueGnostics GmbH, Vienna, Austria). The neurite extension area and the longest neurite length were determined using ImageJ software with the Neurite-J plug-in, as described by Torres-Espin *et al.*<sup>22</sup>

#### Hydrogel injection into the SCI lesion

Male Wistar rats (250–300 g; Velaz) underwent a hemisection at the level of the 8th thoracic vertebra (Th8). The neutralized and isotonic balanced liquid pregel solution of SC-ECM and UB-ECM hydrogels (8 mg/mL) were acutely injected into the spinal cord defect after hemisection and allowed to gelate *in situ*, followed by histological evaluation 2, 4, and 8 weeks after implantation ( $n=5$  per group, per time point).

The surgery was performed under adequate pentobarbital (PTB) anesthesia (60 mg/kg). The animals received local injections of mesocain (0.3 mL s.c. at the surgery site) in addition to general anesthesia, as well as gentamicin (0.05 mL i.m.; Sandoz) and atropine (0.2 mL, atropine solution 1:5) (both from BB Pharma, Prague, Czech Republic) injections.

First, a microsection of the skin was made at the level of Th8 spinal process using a scalpel. Then the laminectomy at Th8 was performed using rongeur, and the dura was incised with capsulotomy scissors. A 2 mm long spinal cord segment of the volume ~6 mm<sup>3</sup> was dissected using delicate tissue scissors to generate a hemisection cavity. Then the dissected segment was removed using a small piece of cellulose and fine forceps. The aforementioned instruments were purchased from Medicon® (Tuttlingen, Germany). The dura mater was sutured with 10/0 monofilament nonresorbable thread (B Braun, Aesculap, Melsungen, Germany), and the hydrogels were injected into the cavity in a single injection using an Omnican® Insulin syringe for U-100 Insulin (Melsungen, Germany). The muscles and skin were sutured with 4/0 monofilament nonresorbable thread (4/0 Chirmax, Prague, Czech Republic), and the animals were housed, two rats in a cage, with food and water *ad libitum*.

In the control SCI group ( $n=4$ ) the hemisection defect was filled with saline. In the animal group treated with SC-ECM hydrogel seeded with hWJ-MSCs ( $n=4$ ), the hydrogels were implanted into the hemisection cavity. This animal group received a daily injection of the immunosuppressant cyclosporin A (10 mg/kg, intraperitoneally) (Sandimmune; Novartis, Basel, Switzerland), azathioprine (2 mg/kg, per orally) (Imuran; Aspen Europe GmbH, Bad Oldesloe, Germany), and methylprednisolone (2 mg/kg, i.m.) (Solu-Medrol; Pfizer, Puurs, Belgium) to prevent the rejection of the transplanted cells.

Of the 56 animals that underwent the hemisection, 4 animals died during the operation and 2 animals died 2–4 weeks after operation. All experiments were performed in accordance with the European Communities Council Directive of 24 November 1986 (86/609/EEC), regarding the use of animals in research and were approved by the Ethics Committee of the Institute of Experimental Medicine, Academy of Sciences, Czech Republic (Prague, Czech Republic).

Hindlimb motor function between the first and fourth weeks post-SCI was recorded for the sham-operated control group, SC-ECM alone, and SC-ECM combined with hWJ-MSCs using the Basso–Beattie–Bresnahan (BBB) open field locomotor test<sup>23</sup> (Supplementary Data).

#### Tissue processing and histology

At 2, 4, and 8 weeks after hydrogel injection, the animals were deeply anesthetized with an intraperitoneal injection of overdose PTB and perfused with PBS followed by 4% paraformaldehyde in 0.1 M PBS. The spinal cord was left in the bone overnight, then removed and postfixed in the same fixative for at least 1 week. A 3 cm long segment of the spinal cord containing the lesioned site was dissected out and transferred to 10% and 30% sucrose. After freezing, the spinal cords were cryosectioned into 40 µm thick longitudinal sections. Hematoxylin–Eosin (H&E) and Masson's Trichrome staining was performed using the standard protocol.

For immunohistological analysis, the following antibodies were used: against neurofilament (NF160, 1:200), endothelial cells (RECA-1, 1:500), astrocytes (Cy3-conjugated mouse Glial Fibrillary Acidic Protein, GFAP, 1:200), all from Sigma-Aldrich; Schwann cells p75 (1:200), serotonin-positive axons (R-SERO, 1:100), oligodendrocytes (OSP, 1:1000), macrophages (ED1, 1:100), M1 macrophages (CD86, Cy3-

conjugated donkey anti-rabbit IgG-PerCp-Cy5,5, 1:2500), human mitochondria (MTCO2, 1:250), all from Abcam; and M2 macrophages (CD206, 1:250), axonal growth cone (GAP43, 1:100), all from Santa Cruz (Heidelberg, Germany). Alexa Fluor® 488-conjugated goat anti-mouse IgG (1:200), Alexa Fluor 594-conjugated goat anti-mouse IgG (1:200) and Alexa Fluor 488-conjugated donkey anti-goat IgG (1:700) were used as secondary antibodies. The nuclei were visualized by using 4',6-diamidino-2-phenylindole (DAPI) fluorescent dye. Fluorescent micrographs were taken using an AxioCam HRc Axioskop 2 Plus fluorescence microscope (Zeiss, Jena, Germany) and a LSM 510 DUO laser scanning confocal microscope (Zeiss).

For axonal and vessel analysis, multiple images across the entire lesion were taken using a 20× objective. Five images from each sample were selected and the total area of the axons (NF160 staining) and blood vessels (RECA staining) within the lesion area was outlined using ImageJ software (National Institutes of Health, Bethesda, MD) and divided by the area of the lesion to determine the percentage of the lesion that was occupied by new axons or vasculature.

#### Gene expression analysis

The expressions were studied using quantitative real-time reverse transcription polymerase chain reaction (qPCR) 2, 4, and 8 weeks after the surgery (in all groups  $n=4$ ). RNA was isolated from paraformaldehyde-fixed frozen tissue sections using the High Pure RNA Paraffin Kit (Roche, Penzberg, Germany), following the manufacturer's recommendations. RNA amounts were quantified using a spectrophotometer (NanoPhotometer™ P-Class, Munchen, Germany). The isolated RNA was reverse transcribed into complementary DNA (cDNA) using the Transcriptor Universal cDNA Master (Roche) and a thermal cycler (T100™ Thermal Cycler; Bio-Rad, Hercules, CA).

The qPCR reactions were performed using cDNA solution, FastStart Universal Probe Master (Roche) and TagMan® Gene Expression Assays (Life Technologies), (Supplementary Table S1; Supplementary Data are available online at [www.liebertpub.com/tea](http://www.liebertpub.com/tea)). The qPCR was carried out in a final volume of 10  $\mu$ L containing 25 ng of extracted RNA. Amplification was performed on the real-time PCR cycler (StepOnePlus™; Life Technologies). All amplifications were run under the same cycling conditions: 2 min at 50°C, 10 min at 95°C, followed by 40 cycles of 15 s at 95°C and 1 min at 60°C.

All samples were run in duplicate, and a negative control was included in each array. Relative quantification of gene expression was determined using the  $\Delta\Delta$ Ct method. Results were analyzed with StepOnePlus software. The gene expression level was normalized on *Gapdh* as a reference gene; control samples from unlesioned spinal cord tissue were used as a calibrator.

#### Statistical evaluation

The statistical significance of the differences in gene expression between the groups at three time points was determined using two-way repeated measurement analysis of variance (ANOVA) with a Student–Newman–Keuls *post hoc* pair-to-pair test. A one-way ANOVA was used for the comparisons of gene expression between groups with SC-ECM hydrogel at 4-week intervals and cell proliferation (SigmaStat 3.1; Systat Software, Inc., San Jose, CA).

## Results

#### In vitro cell culture

The solubilized ECM matrix self-assembles from the pregel form into the hydrogel at 37°C and physiologic pH, as was described in Medberry *et al.*<sup>19</sup> The biocompatibility and

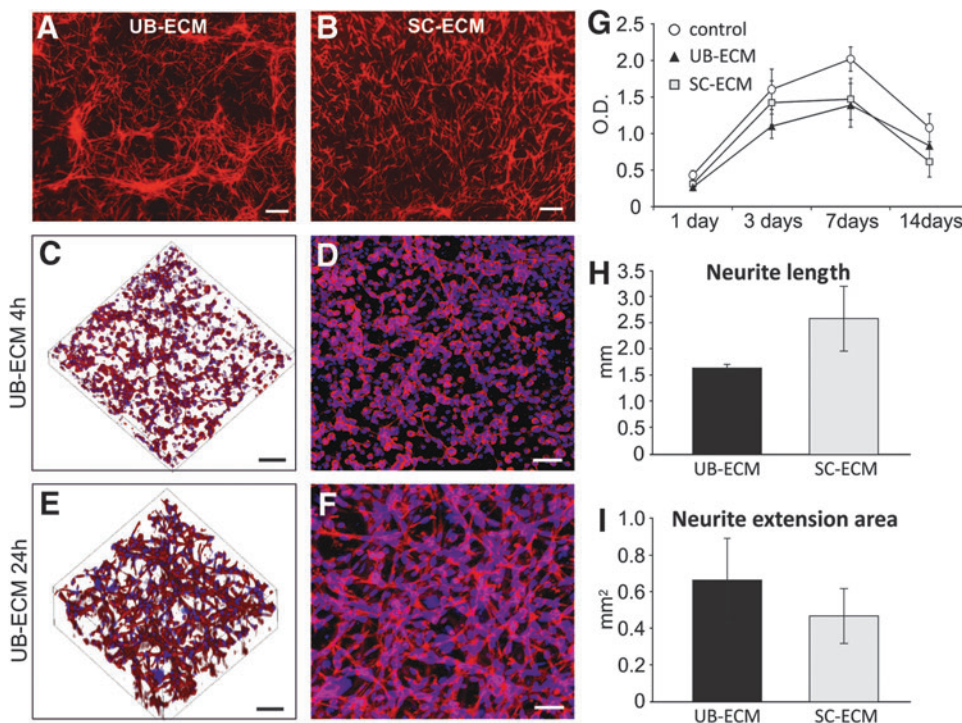


**FIG. 1.** *In vitro* cell growth on extracellular matrix (ECM) hydrogels. Two-dimensional (2D) cell culture on (A) urinary bladder (UB)-ECM and (B) spinal cord (SC)-ECM hydrogels at 3 days. (C–F) Three-dimensional (3D) cell culture in UB-ECM at (C, D) 4 and (E, F) 24 h. Cells were stained for (A–F) phalloidin and (C–F) cell nuclei (DAPI). (G) Proliferation of human Wharton's jelly-derived mesenchymal stem cells (hWJ-MSCs) on ECM hydrogels using WST-1 assay. (H) Quantification of the highest neurite length and (I) neurite extension area of dorsal root ganglia explants on ECM hydrogels using Neurite-J plugin for ImageJ software. Scale bar: (A, B) 100  $\mu$ m, (C–F) 50  $\mu$ m. Color images available online at [www.liebertpub.com/tea](http://www.liebertpub.com/tea)



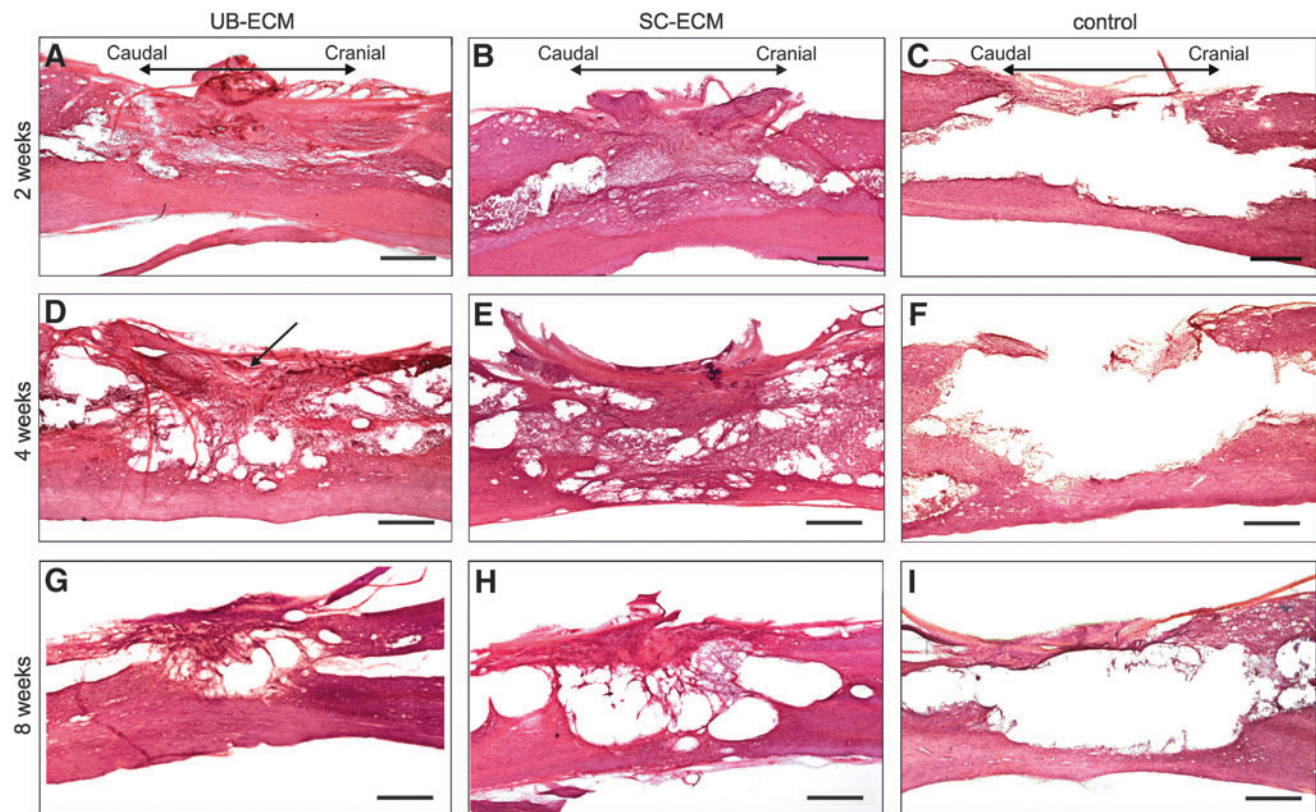


**FIG. 2.** Representative Hematoxylin–Eosin staining of the spinal cord lesion (A–C) 2, (D–F) 4, and (G–I) 8 weeks after injection of (A, D, G) UB-ECM hydrogels; (B, E, H) SC-ECM hydrogels. (C, F, I) Represent a sham-operated control lesion. (D) The *arrow* shows the nondegraded part of the hydrogel. Scale bar: 500  $\mu$ m. Color images available online at [www.liebertpub.com/tea](http://www.liebertpub.com/tea)

bioadhesive properties of ECM hydrogels were confirmed by the *in vitro* use of hWJ-MSCs in the two-dimensional (2D) and 3D cell cultures (Fig. 1). Flow cytometry was performed to detect cell purity, while CD markers were found positive for CD29, CD105, CD90, CD73, and HLA-ABC and negative for CD31, CD34, CD45, CD133, CD235a, and CD271. After seeding onto the ECM hydrogels, cells spread and proliferated on both hydrogel types (Fig. 1).

Cell proliferation was determined using the WST-1 assay after 1, 3, 7, and 14 days of the culture. Both ECM hydrogels showed comparable ability to support *in vitro* cell proliferation, which did not significantly differ from the control cell proliferation on tissue culture plastic (TCP). Cell viability increased until day 7, then, after reaching the confluency of the culture, decreased on both hydrogel types as well as on TCP (Fig. 1G).

When seeded in 3D culture (0.5 million cells per 0.2 mL), hWJ-MSC extended their lamellipodia within the hydrogels and formed a 3D network, as is shown in Figure 1C–F after 4 and 24 h. Rapid hydrogel contraction was observed already after 4 h, which progressed during the culture to at least 10% of the initial area after 7 days (Supplementary Fig. S1).

#### DRG explant culture on ECM hydrogels

DRG explant cultures were used to compare the neurotrophic properties of the CNS and non-CNS-derived ECM hydrogels. After 7 days of culture, neurites densely extended

from the DRG bodies (Supplementary Fig. S2). No significant differences were found between UB-ECM and SC-ECM in both examined parameters, total neurite extension area and longest neurite length (Fig. 1H, I).

#### Histological evaluation after ECM hydrogel injection

Both UB-ECM and SC-ECM hydrogels were injected into the cavity of the spinal cord hemisection and examined at 2, 4, and 8 weeks. The tissue response to the scaffolds was histologically evaluated by analyzing axonal ingrowth, vascularization, and infiltration of macrophages/microglia, astrocytes, and oligodendrocytes within the injury site.

At 2 weeks after injury, H&E staining of longitudinal spinal cord sections demonstrated that both hydrogel types were biocompatible with the surrounding host tissue and entirely filled the lesion cavity (Fig. 2A, B). The hydrogels were mostly degraded, but still detectable in the lesion area (Supplementary Fig. S3) and were densely populated among the host cells.

By 4 weeks postinjury, small areas of the original hydrogel were still present (Fig. 2D), while the newly formed tissue interconnected with the host tissue, bridging the lesion center. Macrophages massively infiltrated the periphery of the lesion where several small cysts developed due to the rapid degradation of the graft. A similar tissue response was found at 8 weeks, when the hydrogels had fully degraded, which was followed by further progression of cyst formation. In contrast

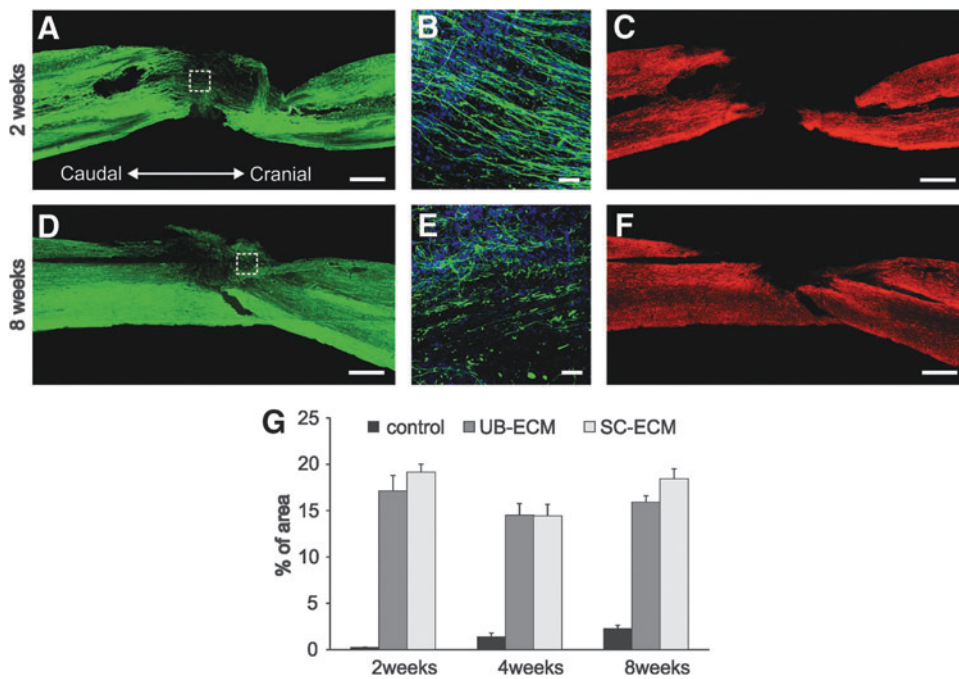


**FIG. 3.** Representative images of the spinal cord lesion (A–C) 2 and (D–F) 8 weeks after injection of SC-ECM hydrogels. Immunofluorescence staining for (A, B, D, E) neurofilaments (NF160), (C, F) astrocytes (GFAP), and (B, E) cell nuclei (DAPI, blue). Squares (A, D) are also shown under the higher magnification insets (B, E). (G) The effect of ECM hydrogels on the ingrowth of NFs. A significantly higher ingrowth of NFs was found in both the ECM hydrogel groups when compared to the control lesion at all time points. Scale bar: (A, C, D, F) 500  $\mu$ m; (B, E) 50  $\mu$ m. Color images available online at [www.liebertpub.com/tea](http://www.liebertpub.com/tea)

to the tissue remodeling process observed in the lesion after hydrogel injection, large pseudocysts formed in the control sham-treated lesion (Fig. 2C, F, I).

To evaluate axonal ingrowth into the hydrogels, a neurofilament marker (NF160) was used (Fig. 3). Robust ingrowth

of NF-positive fibers into the hydrogel-treated lesion was observed from both the rostral and caudal stumps of the lesion, while dense infiltration of NFs was also found in the center of the lesion. Quantification analysis expressed the relative value of NF160 immunopositive area as a percentage

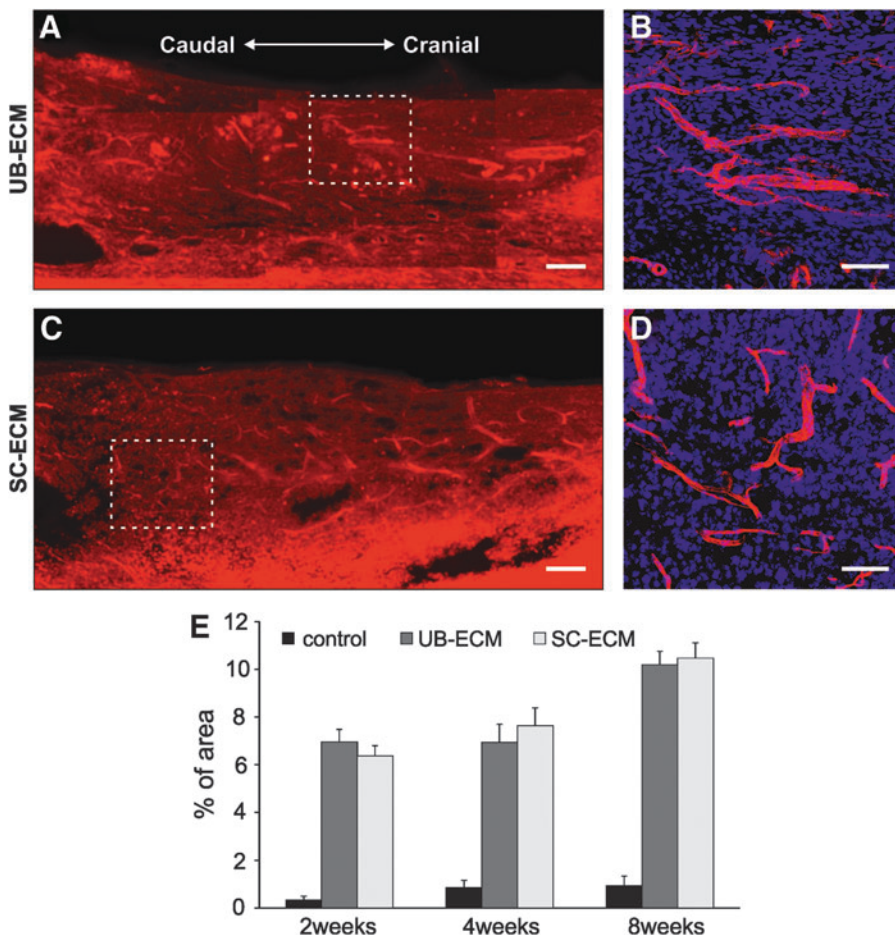
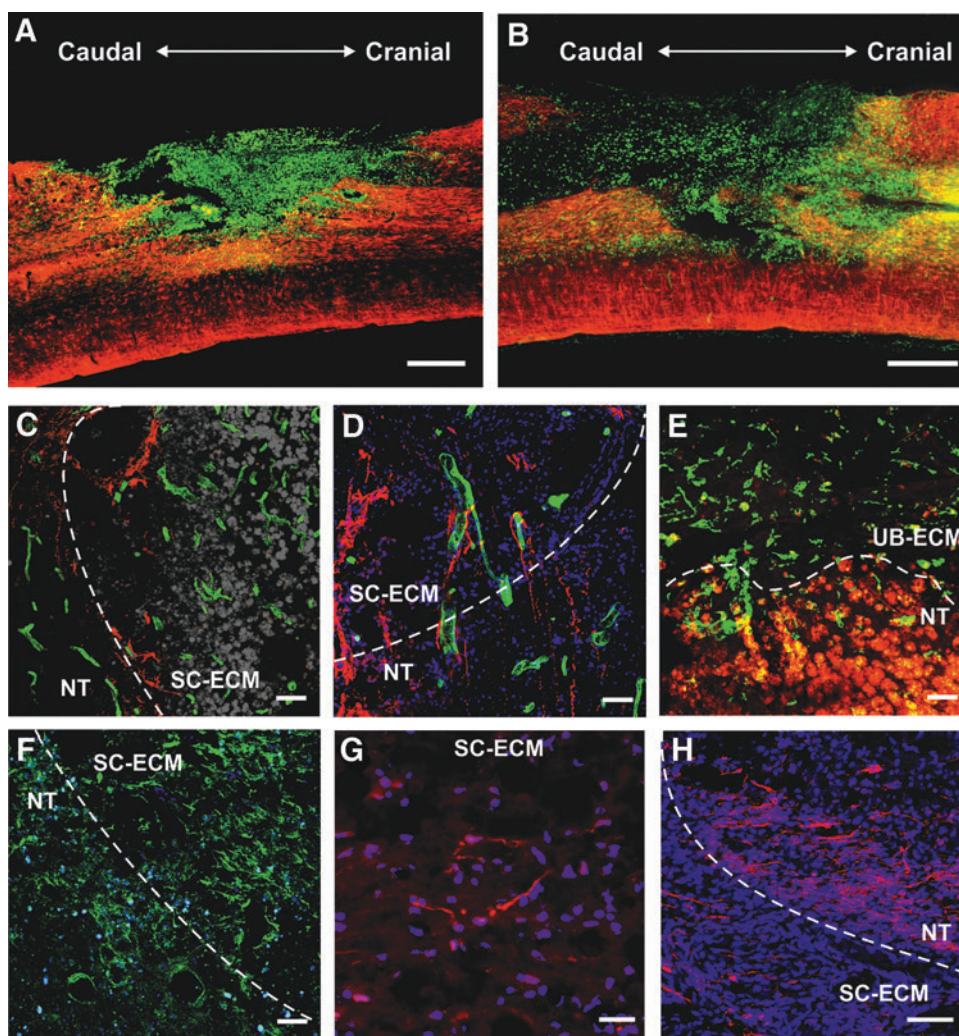


**FIG. 4.** Representative images of the spinal cord lesion at 2 weeks after injection of (A, B) UB-ECM and (C, D) SC-ECM hydrogels. (A–D) Immunofluorescence staining for blood vessels (RECA) and (B, D) cell nuclei (DAPI). Squares (A, C) are also shown under higher magnification insets (B, D). (E) An effect of ECM hydrogels on vascularization. A significantly higher ingrowth of blood vessels was found in both ECM hydrogel groups when compared to the control lesion at all time points. Scale bar: (A, C) 500  $\mu$ m; (B, D) 50  $\mu$ m. Color images available online at [www.liebertpub.com/tea](http://www.liebertpub.com/tea)



**FIG. 5.** Representative immunofluorescence staining for (A, B) macrophages (ED1, green) and astrocytes (GFAP, red) in (A) UB-ECM at 2 weeks and (B) SC-ECM seeded with hWJ-MSCs at 4 weeks. Confocal micrographs of the staining for (C) serotonin-positive axons (5-HT, red) and blood vessels (RECA, green) in SC-ECM at 4 weeks; (D) serotonin-positive axons (5-HT, red), blood vessels (RECA, green), and cell nuclei (DAPI, blue) in SC-ECM seeded with WJ-MSCs at 4 weeks; (E) M1 macrophages (CD86, red) and M2 macrophages (CD206, green) in UB-ECM hydrogel at 2 weeks; (F) oligodendrocytes (OSP, green) and cell nuclei (DAPI, blue) in SC-ECM at 4 weeks; (G) neuronal growth cones (GAP 43, red) and cell nuclei (DAPI, blue) in SC-ECM at 4 weeks; (H) Schwann cells (p75, red) and cell nuclei (DAPI, blue) in SC-ECM at 4 weeks. The dotted line in (C, D, E, F, H) describes the border between ECM hydrogel and neural tissue (NT). Scale bar: (A, B) 500  $\mu$ m; (C, H) 100  $\mu$ m; (D–F) 50  $\mu$ m; (G) 25  $\mu$ m. Color images available online at [www.liebertpub.com/tea](http://www.liebertpub.com/tea)



of the lesion area. The ingrowth of NFs was maximal at 2 weeks in both hydrogel groups and did not further increase at later time points. No differences in the NFs area were found between SC-ECM and UB-ECM hydrogels at all time points (Fig. 3G). Despite the isotropic structure of the ECM hydrogels, the ingrowing axons linearly bridged the SCI lesion while forming multiple bundles organized in the longitudinal direction along the spinal cord (Fig. 3B).

Astrocytes, evaluated by immunofluorescence staining for GFAP, did not migrate inside the lesion and thus served as a clear demarcation of the lesion area (Fig. 3C, F). Only a few astrocytic processes grew into the graft from the lesion border (Fig. 3F).

In terms of neovascularization, a number of blood vessels (RECA staining) grew into the hydrogel-treated lesions and formed a dense network (Fig. 4A–D). The area of blood vessels gradually increased with time, but no differences in blood vessel density were found between the UB-ECM and SC-ECM hydrogels at any time point (Fig. 4E).

The host tissue remodeling response was characterized by robust infiltration of CD68<sup>+</sup> cells throughout the entire lesion area (Fig. 5A, B), which populated the hydrogels at all time points, and remained in the lesion site after the hydrogel had degraded. As is apparent from the staining for

M1 and M2 macrophages in Figure 5E, macrophages at the interface of the ECM hydrogel and the host tissue were predominantly of the M1 phenotype (CD86 staining), while M2 phenotype macrophages (CD206 staining) were mostly present within the hydrogel area.

Infiltration of serotonin-positive axons (Fig. 5C, D) was observed from the rostral part of the hydrogels, but these axons did not spread across the lesion. Infiltration of oligodendrocytes (OSP staining, Fig. 5F) within the lesion site indicated that myelination occurred in some of the regenerated axons. Newly sprouted axonal fibers were also detected using GAP43 staining (Fig. 5G). Numerous endogenous Schwann cells that migrated from the nerve roots were detected within the lesion site as well as in the surrounding tissue (Fig. 5H).

#### *Histological evaluation of implanted ECM hydrogels combined with hWJ-MSCs*

To evaluate the potential of ECM hydrogels as a cell vehicle, the SC-ECM hydrogels were mixed with hWJ-MSCs (0.5 million cells per 0.2 mL), and the cell–hydrogel constructs containing ~15,000 cells were acutely implanted into the hemisection cavity. Four weeks after

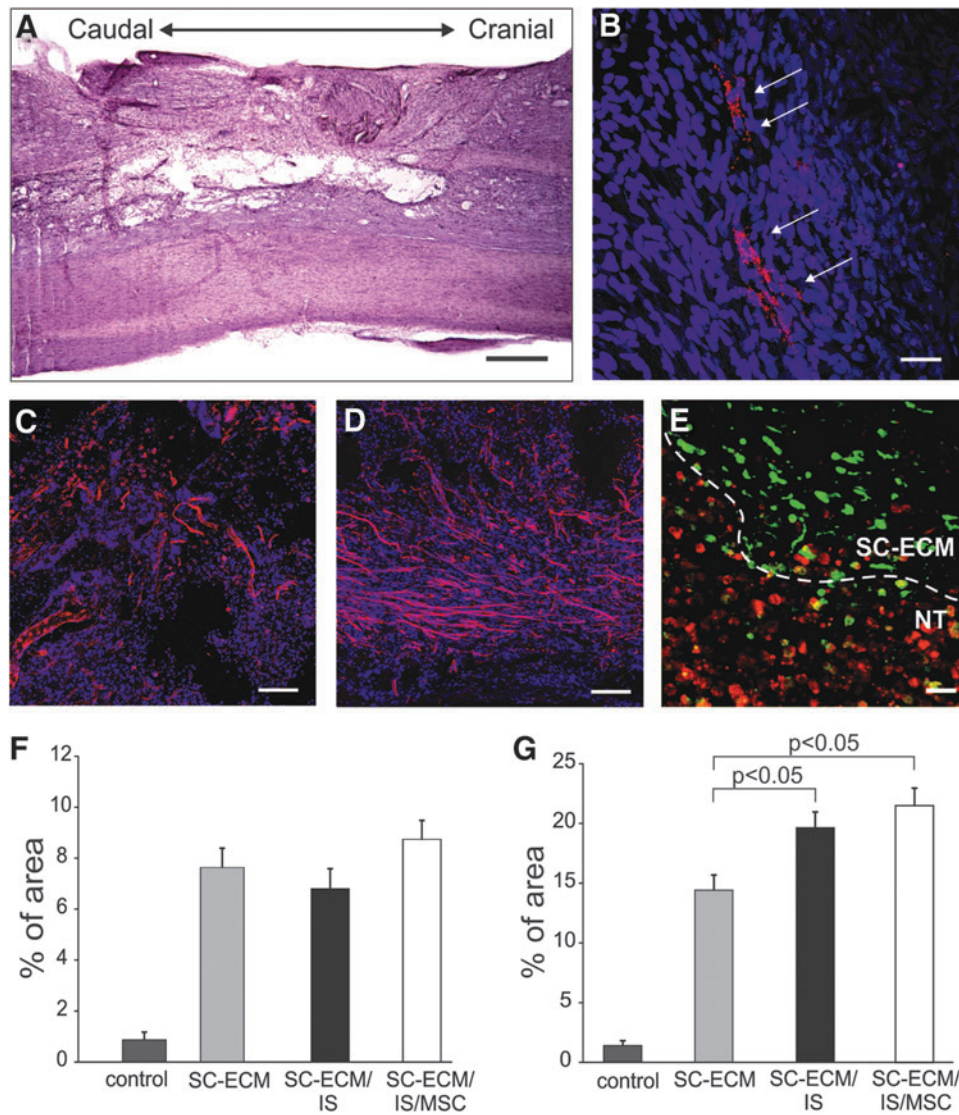


**FIG. 6.** Representative images of the spinal cord lesion after implantation of SC-ECM seeded with hWJ-MSCs at 4 weeks. (A) Hematoxylin-Eosin staining. Confocal micrographs of the staining for (B) human mitochondria (MTCO2); (C) blood vessels (RECA); (D) neurofilaments (NF160) and (B–D) cell nuclei (DAPI, blue); (E) M1 macrophages (CD86, red) and M2 macrophages (CD206, green). The dotted line describes the border between ECM hydrogel and NT. An effect of the SC-ECM hydrogels seeded with hWJ-MSCs on the ingrowth of (F) blood vessels and (G) neurofilaments. (IS)—animal groups that received immunosuppression. Scale bar: (A) 500  $\mu$ m, (B, E) 50  $\mu$ m, (C, D) 100  $\mu$ m. Color images available online at [www.liebertpub.com/tea](http://www.liebertpub.com/tea)

surgery, the grafts were densely infiltrated with endogenous tissue, while cysts had developed at the graft-tissue interface (Fig. 6A). Only very few surviving cells, positive for human mitochondria MTCO2 marker, were detected in the lesion (Fig. 6B). Transplanted cells did not further promote the ingrowth of NF-positive fibers or blood vessels. However, an increase in NF-positive fibers was found in those animal groups that received immunosuppression (Fig. 6F, G). As in the empty ECM hydrogels, M2 phenotype macrophages were mostly present within the hydrogel area (Fig. 6E).

#### Gene expression analysis induced by ECM hydrogels

Changes in the mRNA expression of genes related to inflammation (*Ptgs2*, *Ccl3*, *Ccl5*, *Il2*, *Il6*, *Il12b*), M1 macrophages (*Irf5*, *Cd86*, *Nos2*), M2 macrophages (*Mrc1*, *Cd163*, *Arg1*), growth factors (*NT-3*, *Fgf2*), axonal sprouting (*Gap43*), astrogliosis (*Gfap*), angiogenesis (*Vegfa*), and apoptosis (*Casp3*) were determined at 2, 4, and 8 weeks after hydrogel injection and compared to the control SCI lesion (Fig. 7, Supplementary Table S1).

The most profound host tissue response to the ECM hydrogels was observed 2 weeks after injury, when significant downregulation was found in the expression of *Fgf2*, *Cd163*, *Irf5*, *Ccl5*, and *Gap43* in both hydrogel groups, and of *Gfap* in the UB-ECM hydrogel group only, when compared to the control SCI lesion. At 4 weeks, no significant changes were detected between both hydrogel groups and the control group, except for a significant upregulation of *Arg1* in the UB-ECM hydrogel group compared to SC-ECM (Supplementary Table S2). A potential tissue-specific effect of SC-ECM was observed at 8 weeks, when significant upregulation of mRNA expression was detected for *NT-3*, *Fgf2*, *Irf5*, and *Casp3*. The expression of proinflammatory cytokines *IL-2*, *IL-6*, *Il12b*, and *Nos2* was undetectable in all groups.

The effect of hWJ-MSCs combined with SC-ECM hydrogels was determined 4 weeks after the scaffold implantation. The animals received immunosuppression to prevent rejection of the xenogeneic cells. Interestingly, the immunosuppression significantly decreased the mRNA expression of *Gfap* in both empty and cell-seeded hydrogels and of *Fgf2*, *Casp3*, *Ccl3*, and *Cd86* in empty hydrogels, when compared to the control lesion (Fig. 7, Supplementary



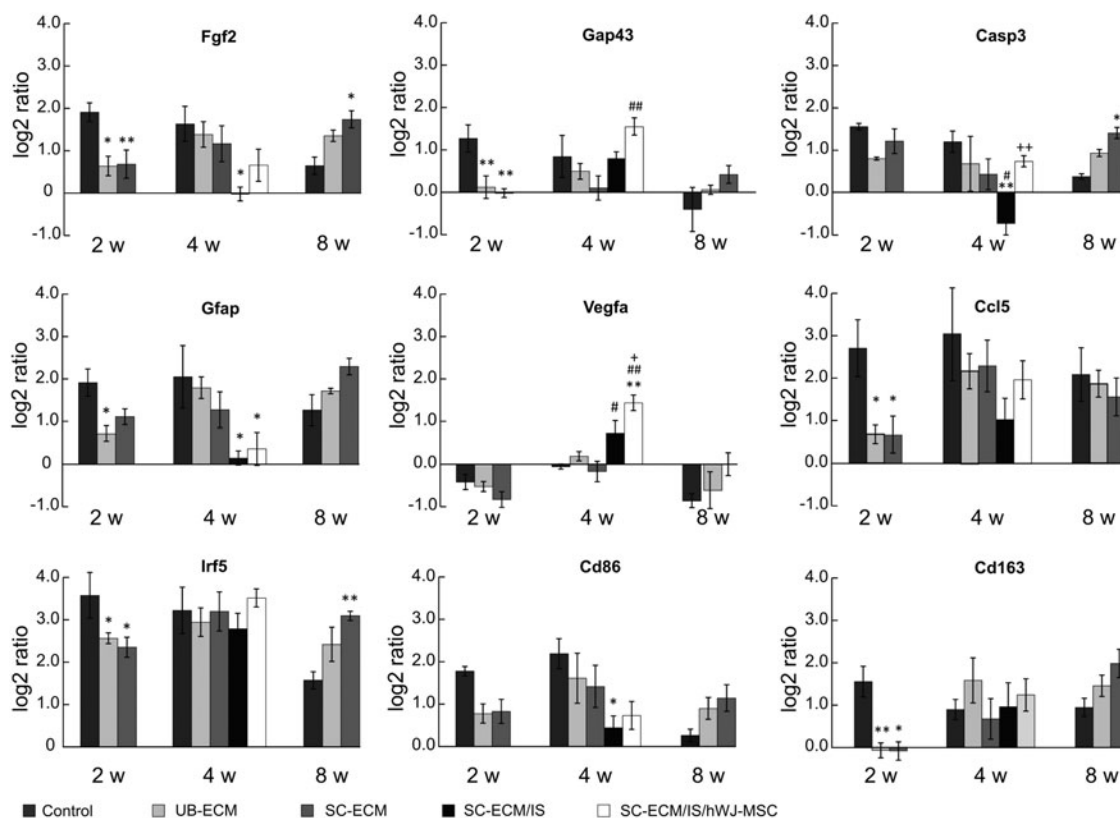


**FIG. 7.** Analysis of messenger RNA (mRNA) gene expression of several genes involved in inflammatory and reparative processes following spinal cord injury (SCI) treated with ECM hydrogels. The graphs show the log<sub>2</sub>-fold changes in gene expression over intact spinal cord tissue. IS, animal groups that received immunosuppression. \* $p < 0.05$ , \*\* $p < 0.01$ :  $\Delta$ Ct values of ECM hydrogel versus control lesion. # $p < 0.05$ , ## $p < 0.01$ :  $\Delta$ Ct values of SC-ECM hydrogel with IS versus SC-ECM. + $p < 0.05$ , ++ $p < 0.01$ :  $\Delta$ Ct values of SC-ECM hydrogel with IS and hWJ-MSCs versus empty SC-ECM with IS.

Table S1). Moreover, a significant increase in the expression of *Vegfa* and *Gap43* was also found in cell-seeded hydrogels when compared to the empty hydrogels.

## Discussion

In this study, we evaluated the *in vivo* neuroregenerative potential of two types of ECM hydrogels based on the CNS and non-CNS tissue, when injected into the spinal cord acutely after SCI. The ECM matrices were derived from porcine spinal cord and urinary bladder and processed into an injectable hydrogel form as was described previously.<sup>19,21</sup> Regarding the different tissue sources used, SC-ECM and UB-ECM hydrogels were prepared using different decellularization methods and differed in their composition as well as in their physical and biological properties.<sup>19,21</sup> Despite the lack of a native 3D ultrastructure from the source tissue, ECM hydrogels retain their biological activity and possess mechanical properties similar to that of soft neural tissue, with the advantage of injectability and *in situ* polymerization, which offer minimally invasive delivery techniques and facilitate the possibility of clinical translation.

When injected into the SCI, both hydrogel types were well integrated into the surrounding tissue, with persisting massive cell infiltration and neovascularization. A potentially important factor for tissue regeneration is tissue specificity

of the ECM hydrogel source. In this study, however, both studied materials proved to be advantageous for providing a supportive environment and revealed similar neurotrophic properties *in vitro* in the DRG explant culture as well as *in vivo* with regard to the ingrowth of NFs and neovascularization. These findings are consistent with those of a previous study, which showed no advantage of CNS-derived ECM materials versus non-CNS-derived ECM materials with respect to effects upon neural stem/progenitor cells.<sup>24</sup>

Macrophages were the predominant infiltrating cells within the grafts that participated in the ECM degradation. As was shown previously, degradation of ECM scaffolds is essential for the constructive tissue remodeling process, by which a degradable biomaterial serves as a temporary inductive niche, which is gradually replaced by anatomically appropriate and functional tissue as opposed to scar tissue.<sup>11,25,26</sup> Moreover, degradation of ECM scaffolds stimulates the release of matricryptic molecules; which possess a variety of bioactive properties, such as antimicrobial activity, angiogenic effects, as well as the recruitment of endogenous stem and progenitor cells.<sup>26</sup>

In the present study, however, despite the fact that the lesion cavity was filled with endogenous cell-populated ECM hydrogels 2 weeks after their injection, further progression in matrix degradation at later time points was not followed by full neural tissue replacement, but rather

resulted in the formation of a dense network of tissue containing axons, blood vessels, and other neural tissue elements interrupted by a number of small cysts.

According to the gene expression analysis, *in vivo* ECM degradation was associated with a significant decrease in mRNA expression of markers for proinflammatory/M1 macrophages (*Irf5*) and regulatory/M2 macrophages (*Cd163*), inflammation (*Ccl5/RANTES*), as well as genes for growth factor *Fgf2*, astrogliosis (*Gfap*), and neuronal growth cones (*Gap43*). The expression of other markers related to immune response, such as *Cd86*, *Mrc1*, and *Ptgs2*, also decreased, but these changes were not found to be significant. Interestingly, these effects were detected during the early phase after injury, but decreased or even reversed at later time points, suggesting that ECM hydrogel degradation played a significant role in the transient modulation of the innate immune and tissue repair response.

Previous reports have shown increased numbers of M2 macrophages and more positive polarization toward an M2 phenotype associated with ECM *in vivo* degradation and the promotion of constructive tissue remodeling.<sup>15,27</sup> Recent studies describe the M2 polarizing effects of ECM derived from several tissues.<sup>28,29</sup> In the present study, the expression of genes related to both M1 and M2 macrophages decreased at 2 weeks, which reflects that both inflammatory as well as anti-inflammatory responses were inhibited after ECM hydrogel treatment. Nevertheless, according to positive staining for CD206, ECM hydrogel treatment led to spatial differences of macrophage distribution within the lesion, where M2 macrophages were mostly accumulated within the hydrogel, and M1 macrophages were in the surrounding tissue.

The ability of ECM hydrogels to promote *in vitro* cell growth and proliferation was examined using hWJ-MSCs. The hWJ-MSCs currently represent a promising cell type in regenerative medicine and are already being evaluated in various clinical trials, including SCI.<sup>30</sup> The *in vitro* 2D cell culture demonstrated that both types of ECM hydrogels promoted adhesion and proliferation of hWJ-MSCs.

However, when seeded in 3D culture, hWJ-MSCs triggered rapid gel contraction. This well-known phenomenon is characteristic for collagen gels seeded with fibroblasts that generate tension on the matrix during both extension and retraction of pseudopodia.<sup>31</sup> A similar effect has also been described for ECM hydrogels derived from porcine dermis as well as urinary bladder seeded with fibroblasts.<sup>21</sup>

When used as a cell vehicle *in vivo* to fill the lesion cavity, the rapid gel contraction may then result in inhomogeneous scaffold distribution within the lesion. Moreover, when injected into the lesion, the ECM hydrogels may further contract over time as they are populated with various endogenous cells, such as fibroblasts or epithelial cells. Of note, a similar collagen concentration ( $\sim 700 \mu\text{g}$  collagen/mg dry weight) as well as gel contraction rate was found for both SC-ECM and UB-ECM, while sulfated glycosaminoglycan concentration was higher for UB-ECM ( $\sim 4 \mu\text{g}/\text{mg}$  dry weight) than for SC-ECM ( $\sim 1 \mu\text{g}/\text{mg}$  dry weight).<sup>19</sup>

To evaluate ECM hydrogels for cell delivery, we prepared the cell seeded gels before their implantation into the lesions, which partly avoids the massive scaffold contraction within the lesion cavity. In spite of this, the inflammatory milieu of the acute lesion together with the massive infiltration of macrophages did not support cell survival. Furthermore, only

few cells were detected within the lesion 4 weeks after the implantation. On the other hand, due to the limited volume of the implanted scaffold, the total number of implanted cells within the hydrogel was relatively small ( $\sim 15,000$ ). By increasing the number of implanted cells a higher *in vivo* cell survival rate could be achieved, however, an increased degree of gel contraction may result in the enhanced formation of dense cell bulks within the lesion cavity.

Notably, immunosuppression significantly promoted axonal ingrowth, decreased expression of *Gfap*, *Fgf2*, *Casp3*, *Ccl3*, and *Cd86*, and increased expression of *Vegfa*, which confirmed the neurotrophic effect of immunosuppressive agents.<sup>32</sup>

In comparison with the synthetic nondegradable materials based on poly(2-hydroxyethyl methacrylate), which we previously developed and evaluated *in vivo*,<sup>33,34</sup> ECM hydrogels are undoubtedly advantageous, in terms of their injectability, degradability, as well as their biological activity, which is able to modulate the immune response and stimulate vascularization and axonal ingrowth. At the same time, there are also two impediments that hinder the use of ECM hydrogels in their current form as optimal materials for CNS repair: (1) progressive hydrogel contraction in combination with fibroblast-like cells, such as MSCs and (2) rapid *in vivo* hydrogel degradation, which was too fast to be followed by full tissue reconstruction in the lesion cavity.

When applied immediately into the SCI, the neuroregenerative potential of ECM hydrogels might be burdened by the hostility of the acute SCI lesion due to the acute inflammatory response, which in turn may significantly influence the speed of hydrogel degradation and thus the character of tissue replacement.

Remarkably, acute lateral hemisection, which we used to evaluate the feasibility of ECM hydrogels in CNS repair, is the least invasive and devastating SCI model. On the other hand, hemisection is a case of partial lesion with a high rate of spontaneous recovery and a high risk of inconsistencies in the injuries from one animal to the next, which might lead to misinterpretation of the behavioral evaluation.<sup>35,36</sup>

Further investigation using a subacute or chronic compression SCI model together with systematic functional evaluation is, therefore, the next step in establishing the link between *in vivo* biological properties of the ECM hydrogel in acute and chronic SCI.

To slow degradation, chemical crosslinking of the ECM hydrogel may offer longer scaffold persistence within the lesion and thus provide more time to complete the tissue remodeling. However, recent studies suggest that degradation of the ECM scaffold is an essential component of a rapid constructive remodeling response. Moreover, crosslinking of the ECM may reduce or eliminate the amount of cellular infiltration into the implant or even cause a foreign body reaction.<sup>15</sup> Alternatively, hydrogels composed of concentrations  $>8 \text{ mg/mL}$  as used in the present study may slow the degradation process.

## Conclusions

This study evaluated the *in vivo* function of two types of ECM hydrogels derived from decellularized porcine spinal cord and urinary bladder tissues as scaffolds for SCI repair. Both ECM hydrogels showed significant immunomodulatory

and neuroregenerative effects and provided the substrate for tissue bridging after SCI. Further studies concerning the optimization of hydrogel degradation time as well as the analysis of the ability to restore neuronal function after SCI in combination with a suitable cell type are needed to consider the potential of ECM hydrogels for clinical translation.

### Acknowledgments

The financial support of the GACR 15-01396S, MEYS 7F14057 from the Czech-Norwegian research program CZ09, GAUK 1846214, GACR 14-10504P and BIOCEV–Biotechnology and Biomedicine Center of the Academy of Sciences and Charles University (CZ.1.05/1.1.00/02.0109), from the European Regional Development Fund is gratefully acknowledged. The authors would like to thank Lucie Svobodová for tissue processing and histology.

### Disclosure Statement

No competing financial interests exist.

### References

- Young, W. Spinal cord regeneration. *Cell Transplant* **23**, 573, 2014.
- Pego, A.P., Kubinova, S., Cizkova, D., Vanicky, I., Mar, F.M., Sousa, M.M., and Sykova, E. Regenerative medicine for the treatment of spinal cord injury: more than just promises? *J Cell Mol Med* **16**, 2564, 2012.
- Kumar, P., Choonara, Y.E., Modi, G., Naidoo, D., and Pillay, V. Multifunctional therapeutic delivery strategies for effective neuro-regeneration following traumatic spinal cord injury. *Curr Pharm Des* **21**, 1517, 2015.
- Kubinova, S., and Sykova, E. Biomaterials combined with cell therapy for treatment of spinal cord injury. *Regen Med* **7**, 207, 2012.
- Assuncao-Silva, R.C., Gomes, E.D., Sousa, N., Silva, N.A., and Salgado, A.J. Hydrogels and cell based therapies in spinal cord injury regeneration. *Stem Cells Int* **2015**, 948040, 2015.
- Macaya, D., and Spector, M. Injectable hydrogel materials for spinal cord regeneration: a review. *Biomed Mater* **7**, 012001, 2012.
- Siebert, J.R., Eade, A.M., and Osterhout, D.J. Biomaterial approaches to enhancing neurorestoration after spinal cord injury: strategies for overcoming inherent biological obstacles. *Biomed Res Int* **2015**, 752572, 2015.
- Ricks, C.B., Shin, S.S., Becker, C., and Grandhi, R. Extracellular matrices, artificial neural scaffolds and the promise of neural regeneration. *Neural Regen Res* **9**, 1573, 2014.
- Crapo, P.M., Medberry, C.J., Reing, J.E., Tottey, S., van der Merwe, Y., Jones, K.E., and Badylak, S.F. Biologic scaffolds composed of central nervous system extracellular matrix. *Biomaterials* **33**, 3539, 2012.
- Badylak, S.F. Decellularized allogeneic and xenogeneic tissue as a bioscaffold for regenerative medicine: factors that influence the host response. *Ann Biomed Eng* **42**, 1517, 2014.
- Badylak, S.F., Freytes, D.O., and Gilbert, T.W. Extracellular matrix as a biological scaffold material: structure and function. *Acta Biomater* **5**, 1, 2009.
- Nakayama, K.H., Lee, C.C., Batchelder, C.A., and Tarantal, A.F. Tissue specificity of decellularized rhesus monkey kidney and lung scaffolds. *PLoS One* **8**, e64134, 2013.
- Adam Young, D., Bajaj, V., and Christman, K.L. Award winner for outstanding research in the PhD category, 2014 Society for Biomaterials annual meeting and exposition, Denver, Colorado, April 16–19, 2014: decellularized adipose matrix hydrogels stimulate in vivo neovascularization and adipose formation. *J Biomed Mater Res A* **102**, 1641, 2014.
- Reing, J.E., Zhang, L., Myers-Irvin, J., Cordero, K.E., Freytes, D.O., Heber-Katz, E., Bedelbaeva, K., McIntosh, D., Dewilde, A., Brauhnut, S.J., and Badylak, S.F. Degradation products of extracellular matrix affect cell migration and proliferation. *Tissue Eng Part A* **15**, 605, 2009.
- Badylak, S.F., and Gilbert, T.W. Immune response to biologic scaffold materials. *Semin Immunol* **20**, 109, 2008.
- Zhang, X.Y., Xue, H., Liu, J.M., and Chen, D. Chemically extracted acellular muscle: a new potential scaffold for spinal cord injury repair. *J Biomed Mater Res* **100**, 578, 2011.
- Li, C., Zhang, X., Cao, R., Yu, B., Liang, H., Zhou, M., Li, D., Wang, Y., and Liu, E. Allografts of the acellular sciatic nerve and brain-derived neurotrophic factor repair spinal cord injury in adult rats. *PLoS One* **7**, e42813, 2012.
- Liu, J., Chen, J., Liu, B., Yang, C., Xie, D., Zheng, X., Xu, S., Chen, T., Wang, L., Zhang, Z., Bai, X., and Jin, D. Acellular spinal cord scaffold seeded with mesenchymal stem cells promotes long-distance axon regeneration and functional recovery in spinal cord injured rats. *J Neurosci* **325**, 127, 2012.
- Medberry, C.J., Crapo, P.M., Siu, B.F., Carruthers, C.A., Wolf, M.T., Nagarkar, S.P., Agrawal, V., Jones, K.E., Kelly, J., Johnson, S.A., Velankar, S.S., Watkins, S.C., MODO, M., and Badylak, S.F. Hydrogels derived from central nervous system extracellular matrix. *Biomaterials* **34**, 1033, 2013.
- DeQuach, J.A., Yuan, S.H., Goldstein, L.S., and Christman, K.L. Decellularized porcine brain matrix for cell culture and tissue engineering scaffolds. *Tissue Eng Part A* **17**, 2583, 2011.
- Wolf, M.T., Daly, K.A., Brennan-Pierce, E.P., Johnson, S.A., Carruthers, C.A., D'Amore, A., Nagarkar, S.P., Velankar, S.S., and Badylak, S.F. A hydrogel derived from decellularized dermal extracellular matrix. *Biomaterials* **33**, 7028, 2012.
- Torres-Espin, A., Santos, D., Gonzalez-Perez, F., del Valle, J., and Navarro, X. Neurite-J: an image-J plug-in for axonal growth analysis in organotypic cultures. *J Neurosci Methods* **236**, 26, 2014.
- Basso, D.M., Beattie, M.S., and Bresnahan, J.C. A sensitive and reliable locomotor rating scale for open field testing in rats. *J Neurotrauma* **12**, 1, 1995.
- Crapo, P.M., Tottey, S., Slivka, P.F., and Badylak, S.F. Effects of biologic scaffolds on human stem cells and implications for CNS tissue engineering. *Tissue Eng Part A* **20**, 313, 2014.
- Tottey, S., Corselli, M., Jeffries, E.M., Londono, R., Peault, B., and Badylak, S.F. Extracellular matrix degradation products and low-oxygen conditions enhance the regenerative potential of perivascular stem cells. *Tissue Eng Part A* **17**, 37, 2011.
- Valentin, J.E., Stewart-Akers, A.M., Gilbert, T.W., and Badylak, S.F. Macrophage participation in the degradation and remodeling of extracellular matrix scaffolds. *Tissue Eng Part A* **15**, 1687, 2009.
- Brown, B.N., Ratner, B.D., Goodman, S.B., Amar, S., and Badylak, S.F. Macrophage polarization: an opportunity for improved outcomes in biomaterials and regenerative medicine. *Biomaterials* **33**, 3792, 2012.



28. Sicari, B.M., Dziki, J.L., Siu, B.F., Medberry, C.J., Dearth, C.L., and Badylak, S.F. The promotion of a constructive macrophage phenotype by solubilized extracellular matrix. *Biomaterials* **35**, 8605, 2014.
29. Slivka, P.F., Dearth, C.L., Keane, T.J., Meng, F.W., Medberry, C.J., Riggio, R.T., Reing, J.E., and Badylak, S.F. Fractionation of an ECM hydrogel into structural and soluble components reveals distinctive roles in regulating macrophage behavior. *Biomater Sci* **2**, 1521, 2014.
30. Cheng, H., Liu, X., Hua, R., Dai, G., Wang, X., Gao, J., and An, Y. Clinical observation of umbilical cord mesenchymal stem cell transplantation in treatment for sequelae of thoracolumbar spinal cord injury. *J Transl Med* **12**, 253, 2014.
31. Brown, R.A. In the beginning there were soft collagen-cell gels: towards better 3D connective tissue models? *Exp Cell Res* **319**, 2460, 2013.
32. Sosa, I., Reyes, O., and Kuffler, D.P. Immunosuppressants: neuroprotection and promoting neurological recovery following peripheral nerve and spinal cord lesions. *Exp Neurol* **195**, 7, 2005.
33. Kubinova, S., Horak, D., Hejcl, A., Plichta, Z., Kotek, J., Proks, V., Forostyak, S., and Sykova, E. SIKVAV-modified highly superporous PHEMA scaffolds with oriented pores for spinal cord injury repair. *J Tissue Eng Regen Med* **9**, 1298, 2013.
34. Kubinova, S., Horak, D., Hejcl, A., Plichta, Z., Kotek, J., and Sykova, E. Highly superporous cholesterol-modified poly(2-hydroxyethyl methacrylate) scaffolds for spinal cord injury repair. *J Biomed Mater Res* **99**, 618, 2011.
35. Cloud, B.A., Ball, B.G., Chen, B.K., Knight, A.M., Hakim, J.S., Ortiz, A.M., and Windebank, A.J. Hemisection spinal cord injury in rat: the value of intraoperative somatosensory evoked potential monitoring. *J Neurosci Methods* **211**, 179, 2012.
36. Fouad, K., Hurd, C., and Magnuson, D.S. Functional testing in animal models of spinal cord injury: not as straight forward as one would think. *Front Integr Neurosci* **7**, 85, 2013.

Address correspondence to:

*Sarka Kubinova, PhD*

*Institute of Experimental Medicine AS CR, v.v.i.*

*Vítěňská 1083*

*142 20 Prague 4-Krč*

*Czech Republic*


*E-mail: sarka.k@biomed.cas.cz*

*Received: September 8, 2015*

*Accepted: December 24, 2015*

*Online Publication Date: January 28, 2016*

# Injectable hydroxyphenyl derivative of hyaluronic acid hydrogel modified with RGD as scaffold for spinal cord injury repair

Kristyna Zaviskova <sup>1,2</sup> Dmitry Tukmachev,<sup>1,2</sup> Jana Dubisova,<sup>1,2</sup> Irena Vackova,<sup>1</sup> Ales Hejcl,<sup>1</sup> Julie Bystronova,<sup>3</sup> Martin Pravda,<sup>3</sup> Ivana Scigalkova,<sup>3</sup> Romana Sulakova,<sup>3</sup> Vladimir Velebny,<sup>3</sup> Lucie Wolfova,<sup>1,3</sup> Sarka Kubinova<sup>1</sup>

<sup>1</sup>Department of Biomaterials and Biophysical Methods, Institute of Experimental Medicine of the Czech Academy of Sciences, Prague, Czech Republic

<sup>2</sup>2nd Medical Faculty, Charles University, Prague, Czech Republic

<sup>3</sup>Department of Tissue Engineering, Contipro a.s., Dolni Dobrouc, Czech Republic

Received 14 September 2017; revised 9 November 2017; accepted 15 December 2017

Published online 23 January 2018 in Wiley Online Library (wileyonlinelibrary.com). DOI: 10.1002/jbm.a.36311

**Abstract:** Hydrogel scaffolds which bridge the lesion, together with stem cell therapy represent a promising approach for spinal cord injury (SCI) repair. In this study, a hydroxyphenyl derivative of hyaluronic acid (HA-PH) was modified with the integrin-binding peptide arginine-glycine-aspartic acid (RGD), and enzymatically crosslinked to obtain a soft injectable hydrogel. Moreover, addition of fibrinogen was used to enhance proliferation of human Wharton's jelly-derived mesenchymal stem cells (hWJ-MSCs) on HA-PH-RGD hydrogel. The neuroregenerative potential of HA-PH-RGD hydrogel was evaluated *in vivo* in acute and subacute models of SCI. Both HA-PH-RGD hydrogel injection and implantation into the acute spinal cord hemisection cavity resulted in the same axonal and blood vessel density in the lesion area after 2 and 8 weeks. HA-PH-RGD hydrogel alone or combined with fibrinogen (HA-PH-RGD/F) and seeded with hWJ-MSCs was

then injected into subacute SCI and evaluated after 8 weeks using behavioural, histological and gene expression analysis. A subacute injection of both HA-PH-RGD and HA-PH-RGD/F hydrogels similarly promoted axonal ingrowth into the lesion and this effect was further enhanced when the HA-PH-RGD/F was combined with hWJ-MSCs. On the other hand, no effect was found on locomotor recovery or the blood vessel ingrowth and density of glial scar around the lesion. In conclusion, we have developed and characterized injectable HA-PH-RGD based hydrogel, which represents a suitable material for further combinatorial therapies in neural tissue engineering. © 2018 Wiley Periodicals, Inc. *J Biomed Mater Res Part A*: 106A: 1129–1140, 2018.

**Key Words:** hyaluronic acid, spinal cord injury, scaffold, mesenchymal stem cells, regenerative medicine

---

**How to cite this article:** Zaviskova K, Tukmachev D, Dubisova J, Vackova I, Hejcl A, Bystronova J, Pravda M, Scigalkova I, Sulakova R, Velebny V, Wolfova L, Kubinova S. 2018. Injectable hydroxyphenyl derivative of hyaluronic acid hydrogel modified with RGD as scaffold for spinal cord injury repair. *J Biomed Mater Res Part A* 2018;106A:1129–1140.

---

## INTRODUCTION

Spinal cord injury (SCI) often results in permanent neurological defects as a consequence of the inability of axons to regenerate across the lesion. Despite progress, which has been made in promoting SCI repair in experimental models, there is still no effective therapy available for the patients.<sup>1</sup> A promising treatment approach is represented by the use of supportive and stimulatory biomaterial, which can serve as a bridge for axonal regrowth and endogenous cell migration as well as a carrier for cell transplantation.<sup>2–4</sup> A convenient way for the development of materials suitable for tissue regeneration is to mimic the structure and components of extracellular matrix (ECM) of the target tissue. Moreover, physical or chemical cues can be incorporated into the biomaterial to influence specific cell behavior.<sup>5</sup>

Natural hydrogels are extensively developed materials for SCI repair. They can be based on an ECM component, such as collagen,<sup>6</sup> fibronectin,<sup>7</sup> hyaluronic acid (HA),<sup>8–12</sup> or other naturally occurring polysaccharides or their combination.<sup>13,14</sup> In addition, hydrogels that retain the composition of tissue-specific ECM can be prepared by the decellularization of various tissues.<sup>15,16</sup>

HA is an important structural component of ECM and it is widely used due to its biocompatibility, biodegradability, and non-immunogenicity as biomaterial in clinical settings. Among its structural functions, HA also acts as a signaling molecule via specific HA receptors to actively modulate tissue regeneration.<sup>17,18</sup>

In neural tissue engineering, HA-based materials have been studied *in vitro* as substrates for neural stem cell cultures,<sup>19</sup> as well as *in vivo*, alone or as carriers for cell delivery

Additional Supporting Information may be found in the online version of this article.

**Correspondence to:** S. Kubinova; e-mail: sarka.k@biomed.cas.cz

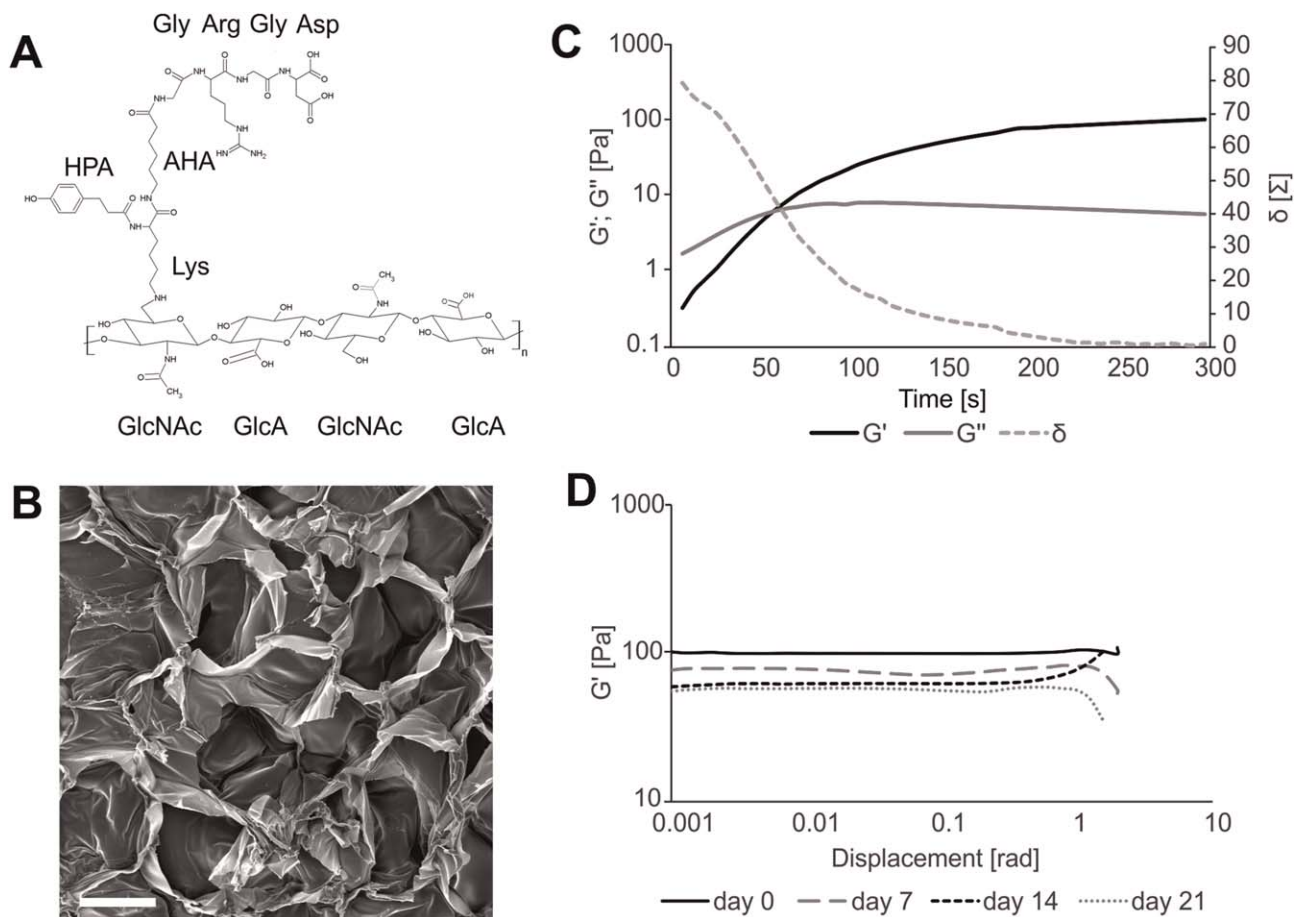


**FIGURE 1.** A: Scheme of hydroxyphenyl derivative of HA with attached RGD peptide sequence. B: SEM image of the HA-PH-RGD hydrogel structure. C: Gelation kinetic of the HA-PH-RGD crosslinked with 0.04 U/mL of HRP and 0.165 mM H<sub>2</sub>O<sub>2</sub>. D: The influence of HA-PH-RGD swelling on the elastic modulus. Scale bar: 100 μm.

to improve cell retention and integration.<sup>10,20,21</sup> Injectable HA-based hydrogels were also developed for localized intrathecal delivery of bioactive molecules into the SCI.<sup>22,23</sup>

Native HA does not form a gel nor support cell adhesion. Therefore, it is necessary to chemically modify the functional groups of HA and tune its chemical, physical or biological properties according to the special demands of the particular application. Concerning the gel formation, various HA derivatives can be stabilized by crosslinking, such as dihydrazide crosslink of HA polyaldehyde, thiol-en click crosslinking of norbornene-HA derivative, initiated by UV light, copper catalyzed 1,3-dipolar cycloaddition reaction, or UV initiated crosslinking of methacrylated HA.<sup>18</sup> To enable cell adhesion, functionalization of HA-based materials has been achieved using a variety of techniques, such as the incorporation of poly-L-lysine,<sup>24</sup> laminin,<sup>25</sup> fibronectin,<sup>26</sup> fibrinogen,<sup>27</sup> blending with methylcellulose,<sup>14</sup> or modifying HA with integrin ligands derived from ECM, such as arginine-glycine-aspartic acid (RGD) sequence.<sup>28</sup>

One of such promising HA-based materials capable to form covalently cross-linked hydrogel with the required mechanical properties, is the hydroxyphenyl derivative of HA (HA-PH).<sup>29,30</sup> The cross-linking reaction of this HA-PH

derivative can be triggered by enzyme horseradish peroxidase (HRP) and hydrogen peroxide (H<sub>2</sub>O<sub>2</sub>) under physiological conditions, without a negative effect on encapsulated cells during cross-linking reaction and gel forming.<sup>31</sup> Previously, we demonstrated the chondrogenic potential of HA-PH derivative based hydrogel *in vitro* as well as *in vivo* in cartilage defects.<sup>31,32</sup>

In this study, we have used the HA-PH derivative bearing the newly developed 3-(4-hydroxyphenyl) propionic acid (PH)—L-lysine—aminohexanoic acid—L-glycine—L-arginine—L-glycine—L-aspartic acid (HA-PH-RGD) sequence [Fig. 1(A)], which allows the attachment of PH moiety and RGD cell adhesive motive to polymer backbone in one synthetic step. The mechanical properties of HA-PH-RGD hydrogel were then optimized to be suitable for the soft neural tissue with an optimal time of gelation, to enable a hydrogel injection into the site of the defect.

The biocompatibility of this material was evaluated *in vitro* in cell culture as well as *in vivo* in an experimental model of SCI in rats. First, we compared two ways of hydrogel delivery into the lesion cavity after acute spinal cord hemisection, where we did not observe any remarkable differences in tissue repair, when the hydrogel was formed



*ex vivo* and then implanted or injected into the lesion and crosslinked *in situ*. Then, we evaluated the neuroregenerative potential of HA-PH-RGD hydrogel alone or in combination with human Wharton's jelly-derived mesenchymal stem cells (hWJ-MSCs) after its injection into the subacute spinal cord hemisection. To further promote hWJ-MSCs adhesion, HA-PH-RGD was combined with fibrinogen (HA-PH-RGD/F), which contains integrin binding sites, such as RGD, and has been widely used as a promising additive to enhance cell survival, growth, and proliferation.<sup>33,34</sup> Moreover, fibrinogen is abundant in a blood plasma and can be easily extracted from the donors for the autologous use. We used hWJ-MSCs, as these cells represent an easily accessible source, with high potential for clinical applications. Moreover, a therapeutic benefit of hWJ-MSCs in SCI alone as well as in combination with a biomaterial has been shown previously in several experimental and clinical studies.<sup>35–37</sup>

## MATERIALS AND METHODS

### Hyaluronan RGD modification

HPA-K-AHA-GRGD oligopeptide sequence was synthesized by solid phase synthesis using Fmoc-SPPS protocol.<sup>38</sup> Briefly, N-termini of the RGD adhesive peptide was modified by subsequent attachment of lysine, 6-aminohexanoic acid (Ahx) and glycine. Furthermore,  $\alpha$ -amino group of lysine was acylated by 3-(4-hydroxyphenyl) propionic acid (HPA). This peptide sequence (HPA-K-Ahx-GRGD) was purified and characterized by <sup>1</sup>H NMR and Mass Spectroscopy.

The RGD sequence was further conjugated with hyaluronan polyaldehyde (HA-CHO; DS = 10%; Mw = 400 kDa; purchased from Contipro a. s.) via reductive amination.<sup>39,40</sup> HA-CHO (1.00 g, 2.50 mmol dimers of HA) was dissolved in 100 mL of demineralized water. Then, HPA-K-Ahx-GRGD (0.25 mmol) was added to the reaction mixture and the mixture was further stirred for 1 h at room temperature. Subsequently, a solution of picoline-borane complex (PIC-BOR; 0.625 mmol) in 10 mL of 50% propan-2-ol was added to the mixture. The reaction mixture was stirred for another 12 h at room temperature. The final product was obtained after precipitation by propan-2-ol. The degree of substitution (DS) of HPA-K-Ahx-GRGD of such modified HA-PH-RGD derivative was 2.5%.

### Chemical characterization of HA-PHA-RGD derivative

<sup>1</sup>H NMR and HSQC spectroscopy was carried out on a Bruker Advance III 500 MHz instrument operating at a proton frequency of 500.25 MHz, and elaborated by Bruker 2.1 Topspin software. Samples were dissolved in a mixture of D<sub>2</sub>O and NaOD (0.75 mL) and transferred into 5 mm NMR quartz tubes. <sup>1</sup>H NMR was also used to determinate the DSs of the prepared HA-PHA-RGD derivative. The DS was calculated from the ratio of the signal intensity of aromatic protons of the HPA (doublets 6.47 and 6.89 ppm) with respect to the signal of hydrogens of the *N*-acetyl group (singlet 2.01 ppm) (Supporting Information Figs. S1–S3).

LCMS-2020 Single Quadrupole Liquid Chromatograph Mass Spectrometer (LC/MS) with the column C18 (250 × 10.00 mm, Jupiter 4 u Proteo 90 A) was used for RGD

sequence isolation. Gradient elution was used for peptide purification (phase A 0.1% formic acid; phase B – acetonitrile). The gradient was set as follows: 0–8 min 30% B, 8–15 min 30–50% B, 15–16 min 50–95% B, 16–20 min 95% B, 20–22 min 95–30% B, 22–32 min 30% B. Chromatographs and the MS detector record are shown in Supporting Information Figure 4.

Size exclusion chromatography combined with a multi-angle laser light scattering detector was used to determine the molecular weight of the HA-PH-RGD. A refractive index increment (dn/dc) of 0.155 mL g<sup>-1</sup> was used to calculate the molecular weight and polydispersity (Mw/Mn).

### Hydrogel preparation and crosslinking

The HA-PH-RGD (20 mg/mL) was dissolved in 0.9% NaCl and stirred for a period of at least 6 h at room temperature to gain homogenous solutions. The crosslinking of HA-PH-RGD solution and hydrogel formation was initiated by the addition of 0.04 U/mL HPR (Sigma) and 0.165 mM H<sub>2</sub>O<sub>2</sub> (Merck, Germany) to the HA-PH-RGD solution. Cylindric teflon moulds with a volume of 0.4 mL were used for gel forming and maturing.

### Hydrogel characterization

Rheological measurements were performed using TA Instruments AR-G2 rheometer and Rheology Advantage Data Analysis software. The device settings were as follows: parallel plate (40 mm), gap 400  $\mu$ m, dose volume 500  $\mu$ L and temperature 37°C. For evaluation of the viscoelastic properties of material, that is, storage modulus  $G'$ , loss modulus  $G''$  and shear loss angle  $\delta$  ( $\tan \delta = G''/G'$ ), strain sweep mode was used (frequency 1 Hz and displacement from 0.001 to 2 rad). Crosshatched geometry was used to avoid slippage of the samples. The time of gelation was evaluated from the intersection of the  $G'$  and  $G''$  moduli using time sweep step mode (frequency 1 Hz and displacement 0.001 rad).

Hydrogels used for the stability study were prepared using the teflon moulds. The samples with a volume of 0.4 mL were immersed in phosphate-buffered saline (PBS) for 7, 14 and 21 days. Then, the swollen hydrogel disks were gently blotted dry and measured on a rheometer in strain sweep mode. The increasing deformation—displacement set from 0.001 to 2 rad was performed at 1 Hz, in order to achieve elastic modulus of the material. Crosshatched geometry was used to avoid slippage of the samples. The swelling ratio of the samples could not be properly evaluated. Due to the swollen hydrogel consistency, it was not possible to completely and equivalently blot up the swollen samples, which would have affected the obtained values. Moreover, this procedure would cause destruction of the sample structure. Scanning electron microscope (SEM) was used to show the hydrogel structure (Supporting Information).

### Cell isolation and culture

Human umbilical cord samples were collected from healthy full-term neonates after spontaneous delivery at the Department of Obstetrics and Gynecology, University Hospital of

Pilsen, Czech Republic. The samples were obtained upon written informed consent from mothers using the guidelines approved by the Institutional Ethics Committee. The proximal part of the umbilical cord close to the placenta (10–15 cm), was cut and immersed into the sterile PBS (IKEM, Czech Republic) with antibiotic-antimycotic solution (Sigma). Samples were transferred to the laboratory on ice to be processed within 24 h from partum. After washing in PBS and betadine (EGIS Pharmaceuticals PLC, Hungary) and the removal of blood vessels and amniotic membrane, the remaining tissue (Wharton's jelly) was chopped into small pieces (1–2 mm<sup>3</sup>), and the pieces were transferred to culture dishes (Nunc; Schoeller, Czech Republic) containing the alpha-Minimum Essential Medium (East Port, Czech Republic) supplemented with 5% platelet lysate (IKEM, Czech Republic) and gentamicin 10 mg/mL (Sandoz, Czech Republic), and cultivated at 37°C in a humidified atmosphere containing 5% CO<sub>2</sub>. On day 10, the explants were removed from the culture dishes, and the remaining adherent cells were cultured until 90% confluence and passaged using 0.05% Trypsin/EDTA (Life Technologies, USA). After passaging, the cells were seeded into culture flasks (Nunc) at a density of  $5 \times 10^3$  cells/cm<sup>2</sup>. The medium was changed twice a week. hWJ-MSCs from passage three were used for both *in vitro* and *in vivo* studies. The mesenchymal stem cell phenotype was characterized using fluorescence-activated cell sorting (FACS) analysis of surface marker profiles (FACSARIA; Becton Dickinson, USA) and adipogenic, osteogenic and chondrogenic differentiation (Supporting Information).

### Cell proliferation

To enhance cell proliferation, the initial HA-PH or HA-PH-RGD solutions were mixed with fibrinogen (1 mg/mL, Sigma) in 0.9% NaCl and formed into hydrogel film to cover the 24-well culture plate. The culture wells were seeded by  $1.5 \times 10^5$  of hWJ-MSCs per well. After 3, 7, or 12 days of cultivation, the cell proliferation was evaluated using CellTiter-Glo reagent.

Proliferation of hWJ-MSCs in the presence of HA-PH-RGD hydrogel, combined with fibrinogen (HA-PH-RGD/F) was further determined after 3 h, 1, and 3 days in culture using WST-1 reagent (Roche, Germany). hWJ-MSCs were mixed with HA-PH-RGD/F hydrogel to form 3D culture (20 µL,  $8 \times 10^4$  cells) in 1 mL of medium in a 24-well plate. The same volume of hydrogel without cells served as a background. At the measured time points, WST-1 reagent was added to each well and the plates were incubated for 2 h at 37°C. The absorbance was measured using a Tecan Spectra ELISA plate reader (Tecan Trading) at 450 nm with a reference reading at 620 nm.

The morphology of hWJ-MSCs grown in HA-PH-RGD and HA-PH-RGD/F hydrogel was examined by fluorescent staining for actin filaments. After fixation in 4% paraformaldehyde in 0.1 M PBS for 10 min, the cells were stained with Alexa-Fluor 568 phalloidin (1:400, Molecular Probes, USA), and the nuclei were visualized by using 4,6-diamidino-2-phenylindole (DAPI) fluorescent dye (1:1000, Invitrogen, UK).

### Hydrogel application into the SCI lesion

Male Wistar rats (250–300 g, Velaz, Czech Republic) underwent a hemisection on the right side at the level of the eighth thoracic vertebra (Th8). The surgical procedure was described previously in.<sup>16</sup> Briefly, the animals were induced with pentobarbital anesthesia (60 mg/kg), then the skin above the Th8 was cut and muscles were detached from the spine. The laminectomy at Th8 was performed and dura was incised with micro-scissors. The right half of one spinal cord segment (2-mm long) was dissected to generate a hemisection cavity.

In the animals with acute application of hydrogel ( $n = 3$ , in each time point and group), the cavity was filled with hydrogel immediately after the hemisection was performed. Two methods of hydrogel application were used. First, HA-PH-RGD solution (20 mg/mL) was mixed with crosslinking components to form a gel in the teflon mold as described above. The adjusted hydrogel volume was then implanted into the lesion to fill the hemisection cavity. In the second approach, approximately 5 µL of HA-PH-RGD hydrogel solution mixed with crosslinking agents was immediately injected by Omnican Insulin syringe for U-100 Insulin (B.Braun, Germany) into the lesion cavity, where the complete *in situ* gelation occurred. The control lesion was filled with saline.

Animals with a subacute lesion underwent hemisection one week before hydrogel injection. The liquid pre-gel solution of HA-PH-RGD hydrogel ( $n = 6$ ), HA-PH-RGD/F ( $n = 6$ ) and HA-PH-RGD/F combined with hWJ-MSCs (3 million/0.5 mL, approximately  $3 \times 10^4$  transplanted cells in 5 µL of the hydrogel) ( $n = 7$ ), was mixed with crosslinking agents and immediately injected into the hemisection cavity by Omnican Insulin syringe for U-100 Insulin (B.Braun, Germany), to form gel *in situ*. In the control SCI group ( $n = 8$ ), the hemisection defect was filled with saline. From 5 days after the hemisection induction, all animal groups with a subacute hydrogel injection and controls received a daily injection of the immunosuppressant cyclosporinA (10 mg/kg, i.p.) (Sandimmune; Novartis, Switzerland), azathioprine (2 mg/kg, p.o.) (Imuran; Aspen Europe GmbH, Germany) and methylprednisolone (2 mg/kg, i.m.) (Solu-Medrol; Pfizer Manufacturing, Belgium), to prevent rejection of the transplanted cells.<sup>16</sup> All animals were housed two rats per cage with food and water ad libitum. All experiments were performed in accordance with the European Communities Council Directive of 24 November 1986 (86/609/EEC), regarding the use of animals in research and were approved by the Ethics Committee of the Institute of Experimental Medicine, Academy of Sciences Czech Republic, Prague, Czech Republic.

### Tissue processing and histology

Two and eight weeks after the acute hydrogel application, and 8 weeks after subacute hydrogel injection, the animals were deeply anesthetized with an intraperitoneal injection of overdose chloral hydrate (Sigma) and intracardially perfused with PBS, followed by 4% paraformaldehyde in 0.1 M PBS. The spinal cord was left in the bone for 1 week in 4%

paraformaldehyde in 0.1 M PBS. A 3 cm long segment of the spinal cord containing the lesioned site was dissected out, transferred to sucrose and frozen. Then, a series of 40  $\mu\text{m}$  thick longitudinal sections were collected.

Non-specific immunohistological staining was avoided by the application of blocking goat or donkey serum (1:10; G9023 or D9663, Sigma) depending on the secondary antibody host organism. Triton X-100 (0.1% in 0.1 M PBS; Sigma) was used for the permeabilization of cell membranes. Samples were stained with antibodies against neurofilaments 160 kDa (NF-160, 1:200), glial fibrillary acidic protein (GFAP, conjugated with Cy3, 1:800; all from Sigma); growth associated protein 43 (GAP43, 1:100), M2 macrophages (CD206, 1:250; all from Santa Cruz); endothelial cell (RECA-1, 1:500), microglia/macrophages (ED1, 1:150), human mitochondria (MTCO2, 1:250; all from Abcam, UK); and oligodendrocytes (1:200; CE-1, Merck-Millipore, Germany). Donkey anti-mouse IgG AlexaFluor 488, donkey anti-goat IgG AlexaFluor 594, goat anti-mouse IgG Alexa Fluor 488, goat anti-mouse IgG Alexa Fluor 594 (all 1:400; Life Technologies, USA), and goat anti-mouse IgM Cy3 (1:200; Merck-Millipore, Germany) were used as secondary antibodies. The nuclei were visualized by using DAPI fluorescent dye (1:1000; Invitrogen, UK).

Fluorescent micrographs were taken using fluorescence microscope Observer D1 with AxioVision 4.8.2 software (Zeiss, Germany), LEICA DMI6000B (Leica, Germany) with TissueFAXS software (TissueGnostics GmbH, Austria) and a laser scanning confocal microscope LSM 5 DUO (Zeiss, Germany).

For analysis of axonal and blood vessels ingrowth, three images across the lesion (cranial side, central and caudal side) from three longitudinal sections for each animal were taken using a 20 $\times$  objective. The relative area of the axons (NF160 staining) and blood vessels (RECA staining) within the images was analyzed using ImageJ software (NIH, Bethesda, USA). Quantification analysis expressed the percentage of NF160 or RECA positive area from a total lesion area.

To evaluate glial scarring, three mosaic images of GFAP staining for each animal was taken using a 20 $\times$  objective. Integrated density and mean gray value of three areas around the lesion (cranial side, central and caudal side) and background (uninjured part of spinal cord) were measured by ImageJ software. Results were expressed as the corrected total cell fluorescence (CTCF), while  $\text{CTCF} = \text{Integrated Density} - (\text{Area} \times \text{Mean gray value of background})$ .<sup>41</sup>

### Gene expression analysis

Changes in the mRNA expression of genes related to M1 macrophages (*Irf5*, *Cd86*), M2 macrophages (*Mrc1*, *Cd163*), axonal growth (*Gap43*), angiogenesis (*Vegfa*), growth factor (*Fgf2*), apoptosis (*Casp3*), inflammation (*Ccl3*, *Ccl5*), astrogliosis (*Gfap*), and glial scar related chondroitin sulfate proteoglycans (CSPGs) (*Ncan*, *Ptprz1*, *Cspg4*) were determined 8 weeks after subacute injection of HA-PH-RGD hydrogels by quantitative real-time PCR (qPCR), and plotted against the control lesion. RNA was isolated from paraformaldehyde-fixed frozen

tissue sections using the High Pure RNA Paraffin Kit (Roche, Germany) and RNA amounts were quantified using NanoPhotometer P 330 (Implen, Germany). The isolated RNA was reverse transcribed into complementary DNA using the Transcriptor Universal cDNA Master (Roche, Germany) and T100 Thermal Cycler (Bio-Rad, USA). The qPCR reactions were performed using cDNA solution, FastStart Universal Probe Master (Roche, Germany) and TagMan Gene Expression Assays (Thermo Fisher Scientific) (Supplementary Table 1). The qPCR was carried out in a final volume of 10  $\mu\text{L}$  containing 20 ng of extracted RNA. Amplification was performed on the real-time PCR cyclers (StepOnePlus, Life Technologies). All amplifications were run under the same cycling conditions: 2 min at 50°C, 10 min at 95°C, followed by 40 cycles of 15 s at 95°C and 1 min at 60°C. All samples were run in duplicate and a negative control (water) was included in each array; with *Gapdh* as a reference gene. Results were expressed as log<sub>2</sub>-fold changes of  $\Delta\Delta\text{Ct}$  values relative to control spinal cord lesions treated with saline.

### Analysis of locomotor functions

To investigate the effect of the hydrogel treatment on the gait of the rat, locomotor functions were quantitatively evaluated using MotoRater 303030 and TSE Motion 8.5.11 software (TSE-systems, Germany) (Supporting Information).

### Statistical evaluation

Statistical significance of the differences in histological analysis between the groups with acute hydrogel application at two time points was determined using two-way ANOVA. A one-way ANOVA with Holm-Sidak method for all pairwise multiple comparison was used for the comparisons of histological analysis and gene expression between the groups with subacute injection of hydrogels at 8 weeks (SigmaPlot V13; Systat Software Inc., USA). All data in graphs are expressed as mean  $\pm$  SEM.

## RESULTS

### Characterization of HA-PH-RGD hydrogel

In this study, we developed new peptide sequences composed of HPA-K-AHA-GRGD (PH-RGD). The structure of this sequences allows to attach to the polymer backbone both PH moiety and RGD cell-adhesive motive in one synthetic step. The conjugation of this sequence with hyaluronan polyaldehyde was performed via reductive amination. The DS of the prepared conjugate was determined by <sup>1</sup>H NMR as 2.5%, and thus the achieved concentration of the RGD sequence was 1  $\mu\text{mol/mL}$  in hydrogel, containing 20 mg/mL HA-PH-RGD derivative (NMR spectra in Supporting Information Figs. S1–S3).

HA-PH-RGD derivative was crosslinked by the use of HRP and H<sub>2</sub>O<sub>2</sub>, and the gelation rate was evaluated by the rheological measurement. The dosing of the crosslinking agents (HRP, H<sub>2</sub>O<sub>2</sub>) was optimized to 0.04 U/mL HRP and 0.165 mM H<sub>2</sub>O<sub>2</sub>, to obtain a compressive modulus similar to the native neural tissue and gelation time of 61  $\pm$  4 s ( $n = 3$ ), which is appropriate to achieve a safe application of



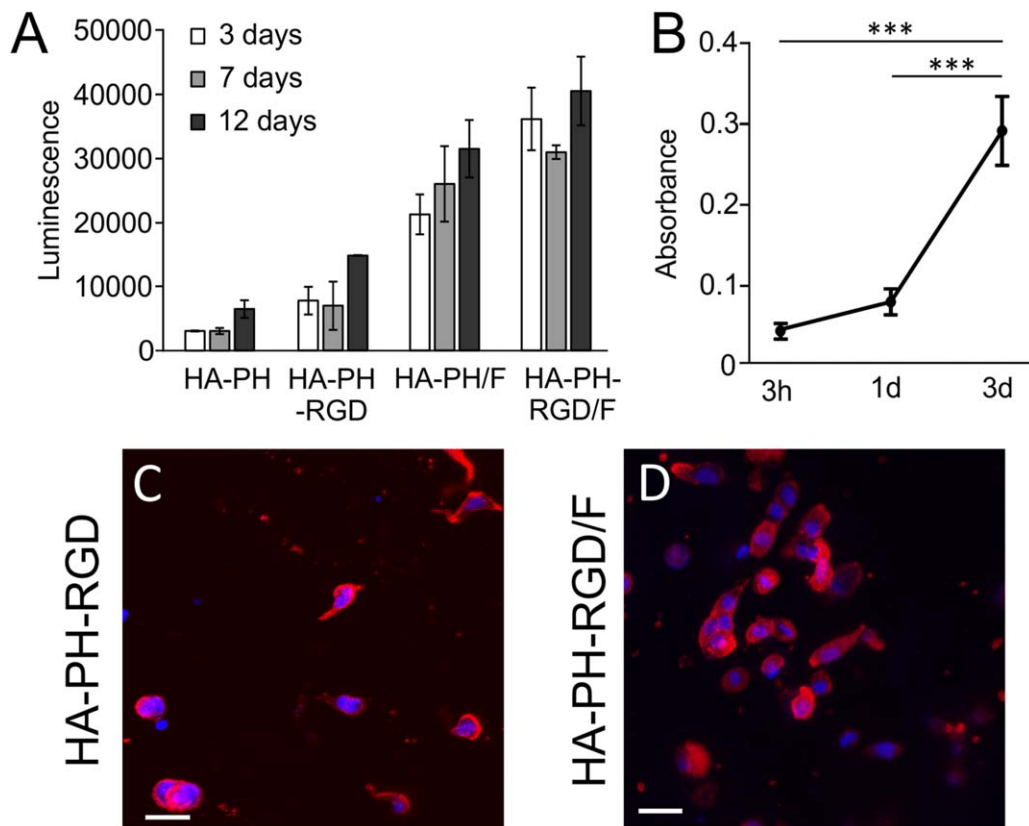


**FIGURE 2.** A: Proliferation of hWJ-MSCs in HA-PH hydrogels on different adhesive substrates (RGD peptide, F-fibrinogen) measured by luminescence of ATP. Statistical differences between the groups are shown in Supporting Information Table S3. B: Proliferation of hWJ-MSCs in 3D culture of HA-PH-RGD/F hydrogel measured by WST-1 assay. \*\*\* $p < 0.001$ , ( $n = 3$ ). C,D: The morphology of hWJ-MSCs in 3D culture in HA-PH-RGD and HA-PH-RGD/F hydrogel after 1 day of cultivation stained for phalloidin (red) and DAPI (blue). Scale bar: 25  $\mu\text{m}$ .

the viscous pre-gel solution into the site of the defect using a syringe [Fig. 1(C)].

The effect of hydrogel swelling on mechanical strength is shown in Figure 1(D). The mechanical strength of the material slightly decreased, which corresponded to the decreasing of  $G'$  modulus of the samples.

#### **In vitro cell culture**

The toxicity of crosslinking agents (HRP and  $\text{H}_2\text{O}_2$ ) was tested by their addition to hWJ-MSC culture, while no cytotoxic effects were observed at concentrations which were used for the hydrogel gelation (Supporting Information Table S2). Proliferation of hWJ-MSCs seeded on HA-PH, and HA-PH-RGD hydrogel, combined with fibrinogen (F) is shown in Figure 2(A). Low cell proliferation was found on the unmodified HA-PH hydrogel, which was further increased on the HA-PH modified with RGD. A remarkable increase in the cell proliferation rate was then achieved when the HA-PH and HA-PH-RGD hydrogels were combined with fibrinogen. Therefore, for cell encapsulation, fibrinogen (1 mg/mL) was added into the HA-PH-RGD hydrogel. The ability of HA-PH-RGD/F to support cell proliferation in 3D culture was further verified by the WST-1 method after 3 h, 1, and 3 days [Fig. 2(B)]. Despite of enhanced cell proliferation, the morphology of hWJ-MSCs after 1 day in 3D culture

was found similar in HA-PH-RGD and HA-PH-RGD/F [Fig. 2(C,D)].

#### **Evaluation of HA-PH-RGD hydrogels in acute SCI lesions**

Two ways of hydrogel application were compared in the acute SCI lesion; implantation of the *in vitro* crosslinked HA-PH-RGD hydrogel and injection of the HA-PH-RGD together with crosslinking agents to form a hydrogel *in situ*. Both implanted and injected HA-PH-RGD hydrogels filled the lesion cavity and were highly populated with endogenous cells. The dense ingrowth of neurofilaments [Fig. 3(A)], as well as blood vessels [Fig. 3(B)] into the hydrogel-treated lesion was observed throughout the whole implant after 2 weeks, and persisted with no considerable changes 8 weeks after application. Quantitative analysis revealed a higher density of neurofilaments [Fig. 3(C)] and blood vessels [Fig. 3(D)] in both hydrogel groups compared with the control lesion, while no differences were found between the lesion treated by hydrogel implantation or injection at any time point. Figure 3(E,G) then depicted migrating astrocytes (staining for GFAP) and Figure 3(H) newly formatted axonal growth cones (staining for GAP43) invading into the hydrogel treated lesion. The results show that the hydrogel injection into the lesion and its subsequent crosslinking *in situ* is not harmful to the surrounding tissue and represents a

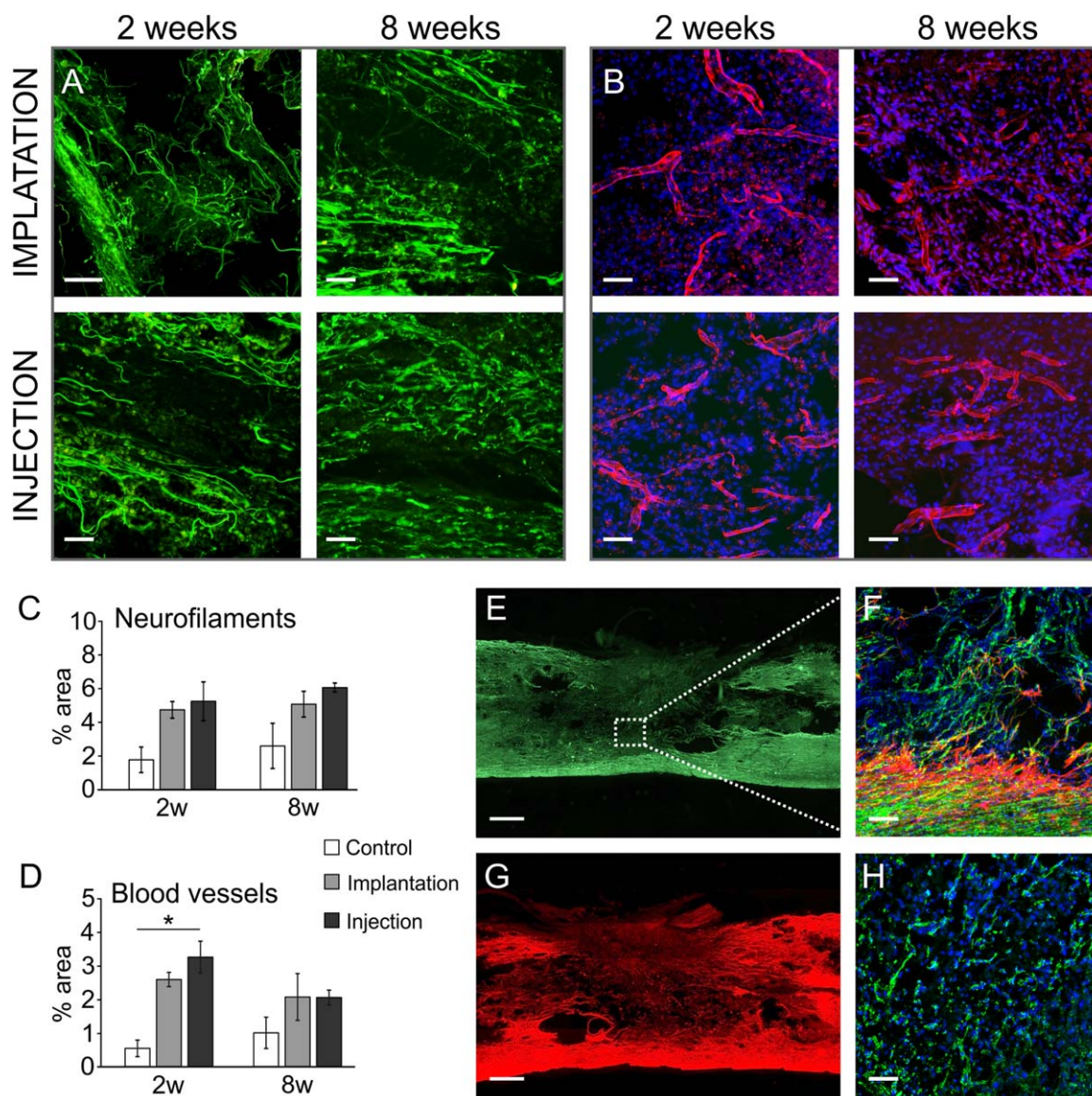


**FIGURE 3.** Representative images of longitudinal sections of the spinal cord lesion 2 and 8 weeks after the acute HA-PH-RGD hydrogel injection or implantation into the hemisection cavity: Staining for (A) neurofilaments (NF-160, green) and (B) blood vessels (RECA, red; DAPI, blue). Quantitative analysis of the ingrowth of (C) neurofilaments and (D) blood vessels into the lesion area 2 and 8 weeks after the injection or implantation of HA-PH-RGD hydrogel. The values are expressed as the percentage of (C) NF-160 or (D) RECA positive area from a total lesion area. ( $n = 3$ ),  $*p < 0.05$ . E: Immunofluorescent staining for neurofilaments (NF-160); square in (E) is shown under the higher magnification inset in (F); (F) immunofluorescent staining for neurofilaments (NF-160, green), astrocytes (GFAP, red) and cell nuclei (DAPI, blue) and (G) immunofluorescent staining for astrocytes (GFAP) 2 weeks after HA-PH-RGD injection. (H) Immunofluorescent staining for growth associated protein 43 (GAP43, green) and cell nuclei (DAPI, blue) 8 weeks after HA-PH-RGD hydrogel implantation. Scale bar: 500  $\mu\text{m}$  (E, G), 50  $\mu\text{m}$  (A, B, F, H).

non-invasive and effective way of hydrogel delivery resulting in tissue repair.

#### Histological evaluation of HA-PH-RGD hydrogels in subacute SCI lesion

The tissue response of the subacute injection of HA-PH-RGD, HA-PH-RGD/F, and HA-PH-RGD/F combined with hWJ-MSCs was evaluated after 8 weeks. As is apparent from Figure 4, both HA-PH-RGD and HA-PH-RGD/F hydrogels significantly improved the density of neurofilaments within the lesion when compared to the control untreated lesion, and this effect was further enhanced by the addition of hWJ-

MSCs. Because immunohistochemical results of HA-PH-RGD/F did not significantly differ from the results obtained with HA-PH-RGD, we did not show the immunohistochemistry of this group.

Astrocytes, detected by immunofluorescence staining for GFAP (Fig. 5), migrated from the lesion border to the lesion area treated by hydrogel, which suggests the formation of a permissive environment promoting glial cell infiltration [Fig. 5(D,F)]. Quantitative evaluation of the GFAP staining density around the lesion, which should reflect the density of the glial scar, did not reveal significant differences between the control and hydrogel treated groups [Fig. 5(G)]. Blood vessels densely



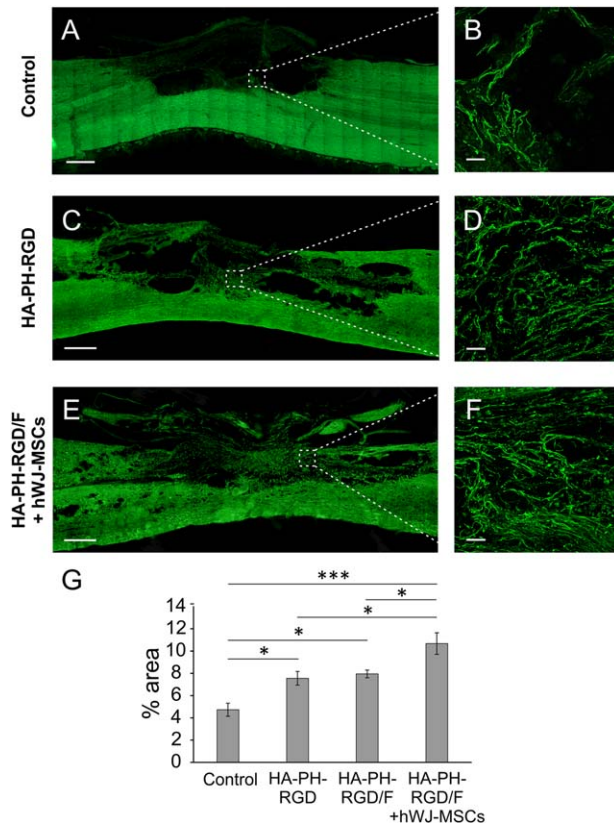


**FIGURE 4.** Representative images of the longitudinal sections of the spinal cord lesion in (A,B) controls and at 8 weeks after the subacute injection of (C,D) HA-PH-RGD and (E,F) HA-PH-RGD/F hydrogels combined with hWJ-MSCs, stained for neurofilaments (NF-160). Squares (A,C,E) are also shown under the higher magnification insets (B,D,F). G: Quantitative analysis of axonal ingrowth is expressed as the percentage of NF-160 positive area from a total lesion area ( $n=6$ ). \* $p < 0.05$ , \*\*\* $p < 0.001$ . Scale bar: 500  $\mu\text{m}$  (A,C,E), 50  $\mu\text{m}$  (B,D,F).

infiltrated the hydrogel treated lesion, however the increase in blood vessel density was not found to be significant when compared with the control lesion (Fig. 6).

ED1 staining, specific for microglia/macrophages, combined with CD206 staining specific for M2 macrophages confirmed the migration of both M1 and M2 macrophages into the hydrogel treated lesion, however, no quantification was performed to detect the M1/M2 ratio [Fig. 7(A-D)]. Oligodendrocytes were detected in the area of hydrogel treated lesions, but not in the control lesion [Fig. 7(E-H)].

Of note, we did not observe any hWJ-MSCs in the spinal cord tissue eight weeks after cell application, on the basis of staining for the human mitochondria (MTCO2) marker used for the detection of human MSCs in the host tissue.

#### Gene expression analysis in subacute SCI lesions

Changes in the mRNA expression of selected genes were determined 8 weeks after the injection of HA-PH-RGD, HA-PH-RGD/F and HA-PH-RGD/F hydrogel combined with hWJ-MSCs (Fig. 8).

Both the HA-PH-RGD and HA-PH-RGD/F hydrogel injections resulted in a decrease in mRNA expression of genes related to macrophages (*Irf5*, *Cd86*), inflammation (*Ccl3*) or

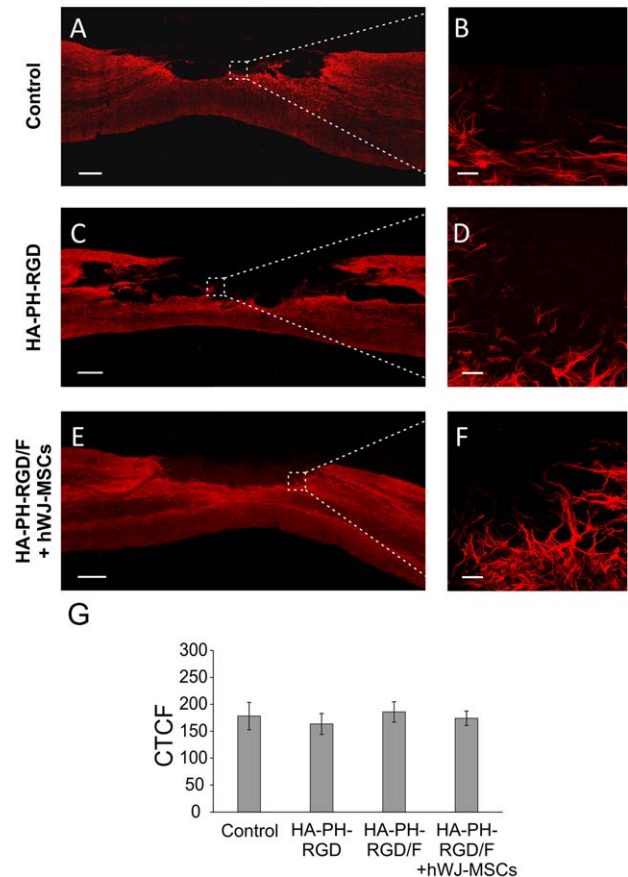


**FIGURE 5.** Representative images of the longitudinal sections of the spinal cord lesion in (A,B) control and at 8 weeks after subacute injection of (C,D) HA-PH-RGD and (E,F) HA-PH-RGD/F hydrogels combined with hWJ-MSCs, stained for astrocytes (GFAP). Squares (A,C,E) are also shown under the higher magnification insets (B,D,F). G: Quantitative analysis of the glial scar density around the lesion was expressed as the CTCF of GFAP staining ( $n=6$ ). Scale bar: 500  $\mu\text{m}$  (A,C,E), 50  $\mu\text{m}$  (B,D,F).

glial scar formation (*Gfap*, *Ptprz1*), but these changes were not significant. Significant downregulation was then found for the expression of *Gap43* when compared with the untreated control lesion. On the contrary, the expression of *Gap43* was significantly increased when the HA-PH-RGD/F was combined with hWJ-MSCs. Similarly, a combination with hWJ-MSCs led to significant upregulation of both M1 (*Irf5*, *Cd86*) and M2 macrophages markers (*Mrc1*).

#### Analysis of locomotor functions in subacute SCI lesions

The effect of the hydrogel treatment on the locomotor functions, such as knee and ankle angles and hind limb retraction and protraction (distance on x-axis of metatarsophalangeal joint in relation to iliac crest), was measured using the TSE Motion 8.5.11. No statistical differences between the control and hydrogel treated animals was found at 2, 5 and 8 weeks (Supporting Information Fig. S7).

#### DISCUSSION

HA-based hydrogels have great potential as scaffold materials for cell delivery in various tissue engineering applications.



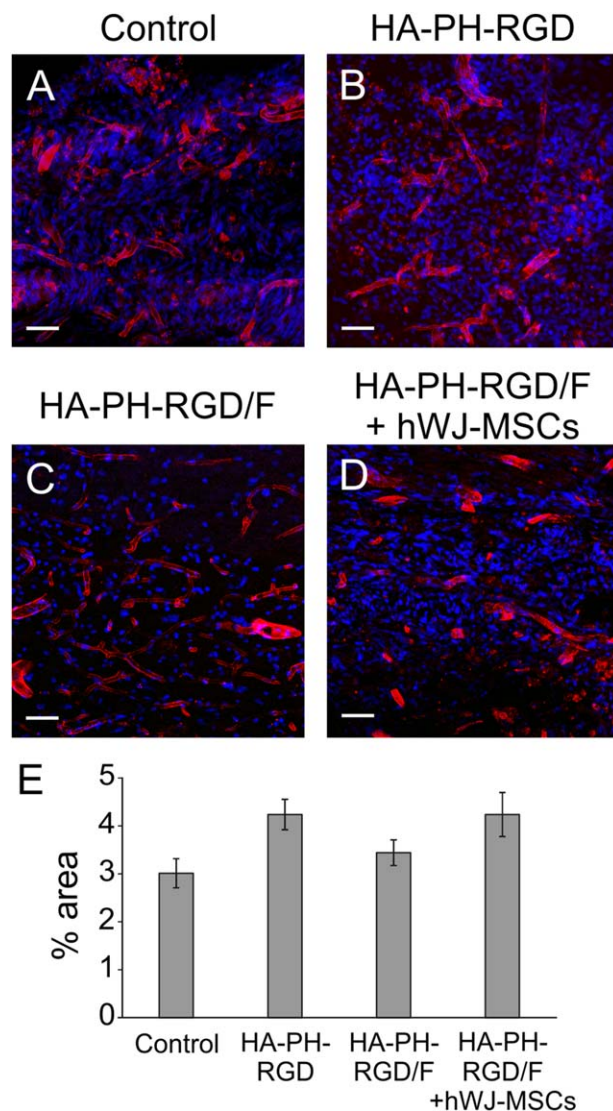


**FIGURE 6.** Representative images of the longitudinal sections of the spinal cord lesion in (A) control and at 8 weeks after subacute injection of (B) HA-PH-RGD, (C) HA-PH-RGD/F and (D) HA-PH-RGD/F hydrogel combined with hWJ-MSCs, stained for blood vessels (RECA, red) and DAPI (blue). E: Quantitative analysis of blood vessel ingrowth is expressed as the percentage of RECA positive area from a total lesion area ( $n = 6$ ). Scale bar: 50  $\mu\text{m}$ .

In the present study, we prepared and characterized injectable HA-PH derivative based hydrogel, specifically developed for neural tissue repair. The big advantage of this material over the others is that it can be manufactured in a reproducible manner under GMP (Good Manufacture Practice) conditions, which are required to allow the transfer of its production from bench-to-bedside in clinical practise.

To form a hydrogel, we used an enzymatic crosslink reaction initiated by HRP and  $\text{H}_2\text{O}_2$ . The concentration of the cross-linking agents was optimized to set mechanical properties comparable to the native spinal cord tissue, and to get the optimal time of gelation for material application into the site of the defect. Moreover, the used crosslink reaction is non-cytotoxic and enabled to form cell-laden hydrogel under physiological conditions.

To enhance cell adhesion and migration into implants, the HA-PH was functionalized with RGD oligopeptide sequence, which has affinity for multiple integrin receptors, and has been previously shown to support effective cell spreading and cytoskeletal organization, as well as cell proliferation.<sup>42</sup> However, an important factor in the establishment of cell adhesion is ligand density, which is, in the case of used HA-PH-RGD derivative, limited to the DS of PH-RGD oligopeptide. Hydrogel containing 20 mg/mL of the new designed HA-PH-RGD conjugate with a DS of 2.5% achieved a concentration of RGD sequence 1  $\mu\text{mol/mL}$  of hydrogel. As was shown in the experiments *in vitro*, the presence of the RGD motive in the HA-PH hydrogel structure improved its cell affinity, but in a limited way. Therefore, for the cell encapsulation, the bioadhesive properties of the HA-PH-RGD hydrogel were further enhanced by the incorporation of fibrinogen which offers cellular adhesive domains and has been previously proved as a natural additive to enhance cell survival, growth and proliferation.<sup>33,34</sup>

On the other hand, the addition of fibrinogen to HA-PH-RGD hydrogel had no effect on the assessed tissue repair parameters in subacute SCI. Notably, when exposed to *in vivo* conditions within the SCI lesion, the hydrogel is infiltrated with extracellular fluid containing various proteins which together with endogenous cell infiltration and degradation of the hydrogel implant may overlap the potential benefit of fibrinogen in HA-PH-RGD/F hydrogel.

To evaluate the repair potential of the HA based hydrogels, the subacute SCI lesion was treated by injection of HA-PH-RGD, HA-PH-RGD/F and HA-PH-RGD/F combined with hWJ-MSCs one week after the lesion induction, and compared with the control injection of saline. Notably, despite the tissue removal after hemisection, the lesion cavity did not remain empty and was commonly filled with debris and connective tissue that enable vascularization with poor axonal infiltration. However, after injection of both HA-PH-RGD and HA-PH-RGD/F, the density of NF-positive fibers in the lesion cavity significantly increased, and this effect was further enhanced when the HA-PH-RGD/F was combined with hWJ-MSCs. Contradictorily, the robust axonal ingrowth into HA-PH-RGD and HA-PH-RGD/F revealed by the histological analysis did not correlate with decreased mRNA expression of gene related to axonal growth (*Gap43*). On the other hand, *Gap43* was upregulated in group with hWJ-MSCs. *Gap43*, which is expressed at high levels in newly created neuronal growth cones during axonal regeneration, is considered a crucial component of effective regenerative response in the nervous system. It is likely that axonal sprouting into HA-PH-RGD and HA-PH-RGD/F hydrogels might culminate during an earlier period after injury, while still persist in the group with hWJ-MSCs. Therefore, NF160 staining of HA-PH-RGD and HA-PH-RGD/F hydrogel groups carried out at 8 weeks revealed already matured sprouting neurons.

Similarly, the expression of both markers of M1 and M2 macrophage/microglia has been increased when the HA-PH-RGD/F was combined with hWJ-MSCs. It suggests that tissue repair processes, facilitated by the stem cells treatment,

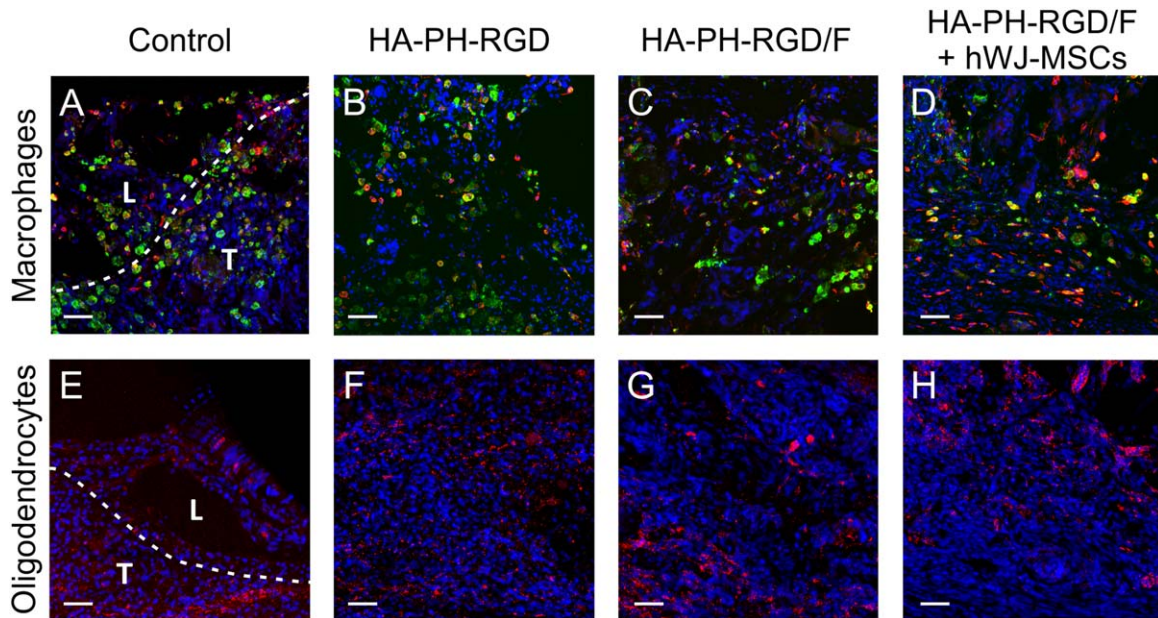


**FIGURE 7.** Representative images of the longitudinal sections of the spinal cord lesion in (A,E) control and at 8 weeks after subacute injection of (B,F) HA-PH-RGD, (C,G) HA-PH-RGD/F and (D,H) HA-PH-RGD/F hydrogel combined with hWJ-MSCs. Staining for (A–D) macrophages (ED1, green) and M2 macrophages (CD206, red), (E–H) oligodendrocytes (MOSP, red) and (A–H) DAPI (blue). The dotted lines in (A,E) outline the border of the tissue (T) and the lesion area (L). Other images are taken from the center of the lesion. Scale bar: 50  $\mu\text{m}$ .

involves orchestrated activation of different macrophage phenotype.<sup>43</sup>

Despite immunosuppression using the combination of three agents, hWJ-MSCs did not survive in the host tissue over the period of 8 weeks. On the other hand, we proved the effect of the cells using immunohistochemical and qPCR analysis, which supports the commonly proposed hypothesis that transplanted cells release trophic factors that provide long lasting neurotrophic and immunomodulatory effects.<sup>44–46</sup>

In contrast to improvement in tissue repair parameters, no significant improvement in locomotor functions was observed in animals treated with both hydrogel alone or in combination with hWJ-MSCs. Although it is unlikely that HA scaffolds alone can lead to behavioral restoration without additional treatment, the combination of hydrogels with various stem cells may have beneficial effects on the repair of the injured spinal cord by providing trophic support.<sup>2–4</sup> However, an important factor which significantly affects the

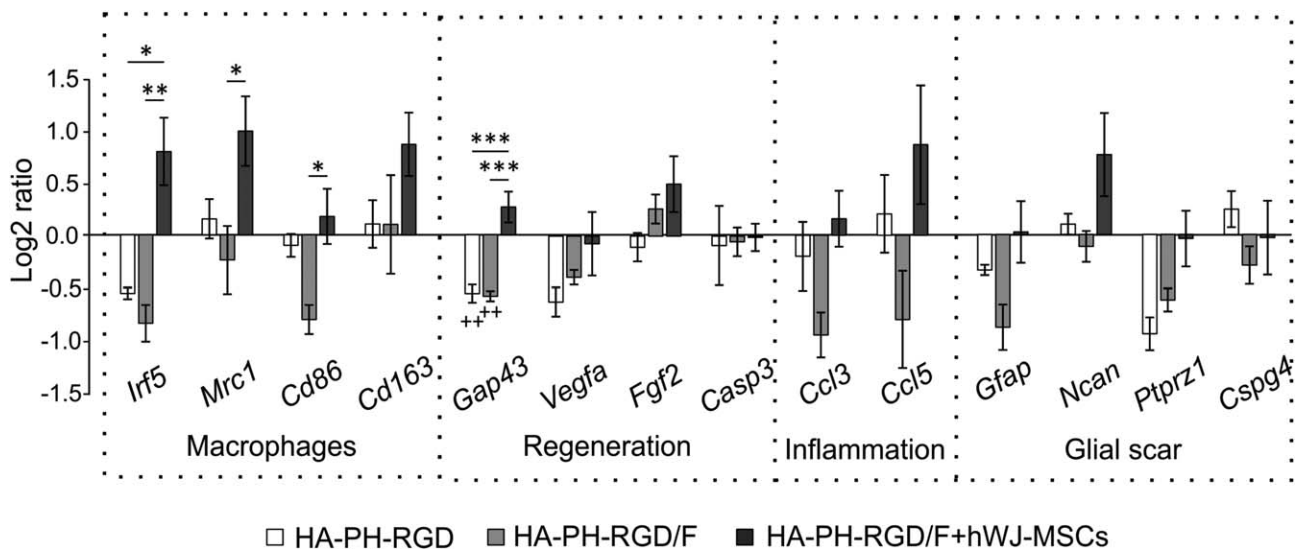


**FIGURE 8.** Analysis of mRNA gene expression of selected genes involved in the reparative processes following SCI treated with HA-PH-RGD, HA-PH-RGD/F, and HA-PH-RGD/F hydrogel combined with hWJ-MSCs. The graph shows the log<sub>2</sub>-fold changes in gene expression over the control lesion with saline. Significance is calculated between  $\Delta\text{Ct}$  values. ++ $p < 0.01$ : versus control lesion, \* $p < 0.05$ , \*\* $p < 0.01$ , \*\*\* $p < 0.001$ , ( $n = 5$ ).



behavioral outcome after SCI is the number of transplanted cells.

In our previous study, an effective hWJ-MS-C dose, necessary to induce functional improvement after contusion SCI, was determined as 1.5 million cells in a single intrathecal application (unpublished data). The higher dose of transplanted cells would probably increase number of surviving cells as well as behavioural outcome. However, in this study, we primarily evaluate the feasibility of HA-PH-RGD hydrogel for neural tissue repair and as a cell carrier *per se*. Therefore, the number of transplanted cells (approximately  $3 \times 10^4$  cells) was limited by the size of the lesion and hydrogel volume (approximately 5  $\mu$ L), and did not exceed the level at which the functional locomotor improvement could be achieved. To overcome the limitation of the number of cells that can be implanted with the hydrogel, we propose a combination of hydrogel with additional cell application via direct cell injection into the lesion site or via intrathecal application.

To test the therapeutic approach, we used a spinal cord hemisection, because it is the least invasive and devastating SCI model for the evaluation of new biomaterials, allows filling the lesion cavity with the material and clear analysis of the endogenous infiltration into the implant.<sup>16,47,48</sup> On the other hand, this model is a case of partial lesions with a high rate of spontaneous recovery and a high risk of inconsistencies in the injuries from one animal to the next, which might lead to misinterpretation of the behavioral evaluation.<sup>49</sup> Further investigation using the SCI model, which completely cuts a projecting system of axons together with systematic functional evaluation is therefore the next step in establishing the HA-PH-RGD hydrogel as a scaffold for SCI repair.

In conclusion, many types of scaffolds are able to support axonal growth and sprouting after SCI, but are unable to achieve significant functional recovery, due to the reduced regeneration of long-tract axons through sites of SCI. Besides the development of optimal materials for bridging the lesion, modifying the extrinsic and intrinsic factors limiting regrowth after SCI represent the current challenge of how to overcome the inhibitory properties of the axon-scar environment. Combinatorial therapies will probably be essential to achieve such functional connectivity.<sup>50</sup>

## CONCLUSION

This study showed that injectable HA-PH-RGD based hydrogel may be a promising material for SCI repair in rats. Injection of HA-PH-RGD hydrogels bridged the lesion cavity, supported vascularization and increased axonal sprouting into the lesion, which was further improved by its combination with hWJ-MS-C. However, enhancement of transplanted cell survival as well as additional treatments that would further stimulate axonal reconnection, are required to overcome HA-PH-RGD hydrogel limitation in functional SCI restoration.

## ACKNOWLEDGMENTS

This work was supported by GACR 15-01396S, Ministry of Education, Youth and Sports of CR within the L01309, and CZ.02.1.01/0.0./0.0/15\_003/0000419.

## DISCLOSURE

Kristyna Zaviskova, Dmitry Tukmachev, Jana Dubisova, Irena Vackova, Ales Hejcl, and Sarka Kubinova have no affiliations with or involvement in any organization or entity with any financial interest, or non-financial interest in the subject matter or materials discussed in this article. Julie Bystrova, Martin Pravda, Ivana Scigalkova, Romana Sulakova, and Lucie Wolfova are employees of Contipro a.s. which is a producer of HA and derivatives of HA, and which provided hyaluronan based materials for the article.

## REFERENCES

- Hill CE. A view from the ending: axonal dieback and regeneration following SCI. *Neurosci Lett* 2016;652:11–24.
- Kubinova S, Sykova E. Biomaterials combined with cell therapy for treatment of spinal cord injury. *Regen Med* 2012;7:207–224.
- Pego AP, Kubinova S, Cizkova D, Vanicky I, Mar FM, Sousa MM, Sykova E. Regenerative medicine for the treatment of spinal cord injury: more than just promises? *J Cell Mol Med* 2012;16:2564–2582.
- Shrestha B, Coykendall K, Li YC, Moon A, Priyadarshani P, Yao L. Repair of injured spinal cord using biomaterial scaffolds and stem cells. *Stem Cell Res Ther* 2014;5:91.
- Park J, Lim E, Back S, Na H, Park Y, Sun K. Nerve regeneration following spinal cord injury using matrix metalloproteinase-sensitive, hyaluronic acid-based biomimetic hydrogel scaffold containing brain-derived neurotrophic factor. *J Biomed Mater Res A* 2010;93:1091–1099.
- Li X, Zhao Y, Cheng S, Han S, Shu M, Chen B, Chen X, Tang F, Wang N, Tu Y, Wang B, Xiao Z, Zhang S, Dai J. Cetuximab modified collagen scaffold directs neurogenesis of injury-activated endogenous neural stem cells for acute spinal cord injury repair. *Biomaterials* 2017;137:73–86.
- King VR, Hewazy D, Alovskaya A, Phillips JB, Brown RA, Priestley JV. The neuroprotective effects of fibronectin mats and fibronectin peptides following spinal cord injury in the rat. *Neuroscience* 2010;168:523–530.
- Khaing ZZ, Milman BD, Vanscoy JE, Seidlits SK, Grill RJ, Schmidt CE. High molecular weight hyaluronic acid limits astrocyte activation and scar formation after spinal cord injury. *J Neural Eng* 2011;8:046033.
- Kushchayev SV, Giers MB, Hom Eng D, Martirosyan NL, Eschbacher JM, Mortazavi MM, Theodore N, Panitch A, Preul MC. Hyaluronic acid scaffold has a neuroprotective effect in hemisection spinal cord injury. *J Neurosurg Spine* 2016;25:114–124.
- Mothe AJ, Tam RY, Zahir T, Tator CH, Shoichet MS. Repair of the injured spinal cord by transplantation of neural stem cells in a hyaluronan-based hydrogel. *Biomaterials* 2013;34:3775–3783.
- Raynald, Li Y, Yu H, Huang H, Guo M, Hua R, Jiang F, Zhang K, Li H, Wang F, Li L, Cui F, An Y. The hetero-transplantation of human bone marrow stromal cells carried by hydrogel unexpectedly demonstrates a significant role in the functional recovery in the injured spinal cord of rats. *Brain Res* 2016;1634:21–33.
- Wang X, He J, Wang Y, Cui FZ. Hyaluronic acid-based scaffold for central neural tissue engineering. *Interface Focus* 2012;2:278–291.
- Gomes ED, Mendes SS, Leite-Almeida H, Gimble JM, Tam RY, Shoichet MS, Sousa N, Silva NA, Salgado AJ. Combination of a peptide-modified gellan gum hydrogel with cell therapy in a lumbar spinal cord injury animal model. *Biomaterials* 2016;105:38–51.
- Caicco MJ, Zahir T, Mothe AJ, Ballios BG, Kihm AJ, Tator CH, Shoichet MS. Characterization of hyaluronan-methylcellulose hydrogels for cell delivery to the injured spinal cord. *J Biomed Mater Res A* 2013;101:1472–1477.
- Koci Z, Vyborny K, Dubisova J, Vackova I, Jager A, Lunov O, Jirakova K, Kubinova S. ECM hydrogel derived from human umbilical cord as a scaffold for neural tissue repair and its comparison to ECM from CNS and non-CNS porcine tissues. *Tissue Eng Part C Methods* 2017;23:333–345.
- Tukmachev D, Forostyak S, Koci Z, Zaviskova K, Vackova I, Vyborny K, Sandvig I, Sandvig A, Medberry CJ, Badylak SF, Sykova E,



- Kubinova S. Injectable extracellular matrix hydrogels as scaffolds for spinal cord injury repair. *Tissue Eng A* 2016;22:306–317.
17. Litwiniuk M, Krejner A, Speyrer MS, Gauto AR, Grzela T. Hyaluronic acid in inflammation and tissue regeneration. *Wounds* 2016;28:78–88.
  18. Knopf-Marques H, Pravda M, Wolfova L, Velebny V, Schaaf P, Vrana NE, Lavallo P. Hyaluronic acid and its derivatives in coating and delivery systems: applications in tissue engineering, regenerative medicine and immunomodulation. *Adv Healthcare Mater* 2016;5:2841–2855.
  19. Seidlits SK, Khaing ZZ, Petersen RR, Nickels JD, Vanscoy JE, Shear JB, Schmidt CE. The effects of hyaluronic acid hydrogels with tunable mechanical properties on neural progenitor cell differentiation. *Biomaterials* 2010;31:3930–3940.
  20. Liang Y, Walczak P, Bulte JW. The survival of engrafted neural stem cells within hyaluronic acid hydrogels. *Biomaterials* 2013;34:5521–5529.
  21. Li L-M, Han M, Jiang X-C, Yin X-Z, Chen F, Zhang T-Y, Ren H, Zhang J-W, Hou T-J, Chen Z, Ou-Yang H-W, Tabata Y, Shen Y-Q, Gao J-Q. Peptide-tethered hydrogel scaffold promotes recovery from spinal cord transection via synergism with mesenchymal stem cells. *ACS Appl Mater Interfaces* 2017;9:3330–3342.
  22. Fuhrmann T, Obermeyer J, Tator CH, Shoichet MS. Click-cross-linked injectable hyaluronic acid hydrogel is safe and biocompatible in the intrathecal space for ultimate use in regenerative strategies of the injured spinal cord. *Methods* 2015;84:60–69.
  23. Gupta D, Tator CH, Shoichet MS. Fast-gelling injectable blend of hyaluronan and methylcellulose for intrathecal, localized delivery to the injured spinal cord. *Biomaterials* 2006;27:2370–2379.
  24. Wei YT, He Y, Xu CL, Wang Y, Liu BF, Wang XM, Sun XD, Cui FZ, Xu QY. Hyaluronic acid hydrogel modified with nogo-66 receptor antibody and poly-L-lysine to promote axon regrowth after spinal cord injury. *J Biomed Mater Res B Appl Biomater* 2010;95:110–117.
  25. Hou S, Xu Q, Tian W, Cui F, Cai Q, Ma J, Lee IS. The repair of brain lesion by implantation of hyaluronic acid hydrogels modified with laminin. *J Neurosci Methods* 2005;148:60–70.
  26. Seidlits SK, Drinnan CT, Petersen RR, Shear JB, Suggs LJ, Schmidt CE. Fibronectin-hyaluronic acid composite hydrogels for three-dimensional endothelial cell culture. *Acta Biomater* 2011;7:2401–2409.
  27. Snyder TN, Madhavan K, Intrator M, Dregalla RC, Park D. A fibrin/hyaluronic acid hydrogel for the delivery of mesenchymal stem cells and potential for articular cartilage repair. *J Biol Eng* 2014;8:10.
  28. Cui FZ, Tian WM, Hou SP, Xu QY, Lee IS. Hyaluronic acid hydrogel immobilized with RGD peptides for brain tissue engineering. *J Mater Sci Mater Med* 2006;17:1393–1401.
  29. Darr A, Calabro A. Synthesis and characterization of tyramine-based hyaluronan hydrogels. *J Mater Sci Mater Med* 2009;20:33–44.
  30. Wolfova L, Pravda M, Foglarova M, Memcova M, Niedoba K, Velebny V. Derivates based on hyaluronic acid, capable of forming hydrogels, method of preparation thereof, hydrogels based on said derivatives, method of preparation thereof and use. Patent WO2013127374 A1; 2013.
  31. Kučera L, Weinfurterová R, Dvořáková J, Kučera J, Pravda M, Foglarová M, Švík K, Klein P, Velebný V, Kubala L. Chondrocyte cultivation in hyaluronan-tyramine cross-linked hydrogel. *Int J Polymer Mater PolymerBiomaterials* 2015;64:661–674.
  32. Dvořáková J, Kučera L, Kučera J, Švík K, Foglarová M, Muthný T, Pravda M, Němcová M, Velebný V, Kubala L. Chondrogenic differentiation of mesenchymal stem cells in a hydrogel system based on an enzymatically crosslinked tyramine derivative of hyaluronan. *J Biomed Mater Res A* 2014;102:3523–3530.
  33. Karoubi G, Ormiston ML, Stewart DJ, Courtman DW. Single-cell hydrogel encapsulation for enhanced survival of human marrow stromal cells. *Biomaterials* 2009;30:5445–5455.
  34. Zapotocky V, Pospisilova M, Janouchova K, Svadlak D, Batova J, Sogorkova J, Cepa M, Betak J, Stepankova V, Sulakova R, Kulhanek J, Pitucha T, Vranova J, Duffy G, Velebny V. Fabrication of biodegradable textile scaffold based on hydrophobized hyaluronic acid. *Int J Biol Macromol* 2017;95:903–909.
  35. Cheng H, Liu X, Hua R, Dai G, Wang X, Gao J, An Y. Clinical observation of umbilical cord mesenchymal stem cell transplantation in treatment for sequelae of thoracolumbar spinal cord injury. *J Transl Med* 2014;12:253.
  36. Li X, Tan J, Xiao Z, Zhao Y, Han S, Liu D, Yin W, Li J, Li J, Wanggou S, Chen B, Ren C, Jiang X, Dai J. Transplantation of hUC-MSCs seeded collagen scaffolds reduces scar formation and promotes functional recovery in canines with chronic spinal cord injury. *Sci Rep* 2017;7:43559.
  37. Zhao Y, Tang F, Xiao Z, Han G, Wang N, Yin N, Chen B, Jiang X, Yun C, Han W, Zhao C, Cheng S, Zhang S, Dai J. Clinical study of neuroregen scaffold combined with human mesenchymal stem cells for the repair of chronic complete spinal cord injury. *Cell Transplant* 2017;26:891–900.
  38. Amblard M, Fehrentz J-A, Martinez J, Subra G. Methods and protocols of modern solid phase peptide synthesis. *Mol Biotechnol* 2006;33:239–254.
  39. Huerta-Angeles G, Němcová M, Příkopová E, Šmejkalová D, Pravda M, Kučera L, Velebný V. Reductive alkylation of hyaluronic acid for the synthesis of biocompatible hydrogels by click chemistry. *Carbohydr Polym* 2012;90:1704–1711.
  40. Šedová P, Buffa R, Kettou S, Huerta-Angeles G, Hermannová M, Leierová V, Šmejkalová D, Moravcová M, Velebný V. Preparation of hyaluronan polyaldehyde—a precursor of biopolymer conjugates. *Carbohydr Res* 2013;371:8–15.
  41. McCloy RA, Rogers S, Caldon CE, Lorca T, Castro A, Burgess A. Partial inhibition of Cdk1 in G 2 phase overrides the SAC and decouples mitotic events. *Cell Cycle* 2014;13:1400–1412.
  42. Mackova H, Plichta Z, Proks V, Kotelnikov I, Kucka J, Hlidkova H, Horak D, Kubinova S, Jirakova K. RGDS- and SIKVAVS-modified superporous poly(2-hydroxyethyl methacrylate) scaffolds for tissue engineering applications. *Macromol Biosci* 2016;16:1621–1631.
  43. Gensel JC, Zhang B. Macrophage activation and its role in repair and pathology after spinal cord injury. *Brain Res* 2015;1619:1–11.
  44. Urdziková L, Růžička J, LaBagnara M, Kárová K, Kubinová Š, Jiráková K, Murali R, Syková E, Jhanwar-Uniyal M, Jendelová P. Human mesenchymal stem cells modulate inflammatory cytokines after spinal cord injury in rat. *Int J Mol Sci* 2014;15:11275–11293.
  45. Petrenko Y, Sykova E, Kubinova S. The therapeutic potential of three-dimensional multipotent mesenchymal stromal cell spheroids. *Stem Cell Res Ther* 2017;8:94.
  46. Assinck P, Duncan GJ, Hilton BJ, Plemel JR, Tetzlaff W. Cell transplantation therapy for spinal cord injury. *Nat Neurosci* 2017;20:637–647.
  47. Kubinova S, Horak D, Hejcl A, Plichta Z, Kotek J, Proks V, Forostyak S, Sykova E. SIKVAV-modified highly superporous PHEMA scaffolds with oriented pores for spinal cord injury repair. *J Tissue Eng Regen Med* 2015;9:1298–1309.
  48. Kubinova S, Horak D, Hejcl A, Plichta Z, Kotek J, Sykova E. Highly superporous cholesterol-modified poly(2-hydroxyethyl methacrylate) scaffolds for spinal cord injury repair. *J Biomed Mater Res A* 2011;99:618–629.
  49. Fouad K, Hurd C, Magnuson DS. Functional testing in animal models of spinal cord injury: not as straight forward as one would think. *Front Integr Neurosci* 2013;7:85.
  50. Chew DJ, Fawcett JW, Andrews MR. The challenges of long-distance axon regeneration in the injured CNS. *Prog Brain Res* 2012;201:253–294.



Article

# The Effect of Human Mesenchymal Stem Cells Derived from Wharton's Jelly in Spinal Cord Injury Treatment Is Dose-Dependent and Can Be Facilitated by Repeated Application

Petr Krupa <sup>1,2</sup>, Irena Vackova <sup>2</sup>, Jiri Ruzicka <sup>2</sup>, Kristyna Zaviskova <sup>2,3</sup> , Jana Dubisova <sup>2,3</sup>, Zuzana Koci <sup>2,3</sup>, Karolina Turnovcova <sup>2</sup>, Lucia Machova Urdzikova <sup>2</sup>, Sarka Kubinova <sup>2</sup>, Svatopluk Rehak <sup>1</sup> and Pavla Jendelova <sup>2,3,\*</sup>

<sup>1</sup> Department of Neurosurgery, Charles University, Medical Faculty and University Hospital Hradec Králové, Sokolska 581, 50005 Hradec Kralove, Czech Republic; petr.krupa@fnhk.cz (P.K.); rehak@lfhk.cuni.cz (S.R.)

<sup>2</sup> Institute of Experimental Medicine, Czech Academy of Sciences, Vídeňská 1083, 14220 Prague 4, Czech Republic; irena.vackova@biomed.cas.cz (I.V.); j.ruzicka@biomed.cas.cz (J.R.); kristyna.zaviskova@biomed.cas.cz (K.Z.); jana.dubisova@biomed.cas.cz (J.D.); zuzana.koci@biomed.cas.cz (Z.K.); karolina.turnovcova@biomed.cas.cz (K.T.); urdzikl@biomed.cas.cz (L.M.U.); sarka.k@biomed.cas.cz (S.K.)

<sup>3</sup> Department of Neuroscience, Charles University, Second Faculty of Medicine, 15006 Prague 5, Czech Republic

\* Correspondence: jendel@biomed.cas.cz; Tel.: +420-241062828

Received: 9 April 2018; Accepted: 15 May 2018; Published: 17 May 2018



**Abstract:** Human mesenchymal stem cells derived from Wharton's jelly (WJ-MSCs) were used for the treatment of the ischemic-compression model of spinal cord injury in rats. To assess the effectivity of the treatment, different dosages (0.5 or 1.5 million cells) and repeated applications were compared. Cells or saline were applied intrathecally by lumbar puncture for one week only, or in three consecutive weeks after injury. Rats were assessed for locomotor skills (BBB, rotarod, flat beam) for 9 weeks. Spinal cord tissue was morphometrically analyzed for axonal sprouting, sparing of gray and white matter and astrogliosis. Endogenous gene expression (*Gfap*, *Casp3*, *Irf5*, *Cd86*, *Mrc1*, *Cd163*) was studied with quantitative Real-time polymerase chain reaction (qRT PCR). Significant recovery of functional outcome was observed in all of the treated groups except for the single application of the lowest number of cells. Histochemical analyses revealed a gradually increasing effect of grafted cells, resulting in a significant increase in the number of GAP43+ fibers, a higher amount of spared gray matter and reduced astrogliosis. mRNA expression of macrophage markers and apoptosis was downregulated after the repeated application of 1.5 million cells. We conclude that the effect of hWJ-MSCs on spinal cord regeneration is dose-dependent and potentiated by repeated application.

**Keywords:** spinal cord injury; human mesenchymal stem cells; Wharton's jelly; inflammatory response; neuroregeneration; astrogliosis; axonal growth

## 1. Introduction

Spinal cord injury (SCI) is a serious mutilating injury, resulting in loss of motor, sensory, and autonomic functions, and remains a challenging medical and social problem even in the 21st century. The final neurological deficit is determined by two mechanisms—primary and secondary injury. Primary injury represents the mechanism and strength of the direct trauma. Secondary injury is characterized by the local immune reaction followed by apoptosis of the injured and vulnerable

neurons, tissue atrophy with cavitation, and glial scar formation [1]. Since there is no specific treatment for primary injury, and the endogenous potential to regenerate the spinal cord neurons is very limited [2], several treatments are focused on neuroprotection and/or reducing the impact of secondary pathological processes. Promising results in alleviation of the pathological chain of secondary damage were found in the last decade by application of mesenchymal stem cells (MSCs).

MSCs are multipotent cells with multi-differentiation and self-renewal capacity. Many types of adult and embryonic tissue have been proven as a source of MSCs—adipose tissue, peripheral blood, lung, heart, corneal stroma, dental pulp, placenta, endometrium, amniotic membrane, and umbilical cord blood and tissue (Wharton's jelly). Under special conditions *in vitro*, they are capable of differentiating into various tissue cells such as osteocytes or osteoblasts, adipocytes, and chondrocytes [3–5]. However, the regenerative potential of MSCs as a therapeutic tool can be provided mainly by the paracrine effect, interacting with the environment around the injured tissue. In nervous tissue repair and regeneration, MSCs support revascularization, modulate inflammatory response [6], produce different growth factors and cytokines [7], and protect vulnerable cells from oxidative stress, causing stress-induced apoptosis [8]. Therefore, it was recently suggested by Caplan [9] that they should be renamed to medicinal signaling cells (MSCs).

In the current study, we used MSCs isolated from human Wharton's jelly (WJ-MSCs). Wharton's jelly is the primitive gelatinous connective tissue of the umbilical cord, first described by Thomas Wharton in 1656. Compared to other sources of MSCs (bone marrow, adipose tissue), WJ-MSCs are more primitive with higher proliferating potential [10], have lower immunogenicity because of a lower major histocompatibility complex class I (MHC-I) and the absence of major histocompatibility complex class II (MHC-II) expression [11], and are proven to be non-tumorigenic [12]. Furthermore, WJ-MSCs can be easily and non-invasively obtained from discarded umbilical tissue, and represent neither potential danger for the donor, nor ethical concerns [13]. They are highly proliferative and can be easily expanded.

The delivery route of stem cells is a frequently discussed issue, as the mode of delivery is an important factor in translation to clinical practice. Therefore, several studies have compared the intraspinal, intrathecal (or intracisternal), intraarterial and intravenous application of MSCs. Regardless of the delivery route, MSC treatment has improved functional recovery after SCI. Whilst the engraftment of the transplanted cells was higher in animals with intraspinal delivery [14,15], injections into the parenchyma of the spinal cord may further damage the spinal cord tissue; therefore, less invasive methods, such as intrathecal or intravenous delivery, are preferable. Indeed, the cells grafted via lumbar puncture, or intracisternally have shown the best functional recovery, even though they often remained in the intrathecal space [16,17] or accumulated around the anterior spinal artery [18]. Rats intrathecally grafted with human bone marrow MSCs (hBM-MSCs) had reduced inflammatory reactions and apoptosis, improved functional recovery, and the glial scar formation had been rearranged after SCI, though no cells were detected in the spinal cord parenchyma two months after transplantation [19,20]. Because of the relatively short survival time of MSCs in the host tissue the repetitive delivery of MSCs may prolong the beneficial effects induced by MSC application by potentiating their regenerative potential [18].

The main goal of this study was to assess the dose of the applied WJ-MSCs, and the difference between single and repetitive application on functional recovery and tissue repair after SCI in rats. WJ-MSCs were applied intrathecally by a lumbar puncture into rats with balloon-induced spinal cord compression lesion. This model simulates the compression of the human spinal cord by an unreduced dislocation or a fracture dislocation of the spine. It is assumed that both mechanical and vascular factors are involved in the pathogenesis of spinal cord injury in this model. Moreover, it is simple and reproducible and requires minimal surgical preparation of the animal (no laminectomy) [21]. The functional outcome was assessed using a set of behavioral tests (BBB, flat beam test, and rotarod). Furthermore, histological and immunohistochemical analyses were performed to evaluate the sparing



of gray and white matter, axonal sprouting, and formation of glial scar. Finally, quantitative PCR analyses of selected endogenous genes were performed.

## 2. Results

### 2.1. Cell Culture

hWJ-MSCs phenotype, their multipotent differentiation potential, and high proliferation capacity was evaluated prior to transplantation (see Supplement 1, Figures S1–S3).

### 2.2. Behavioral Analysis

#### 2.2.1. BBB Test

Recovery of the hind limb locomotor function was evaluated every week starting the first week after SCI. The BBB score was calculated as a mean value from the scores of both legs (Figure 1A). One week after SCI, all tested animals had severe paraparesis or paraplegia. The average score was  $1.28 \pm 0.15$ . No differences between the groups were observed. The second week after SCI animals in all groups showed new motions in one or two joints. Among the groups, a significant difference was found between the control group ( $2.1 \pm 0.43$ ) and the group treated with a single dose of 1.5 M hWJ-MSCs ( $5.28 \pm 0.59$ ) ( $p < 0.05$ ). In the third week after SCI, a rapid improvement of the locomotor functions was observed in the groups treated with a single dose of 1.5 M, and the groups with repeated treatment of 0.5 and 1.5 M, respectively. All three groups recovered significantly better than the control group ( $p < 0.05$ ,  $p < 0.001$ ). Animals treated with only 0.5 M showed little improvement over the control group, which was not statistically significant. In the following weeks, improvement of movement and strength of the hind limbs continued but not so rapidly as was seen during the first three weeks. From the fourth week onward, until the end of the experiment, rats treated with 1.5 M and  $3 \times 0.5$  M and  $3 \times 1.5$  M had comparable results, which were significantly better than the control group and animals treated by 0.5 M ( $p < 0.01$ ,  $p < 0.001$ ). No significant difference between the control group and the 0.5 M group was found. The final results at the end of the ninth week were  $4.29 \pm 0.57$  for the control group,  $5.19 \pm 0.36$  for 0.5 M,  $9.81 \pm 0.88$  for  $3 \times 0.5$  M,  $8.67 \pm 0.88$  for 1.5 M and  $9.21 \pm 0.45$  for  $3 \times 1.5$  M. Animals in the groups with repetitive treatment were mostly able to achieve effective weight support of their body when standing, or even walking. The gap between scores 8 (and lower) and 9 (and higher) is substantial when comparing the strength of the muscles of the hindlimbs.

(Two-way RM ANOVA, Treatment;  $F = 8.481$ ,  $p < 0.001$ ; for  $p$  values of post hoc pair-to-pair test, see Supplement 2).

#### 2.2.2. Rotarod Test

Coordination of the limb movements was tested by a rotarod test (Figure 1B). All animals were trained in this task before surgery at a fixed speed of 10 rpm. Testing was then performed every two weeks—2nd, 4th, 6th, and 8th week after SCI. Due to the severity of the lesion and limited recovery, no significant differences were observed between the groups.

(Two-way RM ANOVA, Treatment;  $F = 0.490$ ,  $p = 0.743$ ; for  $p$  values of post hoc pair-to-pair test, see Supplement 2).

#### 2.2.3. Beam Walk Test

Advanced locomotor skills and coordination of the hind limbs was measured by walking on the flat beam. Results were evaluated using a 0–7 scale modified from Metz and Whishaw. All animals were firstly trained in this task before surgery and then tested every week starting the second week after SCI (Figure 1C). Due to the severity of the lesion, most of the rats showed minimal ability to cross the beam and often just stayed and balanced at the starting point of the beam. The best scores

(7th week after SCI  $3.1 \pm 0.33$ ) were obtained in animals treated by  $3 \times 1.5$  M, which were significantly better, when compared to all of the other groups. For the first three weeks, animals treated with 0.5 M achieved significantly better results than the control group, but in subsequent weeks they gradually worsened and the significant difference was lost. This was most probably due to the gaining of weight, lack of motivation, and fear of falling off the beam.

(Two-way RM ANOVA, Treatment;  $F = 20.656$ ,  $p < 0.001$ ; for  $p$  values of post hoc pair-to-pair test, see Supplement 2).

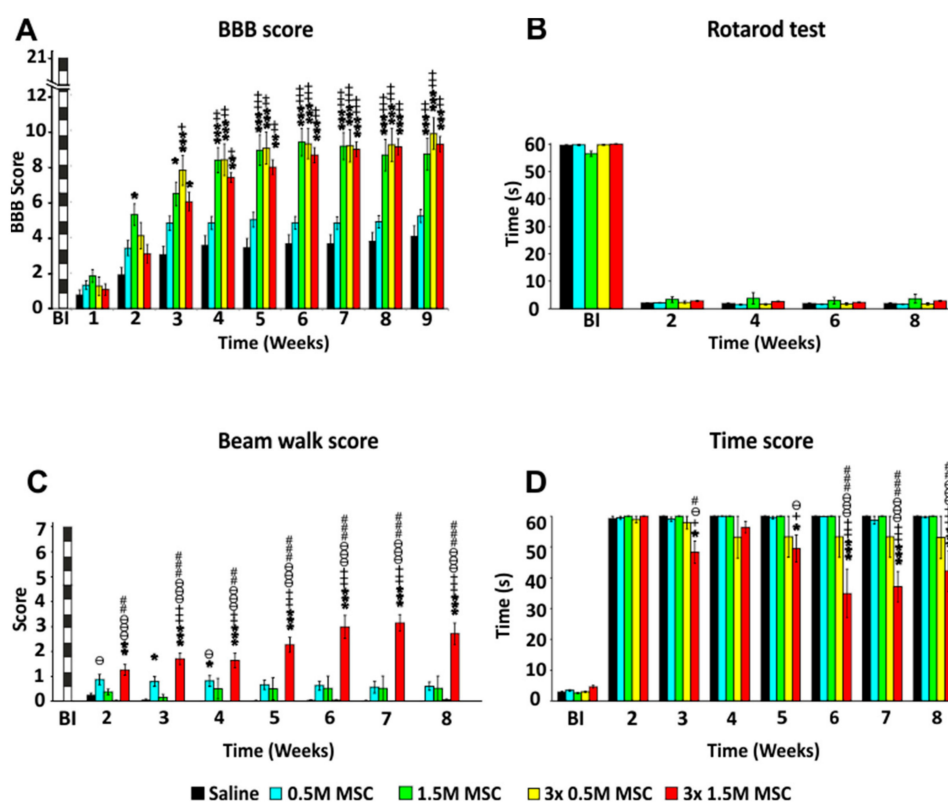


**Figure 1.** Recovery of locomotor functions following hWJ-MSCs transplantation after SCI. Treatments by a different number of administrated cells. The locomotor skills of saline- or stem cell-treated rats were measured using the BBB (A), rotarod (B), beam walk score (C), and time score (D). Animals treated with a higher single dose and by repetitive dose of hWJ-MSCs achieved significantly higher scores in the open-field BBB test when compared to saline controls and animals treated by 0.5 M hWJ-MSCs (A). Strength and limb coordination was measured by rotarod test (B), where no significant differences were found. The flat beam test (C), which is focused on advanced locomotor skills, demonstrated significantly higher scores in the group treated by  $3 \times 1.5$  M hWJ-MSCs. Time score (D) reflects the time the rat needs to cross the beam and shows the overall stability of the rat. Animals treated by  $3 \times 1.5$  M achieved significantly better times than the rest of the rats. \*  $p < 0.05$  versus saline; \*\*  $p < 0.01$  versus saline; \*\*\*  $p < 0.001$  versus saline; +  $p < 0.05$  versus 0.5 M MSCs; ++  $p < 0.01$  versus 0.5 M MSCs; +++  $p < 0.001$  versus 0.5 M MSCs; #  $p < 0.05$  versus  $3 \times 0.5$  M MSCs; ##  $p < 0.01$  versus  $3 \times 0.5$  M MSCs; ###  $p < 0.001$  versus  $3 \times 0.5$  M MSCs;  $\theta$   $p < 0.05$  versus 1.5 M MSCs;  $\theta\theta$   $p < 0.01$  versus 1.5 M MSCs;  $\theta\theta\theta$   $p < 0.001$  versus 1.5 M MSCs. BBB = Basso, Beattie, and Bresnahan test; BI = before injury; MSC = human Wharton Jelly mesenchymal stem cell; SCI = spinal cord injury.

In addition to the beam score, we measured the time needed to cross the beam (maximally for 60 s). During the pre-training, healthy rats were able to cross the beam in approximately 3.0 s (Figure 1D). The measurement was performed weekly starting the second week after SCI. Two weeks after SCI not all the rats were able to cross the beam and did not move from the starting line. In the following weeks,

a significant improvement was observed between the rats treated by  $3 \times 1.5$  M and the other groups. The best score was achieved in the sixth week in the group  $3 \times 1.5$  M, when rats traversed the beam at an average time of  $34.9 \pm 7$  s.

(Two-way RM ANOVA, Treatment;  $F = 5.001$ ,  $p = 0.002$ ; for  $p$  values of post hoc pair-to-pair test, see Supplement 2).

### 2.3. Histology and Immunohistochemistry

#### 2.3.1. Gray and White Matter Sparing

The total area of spared gray/white matter was measured on the 15 cross sections of the spinal cord 9 weeks after the SCI (7 sections cranially and caudally to the center of the lesion, which was determined as the section with the smallest area of the residual spinal cord tissue). Values were averaged and compared to the control, which was set as 100%. Concerning the gray matter preservation (Figure 2A), a significant difference was found between the group  $3 \times 1.5$  M and the control ( $p < 0.05$ ), and a strong trend was observed when compared to the group of 0.5 M ( $p = 0.051$ ). Comparison of the white matter sparing showed no significant difference between the groups as a whole (Figure 2B). Similarly to the gray matter, in the center of the lesion and in the surrounding tissue, we observed significantly more spared white matter in animals treated with  $3 \times 1.5$  M and 1.5 M when compared to the control group and rats treated with 0.5 M.

(Two-way RM ANOVA, Treatment; gray matter –  $F = 3.341$ ,  $p = 0.03$ , white matter –  $F = 1.290$ ,  $p = 0.307$ ; for  $p$  values of post hoc pair-to-pair test, see Supplement 3).

#### 2.3.2. Astrogliosis and Distribution of Protoplasmic Astrocytes

The total area of the glial scar formed around the central cavity was measured on 15 GFAP-CY3 stained cross sections of the spinal cord 9 weeks after the SCI (7 sections cranially and caudally to the center of the lesion, which was determined as the section with the smallest area of the residual spinal cord tissue). Values were averaged and are presented as a ratio of scar tissue to the whole section in percentages (Figure 2C). Groups treated with  $3 \times 1.5$  M as well as  $3 \times 0.5$  M and 1.5 M had a significantly smaller GFAP positive area around the main cavity compared to the control group ( $p < 0.05$ ). The group treated by 0.5 M showed no significant difference compared to saline-treated rats.

(Two-way RM ANOVA, Treatment;  $F = 4.026$ ,  $p = 0.015$ ; for  $p$  values of post hoc pair-to-pair test, see Supplement 3).

On the same slices, the number of protoplasmic astrocytes was counted (Figure 2D). Rats treated by  $3 \times 0.5$  M and 1.5 M as well as  $3 \times 1.5$  M had a significantly lower number of protoplasmic astrocytes compared to the control group.

(Two-way RM ANOVA, Treatment;  $F = 3.997$ ,  $p = 0.015$ ; for  $p$  values of post hoc pair-to-pair test, see Supplement 3).

#### 2.3.3. Axonal Sprouting

Axonal sprouting was determined as the number of GAP43<sup>+</sup> fibers, which were manually counted on the 15 cross sections of the spinal cord 9 weeks after the SCI (7 sections cranially and caudally to the center of the lesion, which was determined as the section with the smallest area of the residual spinal cord tissue). Values were averaged and compared to the control, which was set as 100%. The significant effect of the cell treatment was not only dose-dependent, but further improved after repeated application (Figure 2E). Treatment with the lowest dose—0.5 M, had no or minimal effect on axonal sprouting ( $102 \pm 4\%$ ). In the other cell-treated groups, the number of positive fibers was gradually increasing with the higher number of grafted cells (1.5 M  $140 \pm 4\%$ ), and repeated application had a significantly stronger effect than a single dose ( $3 \times 0.5$  M  $168 \pm 10\%$ ) and ( $3 \times 1.5$  M  $212 \pm 18\%$ ) ( $p < 0.05$ ).

(One-way ANOVA, Treatment;  $H_4 = 21.844$ ,  $p < 0.001$ ).



2.4. qRT-PCR

Expression of Intrinsic Genes after Stem Cell Transplantation, after SCI

Samples from the spinal cord for qPCR analysis were taken 4 (Figure 3A) and 9 weeks (Figure 3B) after the cell transplantation. A comparison was made against the saline-treated rats, which were set as 0. The expression of genes, which are related to the M1 (*Irf5*, *Cd86*) and M2 (*Mrc1*, *Cd163*) macrophage phenotypes, astrogliosis (*Gfap*), and apoptosis (*Casp3*), was analyzed. Pro-inflammatory genes *Irf5* and *CD86* were, 4 weeks after the transplantation of the cells, insignificantly upregulated in the groups treated by 1.5 M and 3 × 0.5 M but, 9 weeks after the transplantation, were downregulated in all groups except the 3 × 0.5 M. Statistical significance against the saline group was found only in the group 3 × 1.5 M ( $p < 0.05$ ).

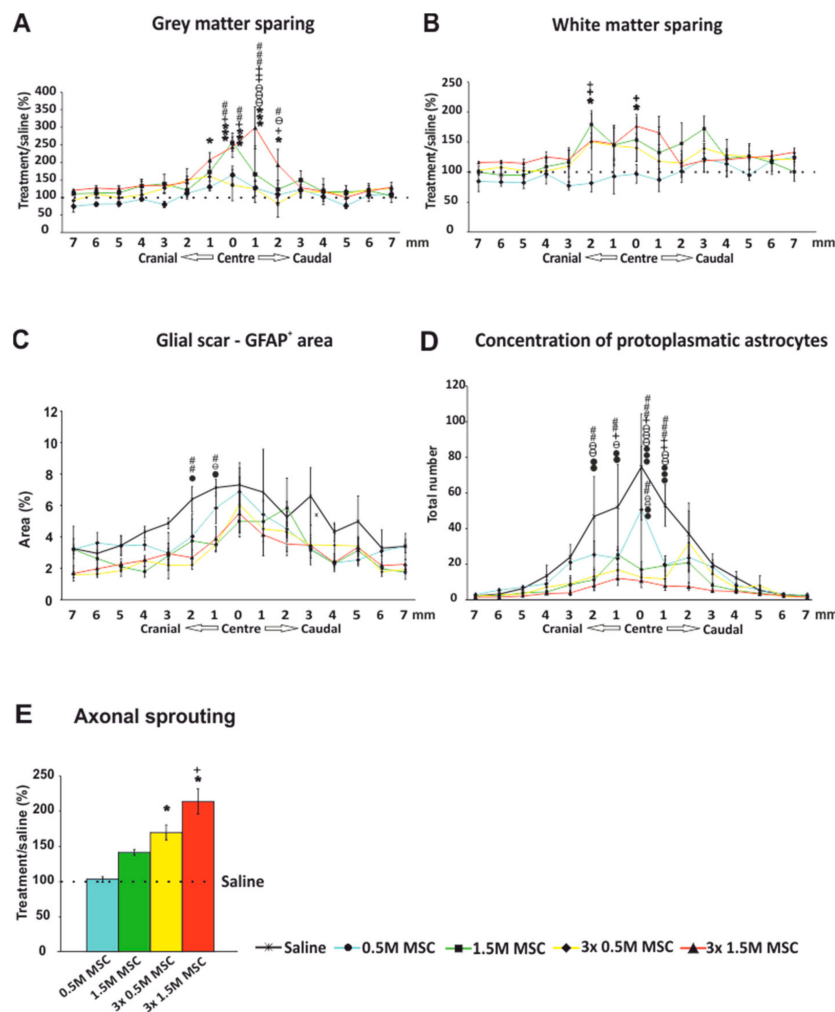


**Figure 2.** Immunohistochemical and histological analysis 9 weeks after SCI. The total area of spared gray matter was significantly higher in the group treated by 3 × 1.5 M hWJ-MSCs, mainly in the slices near the center of the lesion (A). Analysis of the white matter sparing showed similar results to the gray matter, resulting in mild yet still significant preservation in the group treated by 3 × 1.5 M hWJ-MSCs (B). The GFAP-CY3 positive area showing the glial scar formation around the central cavity was slightly smaller in all treated groups compared to the control, with a significant difference near the center of the lesion against the groups treated by repetitive doses (C). The average number of protoplasmic astrocytes near the center of the lesion was significantly higher in the control group than in the cell-treated groups (D). The average number (15 slices per rat; 5 rats) of GAP43+ fibers presented as relative when compared to the control, which is set as 100%. A gradually significant increase with the total number of applied MSCs is shown (E).

The dotted line represents the value of saline-treated rats (100%). \*  $p < 0.05$  versus saline; \*\*\*  $p < 0.001$  versus saline; +  $p < 0.05$  versus 0.5 M MSCs; ++  $p < 0.01$  versus 0.5 M MSCs; +++  $p < 0.001$  versus 0.5 M MSCs; #  $p < 0.05$  versus 3 × 0.5 M MSCs; ##  $p < 0.01$  versus 3 × 0.5 M MSCs; ###  $p < 0.001$  versus 3 × 0.5 M MSCs; ø  $p < 0.05$  versus 1.5 M MSCs; øø  $p < 0.01$  versus 1.5 M MSCs; øøø  $p < 0.001$  versus 1.5 M MSCs; •  $p < 0.05$  versus 3 × 1.5 M MSCs; ••  $p < 0.01$  versus 3 × 1.5 M MSCs; •••  $p < 0.001$  versus 3 × 1.5 M MSCs. MSCs = human Wharton Jelly mesenchymal stem cells; SCI = spinal cord injury; GFAP-CY3 = glial fibrillary acidic protein cyanine 3; GAP43 = growth-associated protein 43.

The anti-inflammatory related genes *Mrc1* and *Cd163* were, 9 weeks after the transplantation, downregulated in all subjected groups with a significant difference in groups 1 × 0.5 M ( $p < 0.05$ ) and 3 × 1.5 M ( $p < 0.001$ ). However, groups treated by a total number of 1.5 M cells (1.5 M and 3 × 0.5 M) were, 4 weeks after transplantation, insignificantly upregulated; thus, their dynamics changed throughout the experiment.

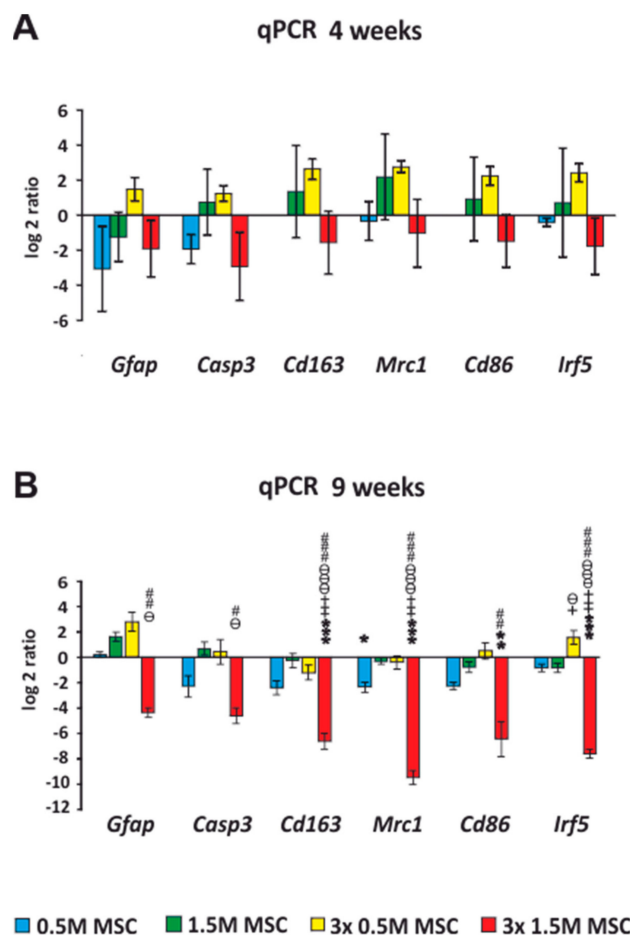


**Figure 3.** mRNA expression of selected genes 4 and 9 weeks after WJ-MSCs transplantation into the SCI. The graphs show the log<sub>2</sub>-fold changes of the  $\Delta\Delta C_t$  values of the indicated genes in comparison to the animals treated with the saline, which were set to 0 and are represented as x axis in the graphs. The expression of genes, which are related to the M1 (*Irf5*, *Cd86*) and M2 (*Mrc1*, *Cd163*) macrophage phenotypes, astrogliosis (*Gfap*), and apoptosis (*Casp3*) are shown 4 weeks after the SCI (A) and 9 weeks after the SCI (B). All of them were significantly downregulated in the group treated by 3 × 1.5 M and remained stable throughout the whole experiment.

Data are expressed as mean  $\pm$  SEM. \*  $p < 0.05$  versus saline; \*\*  $p < 0.01$  versus saline; \*\*\*  $p < 0.001$  versus saline; +  $p < 0.05$  versus 0.5 M MSCs; ++  $p < 0.01$  versus 0.5 M MSCs; +++  $p < 0.001$  versus 0.5 M MSCs; #  $p < 0.05$  versus  $3 \times 0.5$  M MSCs; ##  $p < 0.01$  versus  $3 \times 0.5$  M MSCs; ###  $p < 0.001$  versus  $3 \times 0.5$  M MSCs;  $\theta$   $p < 0.05$  versus 1.5 M MSCs;  $\theta\theta$   $p < 0.01$  versus 1.5 M MSCs;  $\theta\theta\theta$   $p < 0.001$  versus 1.5 M MSCs. MSC: human Wharton Jelly mesenchymal stem cell; SCI: spinal cord injury; *Mrc1*: mannose receptor C type 1; *Casp3*: Caspase-3; *Gfap*: glial fibrillary acidic protein.

Four weeks after the cell implantation, *Gfap*, except in the  $3 \times 0.5$  M group, was downregulated in all groups; 9 weeks after the cell implantation, it remained downregulated only in the  $3 \times 1.5$  M group, with a significant difference that corresponds with the immunohistochemical analysis of the astrogliosis that was lowest in this group. The expression of *Casp3* insignificantly decreased in the 0.5 M and  $3 \times 1.5$  M groups and remained stable throughout the entire experiment.

(One-way ANOVA, Treatment; *Gfap* –  $H_4 = 18.454$ ,  $p = 0.001$ , *Casp3* –  $H_4 = 15.153$ ,  $p = 0.004$ , *Cd163* –  $F = 20.243$ ,  $p < 0.001$ , *Mrc1* –  $F = 59.317$ ,  $p < 0.001$ , *Cd86* –  $H_4 = 19.170$ ,  $p < 0.001$ , *Irf5* –  $F = 47.495$ ,  $p < 0.001$ ; for  $p$  values of post hoc pair-to-pair test, see Supplement 4).

### 2.5. Cell Survival

Survival of the transplanted cells (0.5 M and 1.5 M) was evaluated by staining with the antibody against HuNu, two weeks after the transplantation. Surviving cells were detected as green clusters. Most of the cells remained at the site of the implantation—caught between the folds of arachnoidea mater in the cauda equinae. There was, however, a difference in the number of cells present. While after 0.5 M application only a few cells were detected, the application of 1.5 M resulted in a greater number of trapped cells. No homing into the lesion site was observed.

## 3. Discussion

The present study aimed to determine the effect and optimal dosage of transplanted stem cells derived from Wharton's jelly into injured spinal cord. Cultured human WJ-MSCs were intrathecally implanted into spinal cord compression lesions of Wistar rats, and the impact on the recovery of the spinal cord tissue was described.

We compared single and triple repeated intrathecal delivery of hWJ-MSCs with a different number of cells (0.5 M and 1.5 M) in each application. Since cell survival in the vertebral canal is rather low [20,22,23], we hypothesized that, by repeated application, the trophic and immunomodulatory effect of the cells can be substantially increased. The route of MSC delivery varies in previous studies, and local or systemic approaches have been proposed and investigated, but the optimal method of delivery has yet to be determined.

We have chosen intrathecal delivery in our experiments. It eliminates the risk of direct surgical implantation without the need for deep analgesia and anaesthesia for the animal, and yet still guarantees a wide dissemination of cells through the subarachnoid space and around the lesion site [24]. The procedure can be done either by lumbar puncture or by suboccipital puncture of the cisterna magna. In our study, we chose lumbar puncture because it is more relevant to clinical medicine, where, especially in adult neurosurgery, it is an everyday occurrence. Additionally, repeated application via lumbar puncture is a lesser burden for animals than a suboccipital puncture of the cisterna magna. Since cell survival in the vertebral canal is rather low (approximately 14 days), repeated application substantially increased the trophic and immunomodulatory effect of the cells and could even be feasible in human patients.

Despite reports showing that intralesional transplantation provides better accumulation of the effector cells in the injury site [25], meta-analyses did not prove any statistical significant differences in locomotor improvement after delivery of MSCs using intravenous, intraparenchymal, and intrathecal administration [15,26]. Moreover, Pal et al. compared hBM-MSC injection into the spinal cord parenchyma and application via lumbar puncture. They reported that, while both i.t. and



intraspinal transplantation showed improvement in histological evaluation, only the i.t.-transplanted group performed better in all behavioral tests [27]. Recently intranasal delivery of BM-MSCs with their successful migration into the spinal cord canal was reported, but compared to direct intrathecal delivery, there was significantly lower number of cells detected and the locomotor recovery was insignificant [28].

Besides the determination of transplantation route, optimal timing of transplantation is one of the most important factors to be considered. The subacute phase, defined as the time period between 3 and 14 days post-SCI in rodents and 2 months in humans showed better cell survival as a result of the reduced aggressive host environment due to the inflammation response, and when compared to the acute phase and unlike the chronic phase, the glial scar formation has not yet been formed [18,29,30]. Therefore, we had cell application start 7 days after lesion induction. Another disputable question remains regarding the appropriate dosage of transplanted cells. The vast majority of studies proving the effect of MSCs on SCI have focused only on single transplantation of 0.2–1 M of cells [31–35]. Alternatively, repetition and higher dosage is considered to be superior to single delivery. Li et al. compared single, triple, and quintuple transplantations of 1 M BM-MSCs and concluded that triple delivery is the best [36]. Similar results were found by Cizkova et al. with the conclusion that high doses and/or repetition of the transplantation may lead to higher efficacy of cell survival, more engraftment into the host tissue, and an improvement in functional outcome.

No such experimental study with hWJ-MSCs has been conducted, so evidence of the effect of single vs. multiple deliveries, together with various amounts of cells, is in high demand.

Analysis of behavioral tests revealed that functional recovery of hind limb motion in treated rats was partially dependent on the number of applied cells, which is in agreement with findings by Himes et al., who used a similar number of hBM-MSCs [32]. Whereas the single dose of 0.5 M hWJ-MSCs showed no significant difference in BBB testing, other groups achieved similar significantly higher scores, regardless of repeated application. However, in the advanced motor function testing, such as crossing the beam, the effect was visible in animals with repeated injections. The dose-dependent effect of hBM-MSCs in more advanced motor tests (grid walk and inclined plane test) was also observed by Pal et al. who compared doses of 2 M and 5 M cells/kg body weight [27]. No effect was detected in the rotarod test, which requires a higher level of motor coordination and stepping. Our experimental setting was comparable to our previous study with the hBM-MSCs [20]. However, application of 0.5 M hBM-MSCs resulted in functional improvement similar to the one observed with single application of 1.5 M hWJ-MSCs. It is generally accepted that, due to the low ability of MSCs to survive in the donor tissue, as confirmed in our study, and their limited *in vivo* differentiation, the main therapeutic effect of MSCs lies in their ability to secrete trophic factors promoting local neovascularization, inhibiting cell death, and suppressing the immune response [37]. We did not perform any *in vitro* analysis of growth factors and bioactive molecules, which would compare the paracrine effect of hWJ-MSCs and hBM-MSCs. Though various studies include the analysis of secretory factors, results are not unified in terms of the strength of secretion of regeneration-associated neurotrophic factors. Balasubramanian et al. found that WJ-derived cells secreted higher levels of neurotrophic factors bFGF, NGF, NT3, NT4, and GDNF compared to BM and adipose tissue (AT)-derived cells [38]. Hsieh and colleagues compared MSCs derived from Wharton's jelly and bone marrow regarding their ability to regenerate infarcted myocardia; they described secretome differences that make Wharton's jelly-derived MSCs a more angiogenic, neuroprotective, and neurogenic option [39]. On the other hand, Amable et al. reported that WJ-MSCs secreted very low concentrations of VEGF-4.070 and 4.614 times lower than BM- and adipose tissue MSCs (AT-MSCs), respectively [10]. Most studies agree that hWJ-MSCs have a more effective immunosuppressive function compared to hBM-MSCs [40,41]. However, all those studies were performed *in vitro*, where the proliferation rate of the WJ-MSCs (cell doubling time 40 h) is much higher than the hBM-MSC doubling time of 70 h [42], resulting in more paracrine effective cells in the medium and thus higher overall secretome. Our results confirmed relatively short population doubling

time of hWJ-MSCs, which was approximately 34 h compared to 84 h of hBM-MSCs (see Supplement 1, Figure S1). Another possible explanation of the lesser effect of the same number of transplanted cells in our study is the smaller size of WJ-MSCs when compared with BM-MSCs, which can result in higher dilution in the host environment, or even leakage through the canal after the lumbar puncture. On the other hand, due to a smaller size, more cells can fit into small volumes and these cells can more easily spread through the CSF in the canal. Therefore, the dose-dependent effect can be more visible in the case of hWJ-MSCs than in hBM-MSCs.

Immunohistochemical analyses showed that transplantation of hWJ-MSCs facilitates axonal sprouting and plays a role in decreasing glial scar formation. Astrogliosis, which is closely bound up with reactive astrocytes was significantly less present in cell-treated rats. Axonal sprouting was increasingly enhanced as the total number of transplanted cells increased. This is in agreement with the findings of Li et al., who described the effect of WJ-MSCs in SCI as mainly due to the decreased expression of interleukin-1 $\beta$  (IL-1 $\beta$ ) and the increased expression of nerve growth factor (NGF), which plays an important role in axonal growth [43]. The same trend was present in the measuring of the white and gray matter preservation, which revealed a strong neuroprotective effect in gray matter, mainly in the center of the lesion and only in groups with the highest number of treated cells. A significant effect on tissue sparing was observed only in animals treated by single or triple implantation of 1.5 M hWJ-MSCs. All these findings are in contrast with behavioral analysis, where no differences between higher dosage cell-treated animal groups were found in the BBB test. It is evident that, for the simple locomotor test, such as the BBB test, a threshold of a minimum number of cells is required to trigger functional improvement. However, closer analyses of tissue microstructure have shown that an increased number of cells applied repeatedly further improve the neuroprotective and neuroregenerative properties of the hWJ-MSCs.

Overall, our results proved a substantial benefit from treatment of SCI with MSCs and are in many ways comparable to other studies that used human BM-MSCs, AT-MSCs, or UC-MSCs in rats [27,32,35,44–49] or dogs [50,51]. Meta-analysis from 2014 by Oliveri confirmed the beneficial effect of MSCs in traumatic spinal cord injury but could not detect any clear association between locomotor recovery and MSCs isolated from specific tissues [15]. Still, because of the relative easy harvesting of hWJ-MSCs from otherwise discarded tissue, we believe that hWJ-MSCs are the most suitable for potential wide use in clinics.

Most of the clinical studies with mesenchymal stromal stem cells were performed on chronic lesions with total paraplegia (Frankel A, AIS A), lasting months after the primary injury [52]. Despite some reports that note some neurological improvement after transplantation [53], the effect of WJ-MSCs in the chronic model of SCI must be elucidated. However, we suggest that this treatment should be proposed for patients with spinal trauma that causes “only” compression of the spinal cord, which is visible in the magnetic resonance imaging (MRI) of T2 and STIR sequences as a hyper intense area of the spinal cord—myelopathy. These patients usually have preserved residual motor and sensory functions (Frankel B and above) and have a good prognosis of recovery when the best medical therapy is applied. hWJ-MSCs, since they are allogenic, can be easily up-scaled, prepared in advance, cryopreserved, and made ready for use in a relatively short time. Therefore, repeated application of hWJ-MSCs could add another piece to the yet unsolvable puzzle of how to treat SCI.

## 4. Materials and Methods

### 4.1. Cell Culture

The collection and isolation of WJ-MSCs were performed by explant culture according to the methodology described by Koci et al. [54]. In brief, human WJ-MSCs were obtained from discarded human umbilical cords from healthy full-term neonates after spontaneous delivery, with the informed consent of the donors using the guidelines approved by the Institutional Committee at University Hospital (Pilsen, Czech Republic). About 10–15 cm per umbilical cord were aseptically

transported into sterile phosphate buffered saline (PBS; IKEM, Prague, Czech Republic) with antibiotic-antimycotic solution (Sigma, St. Louis, MO, USA) at 4 °C. After the removal of blood vessels, the remaining tissue was cut into small pieces (cca 1 mm<sup>3</sup>) and put into Nunc culture dishes (Schoeller, Thermo Fisher Scientific, Waltham, MA, USA) containing the alpha-Minimum Essential Medium ( $\alpha$ MEM; East Port, Prague, Czech Republic), supplemented with 5% platelet lysate (IKEM, Prague, Czech Republic) and gentamicin 10 mg/mL (Sandoz, Holzkirchen, Germany), and cultivated at 37 °C in a humidified atmosphere containing 5% CO<sub>2</sub>. After 10 days, the explants were removed from the culture dishes, and the remaining adherent cells were cultured for 3 weeks or until 90% confluence and passaged using 0.05% Trypsin/EDTA (Life Technologies, Carlsbad, CA, USA). After passaging, the cells were seeded into culture flasks (Nunc; Schoeller, Thermo Fisher Scientific, Waltham, MA, USA) at a density of  $5 \times 10^3$  cells/cm<sup>2</sup>. The medium was changed twice a week. Cells of the 3rd passage were characterized by flow cytometry and their growth properties and differentiation potential was assessed (see Supplementary Material 1). For the transplantation, cells in the 3rd passage were used.

#### 4.2. Animals

As an experimental model, adult Wistar male rats were used. Animals were obtained from the breeding facility of the Academy of Sciences of the Czech Republic. All experiments were performed in accordance with the European Communities Council Directive of 22nd of September 2010 (2010/63/EU) regarding the use of animals in research and were approved 8 September 2014 by the Professional Committee for Laboratory Animal Welfare of the Institute of Experimental Medicine, Academy of Sciences of the Czech Republic in Prague as the experimental project number 53/2014. All animals were approximately 10 weeks old, with weight varying between 275–305 g ( $n = 90$ ). The first group of animals ( $n = 47$ ), surviving 9 weeks, was used for behavioral testing, histological, immunohistochemical, and qPCR analysis (9W). The second group of animals ( $n = 39$ ) was used for qPCR evaluation 4 weeks (4W) after SCI and was not included in behavioral testing. An additional four animals in the two groups ( $n = 4$ ) were used for evaluation of surviving cells two weeks after transplantation of 0.5 and 1.5 M hWJ-MSCs.

#### 4.3. Spinal Cord Injury Model

The surgical procedure was performed in an operating theatre under standard conditions. As a model of SCI, a balloon-induced ischemic-compression lesion was used [21,55]. At the beginning of the surgery, the animals were anesthetized with Isoflurane (Forane; Abbott Laboratories, Queenborough, UK), analgesia was induced by intramuscular injection of carprofen (Rimadyl, Cymedica, Horovice, Czech Republic, 4 mg/kg), and surgical prophylaxis was maintained by intramuscular injection gentamicin sulfate (Sandoz, Holzkirchen, Germany 5 mg/kg). After the skin incision, the paravertebral muscles were separated at the level of thoracic vertebra T7–T12 and laminectomy of T 10 was performed. A sterile 2-french Fogarty catheter was carefully inserted into the epidural space until the center of the balloon rested on the level of thoracic vertebra 8 (T8). The balloon was rapidly inflated with 15  $\mu$ L saline and kept for 5 min. During this procedure, 3% isoflurane in air was administered at a flow rate of 0.3 L/min, and the animal's body temperature was kept at 37 °C with a heating pad. After 5 min, the catheter was rapidly deflated and removed, and separated muscles and incised skin were sutured by single non-absorbable stitches. The lesioned animals were assisted in feeding and urination until they had recovered sufficiently to perform these functions on their own. The animals received gentamicin sulfate (5 mg/kg) for 7 days to prevent postoperative infections and were allowed to feed and drink ad libitum.

#### 4.4. Transplantation

Transplantation of hWJ-MSCs was performed on the 7th, 14th, and 21st day after the SCI. Treatment was given intrathecally by a lumbar puncture between L3 and L4 or L4 and L5 through



a 25 G needle under the short-time general anaesthesia described above. Firstly, a small volume of CSF was taped as a proof of the subarachnoid space. During the injection of the saline with hWJ-MSCs there was a movement of the rats tail as a response to irritation of the nerve roots of cauda equina. After injection the needle was rested in situ for 30 s to prevent backflow of the content. Animals were divided into 5 groups with variable treatment. The first group (**0.5 M**) received a single transplantation of 0.5 M hWJ-MSCs in 50  $\mu$ L saline on the 7th day after SCI ( $n = 12$ ). The second group (**1.5 M**) received a single transplantation of 1.5 M hWJ-MSCs in 50  $\mu$ L saline on the 7th day after SCI ( $n = 9$ ). The third group (**3  $\times$  0.5 M**) received a triple transplantation of 0.5 M hWJ-MSCs in 50  $\mu$ L saline on the 7th, 14th, and 21st day after SCI ( $n = 8$ ). The fourth group (**3  $\times$  1.5 M**) received a triple transplantation of 1.5 M hWJ-MSCs in 50  $\mu$ L saline on the 7th, 14th, and 21st day after SCI ( $n = 7$ ). The control group (**saline**) received a single or triple injection of 50  $\mu$ L saline on the 7th (14th and 21st) day after SCI ( $n = 11$ ). No differences between simple and repetitive transplantation of the saline were found, so the results were pooled together as a single control when compared with other types of treatment. The day before the transplantation, all animals received cyclosporine A by an intraperitoneal injection (10 mg/kg), which continued daily until the end of the experiment.

#### 4.5. Behavioral Analysis

##### 4.5.1. BBB Test

The BBB open field test, originally described by Basso, Beattie, and Bresnahan [56] was used to assess the joint movement, weight support, forelimb-hindlimb coordination, paw placement and stability of the body. The rats were placed on the floor surrounded by boundaries making a rectangular shape. Results were evaluated in the range of 0–21 points: 0 indicated complete lack of motor capability and 21 indicated the best possible score (healthy rat). Measurements were performed every week for 8 weeks starting the first week after SCI.

##### 4.5.2. Rotarod Test

A rotarod unit machine (Ugo Basile, Comerio, Italy) was used to test the advanced degree of motor coordination of the limbs according to the method first described by Dunham and Miya [57]. Ability to balance on a rotating rod was recorded. Each animal was taught this task one week before surgery. Animals were placed on a rotating rod at a fixed speed of 10 rpm before surgery and 5 rpm after surgery and were left to walk for 60 s. There were four trials per day within five consecutive days. Between trials there was always a 5 min break. The latency to fall off the rod onto the floor was measured.

##### 4.5.3. Beam Walk Test

In the flat beam test, we tested the ability to cross a 1 m long narrow beam with a flat surface. Rats were placed on one side of the beam, and on the other side an escape box was placed. The latency and the trajectory to traverse the beam were recorded by a video tracking system (TSE-Systems Inc., Bad Homburg, Germany) for a maximum of 60 s. Performance of locomotor coordination was evaluated using a 0–7 point scale modified from Metz and Wishaw [58].

#### 4.6. Histological and Immunohistochemical Analyses

At the end of the experiment (9 weeks after the SCI), all animals were anesthetized with ketamine (100 mg/kg) and xylazine (20 mg/kg) and transcardially perfused with a phosphate buffer solution (250 mL), followed by a 4% paraformaldehyde solution in a phosphate buffer (250 mL). The spinal cord was dissected and removed from the spinal column and embedded in paraffin wax. Serial cross sections (5  $\mu$ m thick) were obtained by microtome within a 2-cm-long segment around the center of the lesion. Samples of five animals from each group were analyzed for the total volume of spared white and gray matter, axonal sprouting, and the extent of glial scar. Sections were stained with Luxol fast

blue and Cresyl violet to distinguish the white and gray matter, with anti-GAP43 antibody to evaluate axonal sprouting or by anti-GFAP primary antibody to visualize the glial scar and reactive astrocytes.

#### 4.6.1. Cresyl Violet-Luxol Staining

For visualizing white and gray matter of the spinal cord, Cresyl violet and Luxol fast blue staining were used. Samples from five animals from each group were obtained. Each sample of the spinal cord was cut at 1 mm intervals. A total number of 15 cross sections, including the center of the lesion, were observed with an Axioskop 2 plus microscope (Zeiss, Oberkochen, Germany). Acquired images were analyzed for the total area of spared gray and white matter by ImageJ software (NIH, Bethesda, MD, USA) (Figure 4A).

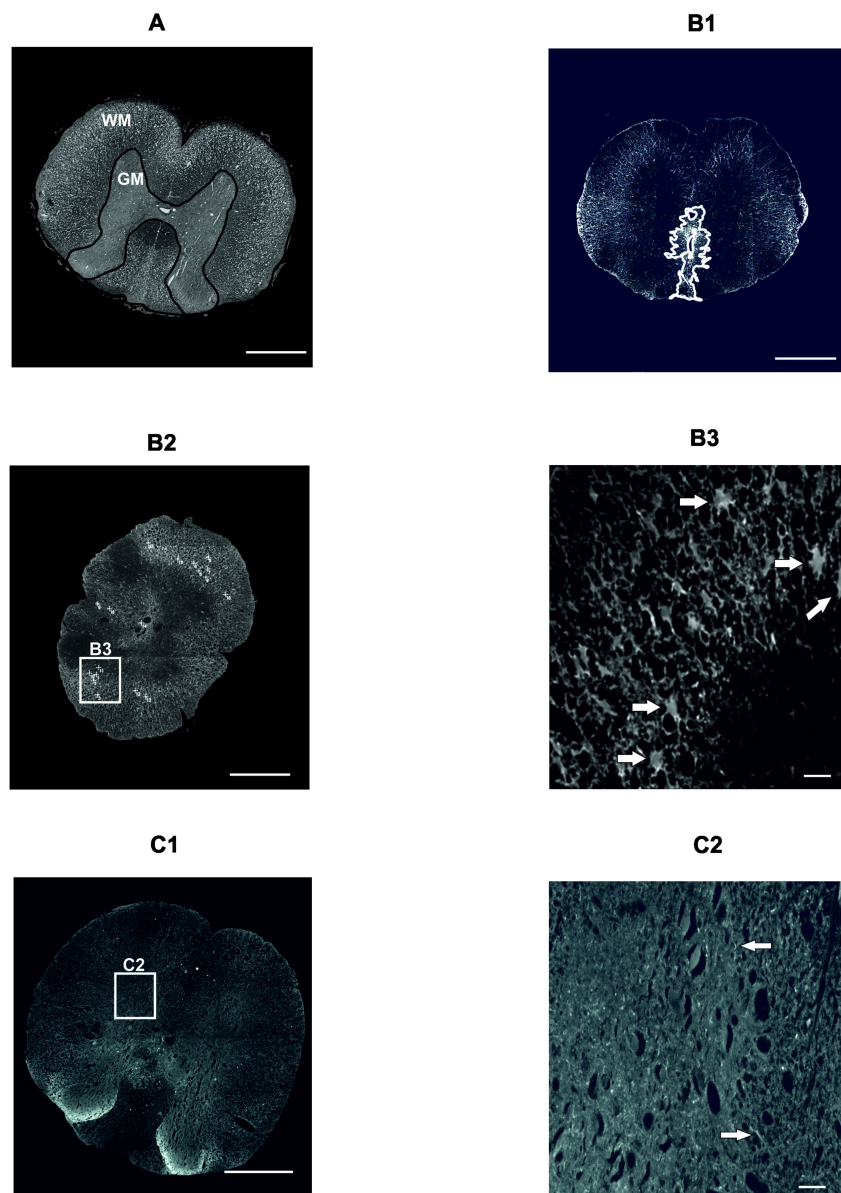


**Figure 4.** Illustrative images of morphometric and immunohistochemical analyses 9 weeks after SCI. Microscopic image of a section stained with Cresyl violet and Luxol fast blue to distinguish the white (WM) and gray (GM) matter (A). Scale bar: 500  $\mu\text{m}$ . The marked glial scar around the main cavity (B1) and the total number of protoplasmic astrocytes (B2) with a detailed inset (B3) from slices stained with GFAP-CY3. Scale bars: 500  $\mu\text{m}$  (B1,B2), 10  $\mu\text{m}$  (B3). Illustrative image of a section labeled with a GAP43<sup>+</sup> antibody (C1) with a detailed inset (C2).

Arrows point at GAP43<sup>+</sup> fibers, which were manually counted as described in the Methods section. Scale bars: 500  $\mu\text{m}$  (C1), 20  $\mu\text{m}$  (C2). SCI: spinal cord injury; GM: gray matter; WM: white matter; GFAP-CY3: glial fibrillary acidic protein cyanine 3; GAP43: growth-associated protein 43.

#### 4.6.2. GFAP Staining

To determine the extent of the glial scar, immunohistochemical analysis of a CY3-conjugated primary antibody against GFAP (Sigma, St. Louis, MO, USA) was used. Samples from five animals from each group were obtained. Each sample of the spinal cord was cut at 1 mm intervals. A total number of 15 cross sections, including the center of the lesion, was observed with an Axioskop 2 plus microscope (Zeiss, Oberkochen, Germany). The acquired images were analyzed using ImageJ software (NIH, Bethesda, MD, USA). The GFAP positive area around the central cavity (Figure 4(B1)) together with the number of protoplasmic astrocytes (Figure 4(B2,B3)) was measured on each section.

#### 4.6.3. GAP43 Staining

The newly sprouted axons were visualized immunohistochemically using a primary antibody against GAP43 (Millipore, Billerica, MA, USA). Samples from five animals from each group were obtained. Each sample of the spinal cord was cut at 1 mm intervals. A total number of 15 cross sections, including the center of the lesion, were observed with an Axioskop 2 plus microscope (Zeiss, Oberkochen, Germany). The acquired images were analyzed and the number of GAP43-positive fibers per section was manually counted (Figure 4(C1,C2)).

#### 4.7. qRT-PCR

To evaluate the up- or downregulation of expression rat target genes (*Gfap*, *Mrc1*, *Irf5*, *Cd163*, *Cd86*, *Casp3*) the quantitative real-time reverse transcription polymerase chain reaction (qRT-PCR) was used. Expression was evaluated at 4 and 9 weeks after hWJ-MSC administration (five animals from each group). Studied RNA was isolated from the paraffin cross sections of injured spinal cord around the center of the lesion using the High Pure RNA Paraffin Kit (Roche, Penzberg, Germany) following the manufacturer's recommendations. The amount of RNA was measured by a spectrophotometer (NanoPhotometer™ P-Class, Munchen, Germany). cDNA was obtained from the isolated RNA by a reverse transcription using the Transcriptor Universal cDNA Master (Roche), and a thermal cycler (T100™ Thermal Cycler, Bio-Rad, Hercules, CA, USA). The qPCR chain reactions were performed using cDNA solution, FastStart Universal Probe Master (Roche, Penzberg, Germany) and the following TagMan® Gene Expression Assays (Life Technologies): *Casp3*/Rn00563902\_m1, *Gfap*/Rn00566603\_m1, *Cd86*/Rn00571654\_m1, *Irf5*/Rn01500522\_m1, *Mrc1*/Rn01487342\_m1, and *Cd163*/Rn01492519\_m1.

The final solution of 25 ng extracted RNA diluted in 10  $\mu\text{L}$  of solution was amplified on a StepOnePlus™ real-time PCR cycler (StepOnePlus™, Life Technologies, Carlsbad, CA, USA). The process of amplification was repeatedly performed under the same standard conditions: 120 s at 50 °C, 300 s at 95 °C, followed by 40 cycles of 15 s at 95 °C and 60 s at 60 °C. Each array included also a negative control (water). As a reference gene, *Gapdh* was used. The  $\Delta\Delta\text{Ct}$  method was used for relative quantification of gene expression. All results were analyzed with StepOnePlus® software (StepOnePlus™, Life Technologies, Carlsbad, CA, USA). Differences between the transplanted and control (saline) groups were analyzed for statistical significance with  $\Delta\text{Ct}$  values level, using a one-way ANOVA test with a post hoc pair-to-pair test. Differences were considered statistically significant if  $p < 0.05$ . Data are expressed as the mean  $\pm$  the standard error of mean. The values of saline-treated animals were set as zero.



#### 4.8. Statistical Analyses

Presented graphs with obtained data are shown as the mean  $\pm$  SEM. The statistical significance between the groups treated by WJ-MSCs and the saline (control) group was assessed using either one-way ANOVA, or two-way ANOVA in the case of a second factor (time). Differences between the groups in behavioral tests and in areal measuring of the gray/white matter sparing and GFAP positive area of glial scar were assessed by two-way repeated measurement (RM) ANOVA. The Student–Newman–Keuls (SNK) post hoc pair-to-pair test was used to specify for which groups and at which time points the changes were significant. Statistical evaluation of the expression of the rat target genes was performed with one-way ANOVA test with a post hoc pair-to-pair test. In case of non-parametric values Kruskal–Wallis one-way ANOVA on ranks test was used. (All in Sigmapstat 3.1, Systat Software Inc., San Jose, CA, USA). Differences were considered statistically significant if  $p < 0.05$ .

#### 5. Conclusions

Implantation of human MSCs derived from Wharton’s jelly improves functional outcome, by modulating the inflammatory response, inducing axonal sprouting and remodeling the glial scar. The effect is dose-dependent, with the best result achieved by repeated delivery.

**Supplementary Materials:** Supplementary materials can be found at <http://www.mdpi.com/1422-0067/19/5/1503/s1>.

**Author Contributions:** P.K.: study conception and design, experimentation, collection and/or assembly of data, data analysis and interpretation, manuscript writing, and final approval of the manuscript; I.V.: study conception and design, and provision of study material; J.R.: study conception and design; L.M.U.: study conception and design; K.Z.: collection and/or assembly of data; J.D.: collection and/or assembly of data; Z.K.: collection and/or assembly of data, data analysis and interpretation, and manuscript writing; K.T.: collection and/or assembly of data; S.K.: qRT PCR data analysis and interpretation, manuscript writing; S.R.: study conception and design, and financial support; P.J.: study conception and design, data analysis and interpretation, manuscript writing, financial support, and final approval of the manuscript.

**Acknowledgments:** This study was supported by the Czech Science Foundation GACR P304/12/G069; GACR 17-03765S, Operational Programme Research, Development and Education in the framework of the project “Center of Reconstructive Neuroscience”, registration number CZ.02.1.01/0.0/0.0/15\_003/0000419 and from EATRIS-CZ (LM2015064). K.Z., S.K., I.V., L.M.U. and P.J. were members of the BIOCEV (CZ.1.05/1.1.00/02.0109) and their work was supported by the Ministry of Education, Youth and Sports of CR within the LQ1604 National Sustainability Program II (Project BIOCEV-FAR).

**Conflicts of Interest:** The authors declare no conflict of interest.

#### References

1. Fawcett, J.W.; Asher, R.A. The glial scar and central nervous system repair. *Brain Res. Bull.* **1999**, *49*, 377–391. [[CrossRef](#)]
2. Zai, L.J.; Wrathall, J.R. Cell proliferation and replacement following contusive spinal cord injury. *Glia* **2005**, *50*, 247–257. [[CrossRef](#)] [[PubMed](#)]
3. Mbalaviele, G.; Jaiswal, N.; Meng, A.; Cheng, L.; Van Den Bos, C.; Thiede, M. Human mesenchymal stem cells promote human osteoclast differentiation from CD34+ bone marrow hematopoietic progenitors. *Endocrinology* **1999**, *140*, 3736–3743. [[CrossRef](#)] [[PubMed](#)]
4. Woodbury, D.; Schwarz, E.J.; Prockop, D.J.; Black, I.B. Adult rat and human bone marrow stromal cells differentiate into neurons. *J. Neurosci. Res.* **2000**, *61*, 364–370. [[CrossRef](#)]
5. Toma, C.; Pittenger, M.F.; Cahill, K.S.; Byrne, B.J.; Kessler, P.D. Human mesenchymal stem cells differentiate to a cardiomyocyte phenotype in the adult murine heart. *Circulation* **2002**, *105*, 93–98. [[CrossRef](#)] [[PubMed](#)]
6. Bai, L.; Lennon, D.P.; Eaton, V.; Maier, K.; Caplan, A.L.; Miller, S.D.; Miller, R.H. Human bone marrow-derived mesenchymal stem cells induce th2-polarized immune response and promote endogenous repair in animal models of multiple sclerosis. *Glia* **2009**, *57*, 1192–1203. [[CrossRef](#)] [[PubMed](#)]
7. Park, C.W.; Kim, K.S.; Bae, S.; Son, H.K.; Myung, P.K.; Hong, H.J.; Kim, H. Cytokine secretion profiling of human mesenchymal stem cells by antibody array. *Int. J. Stem Cells* **2009**, *2*, 59–68. [[CrossRef](#)] [[PubMed](#)]

8. Torres-Espin, A.; Corona-Quintanilla, D.L.; Fores, J.; Allodi, I.; Gonzalez, F.; Udina, E.; Navarro, X. Neuroprotection and axonal regeneration after lumbar ventral root avulsion by re-implantation and mesenchymal stem cells transplant combined therapy. *Neurotherapeutics* **2013**, *10*, 354–368. [[CrossRef](#)] [[PubMed](#)]
9. Caplan, A.I. Mesenchymal stem cells: Time to change the name! *Stem Cells Transl. Med.* **2017**, *6*, 1445–1451. [[CrossRef](#)] [[PubMed](#)]
10. Amable, P.R.; Teixeira, M.V.; Carias, R.B.; Granjeiro, J.M.; Borojevic, R. Protein synthesis and secretion in human mesenchymal cells derived from bone marrow, adipose tissue and wharton's jelly. *Stem Cell Res. Ther.* **2014**, *5*, 53. [[CrossRef](#)] [[PubMed](#)]
11. Zhou, C.; Yang, B.; Tian, Y.; Jiao, H.; Zheng, W.; Wang, J.; Guan, F. Immunomodulatory effect of human umbilical cord wharton's jelly-derived mesenchymal stem cells on lymphocytes. *Cell. Immunol.* **2011**, *272*, 33–38. [[CrossRef](#)] [[PubMed](#)]
12. Kim, D.W.; Staples, M.; Shinozuka, K.; Pantcheva, P.; Kang, S.D.; Borlongan, C.V. Wharton's jelly-derived mesenchymal stem cells: Phenotypic characterization and optimizing their therapeutic potential for clinical applications. *Int. J. Mol. Sci.* **2013**, *14*, 11692–11712. [[CrossRef](#)] [[PubMed](#)]
13. Zhang, J.; Li, Y.; Chen, J.; Yang, M.; Katakowski, M.; Lu, M.; Chopp, M. Expression of insulin-like growth factor 1 and receptor in ischemic rats treated with human marrow stromal cells. *Brain Res.* **2004**, *1030*, 19–27. [[CrossRef](#)] [[PubMed](#)]
14. Bao, X.; Wei, J.; Feng, M.; Lu, S.; Li, G.; Dou, W.; Ma, W.; Ma, S.; An, Y.; Qin, C.; et al. Transplantation of human bone marrow-derived mesenchymal stem cells promotes behavioral recovery and endogenous neurogenesis after cerebral ischemia in rats. *Brain Res.* **2011**, *1367*, 103–113. [[CrossRef](#)] [[PubMed](#)]
15. Oliveri, R.S.; Bello, S.; Biering-Sorensen, F. Mesenchymal stem cells improve locomotor recovery in traumatic spinal cord injury: Systematic review with meta-analyses of rat models. *Neurobiol. Dis.* **2014**, *62*, 338–353. [[CrossRef](#)] [[PubMed](#)]
16. Saito, F.; Nakatani, T.; Iwase, M.; Maeda, Y.; Muraio, Y.; Suzuki, Y.; Fukushima, M.; Ide, C. Administration of cultured autologous bone marrow stromal cells into cerebrospinal fluid in spinal injury patients: A pilot study. *Restor. Neurol. Neurosci.* **2012**, *30*, 127–136. [[PubMed](#)]
17. Forostyak, S.; Jendelova, P.; Sykova, E. The role of mesenchymal stromal cells in spinal cord injury, regenerative medicine and possible clinical applications. *Biochimie* **2013**, *95*, 2257–2270. [[CrossRef](#)] [[PubMed](#)]
18. Cizkova, D.; Novotna, I.; Slovinska, L.; Vanicky, I.; Jergova, S.; Rosocha, J.; Radonak, J. Repetitive intrathecal catheter delivery of bone marrow mesenchymal stromal cells improves functional recovery in a rat model of contusive spinal cord injury. *J. Neurotrauma* **2011**, *28*, 1951–1961. [[CrossRef](#)] [[PubMed](#)]
19. Cheng, I.; Mayle, R.E.; Cox, C.A.; Park, D.Y.; Smith, R.L.; Corcoran-Schwartz, I.; Ponnusamy, K.E.; Oshtory, R.; Smuck, M.W.; Mitra, R.; et al. Functional assessment of the acute local and distal transplantation of human neural stem cells after spinal cord injury. *Spine J.* **2012**, *12*, 1040–1044. [[CrossRef](#)] [[PubMed](#)]
20. Urdzikova, L.M.; Ruzicka, J.; LaBagnara, M.; Karova, K.; Kubinova, S.; Jirakova, K.; Murali, R.; Sykova, E.; Jhanwar-Uniyal, M.; Jendelova, P. Human mesenchymal stem cells modulate inflammatory cytokines after spinal cord injury in rat. *Int. J. Mol. Sci.* **2014**, *15*, 11275–11293. [[CrossRef](#)] [[PubMed](#)]
21. Vanicky, I.; Urdzikova, L.; Saganova, K.; Cizkova, D.; Galik, J. A simple and reproducible model of spinal cord injury induced by epidural balloon inflation in the rat. *J. Neurotrauma* **2001**, *18*, 1399–1407. [[CrossRef](#)] [[PubMed](#)]
22. Antonic, A.; Sena, E.S.; Lees, J.S.; Wills, T.E.; Skeers, P.; Batchelor, P.E.; Macleod, M.R.; Howells, D.W. Stem cell transplantation in traumatic spinal cord injury: A systematic review and meta-analysis of animal studies. *PLoS Biol.* **2013**, *11*, e1001738. [[CrossRef](#)] [[PubMed](#)]
23. Ruzicka, J.; Machova-Urdzikova, L.; Gillick, J.; Amemori, T.; Romanyuk, N.; Karova, K.; Zaviskova, K.; Dubisova, J.; Kubinova, S.; Murali, R.; et al. A comparative study of three different types of stem cells for treatment of rat spinal cord injury. *Cell Transplant* **2017**, *26*, 585–603. [[CrossRef](#)] [[PubMed](#)]
24. Amemori, T.; Ruzicka, J.; Romanyuk, N.; Jhanwar-Uniyal, M.; Sykova, E.; Jendelova, P. Comparison of intraspinal and intrathecal implantation of induced pluripotent stem cell-derived neural precursors for the treatment of spinal cord injury in rats. *Stem Cell Res. Ther.* **2015**, *6*, 257. [[CrossRef](#)] [[PubMed](#)]
25. Paul, C.; Samdani, A.F.; Betz, R.R.; Fischer, I.; Neuhuber, B. Grafting of human bone marrow stromal cells into spinal cord injury: A comparison of delivery methods. *Spine* **2009**, *34*, 328–334. [[CrossRef](#)] [[PubMed](#)]

26. Sareen, D.; Gowing, G.; Sahabian, A.; Staggenborg, K.; Paradis, R.; Avalos, P.; Latter, J.; Ornelas, L.; Garcia, L.; Svendsen, C.N. Human induced pluripotent stem cells are a novel source of neural progenitor cells (iNPCs) that migrate and integrate in the rodent spinal cord. *J. Comp. Neurol.* **2014**, *522*, 2707–2728. [[CrossRef](#)] [[PubMed](#)]
27. Pal, R.; Gopinath, C.; Rao, N.M.; Banerjee, P.; Krishnamoorthy, V.; Venkataramana, N.K.; Totey, S. Functional recovery after transplantation of bone marrow-derived human mesenchymal stromal cells in a rat model of spinal cord injury. *Cytotherapy* **2010**, *12*, 792–806. [[CrossRef](#)] [[PubMed](#)]
28. Ninomiya, K.; Iwatsuki, K.; Ohnishi, Y.; Ohkawa, T.; Yoshimine, T. Intranasal delivery of bone marrow stromal cells to spinal cord lesions. *J. Neurosurg. Spine* **2015**, *23*, 111–119. [[CrossRef](#)] [[PubMed](#)]
29. Okada, S.; Ishii, K.; Yamane, J.; Iwanami, A.; Ikegami, T.; Katoh, H.; Iwamoto, Y.; Nakamura, M.; Miyoshi, H.; Okano, H.J.; et al. In vivo imaging of engrafted neural stem cells: Its application in evaluating the optimal timing of transplantation for spinal cord injury. *FASEB J.* **2005**, *19*, 1839–1841. [[CrossRef](#)] [[PubMed](#)]
30. Parr, A.M.; Kulbatski, I.; Tator, C.H. Transplantation of adult rat spinal cord stem/progenitor cells for spinal cord injury. *J. Neurotrauma* **2007**, *24*, 835–845. [[CrossRef](#)] [[PubMed](#)]
31. Chen, C.; Chen, F.; Yao, C.; Shu, S.; Feng, J.; Hu, X.; Hai, Q.; Yao, S.; Chen, X. Intrathecal injection of human umbilical cord-derived mesenchymal stem cells ameliorates neuropathic pain in rats. *Neurochem. Res.* **2016**, *41*, 3250–3260. [[CrossRef](#)] [[PubMed](#)]
32. Himes, B.T.; Neuhuber, B.; Coleman, C.; Kushner, R.; Swanger, S.A.; Kopen, G.C.; Wagner, J.; Shumsky, J.S.; Fischer, I. Recovery of function following grafting of human bone marrow-derived stromal cells into the injured spinal cord. *Neurorehabil. Neural Repair* **2006**, *20*, 278–296. [[CrossRef](#)] [[PubMed](#)]
33. Amemori, T.; Jendelova, P.; Ruzickova, K.; Arboleda, D.; Sykova, E. Co-transplantation of olfactory ensheathing glia and mesenchymal stromal cells does not have synergistic effects after spinal cord injury in the rat. *Cytotherapy* **2010**, *12*, 212–225. [[CrossRef](#)] [[PubMed](#)]
34. Cho, S.R.; Kim, Y.R.; Kang, H.S.; Yim, S.H.; Park, C.I.; Min, Y.H.; Lee, B.H.; Shin, J.C.; Lim, J.B. Functional recovery after the transplantation of neurally differentiated mesenchymal stem cells derived from bone marrow in a rat model of spinal cord injury. *Cell Transplant.* **2009**, *18*, 1359–1368. [[CrossRef](#)] [[PubMed](#)]
35. Hu, S.L.; Luo, H.S.; Li, J.T.; Xia, Y.Z.; Li, L.; Zhang, L.J.; Meng, H.; Cui, G.Y.; Chen, Z.; Wu, N.; et al. Functional recovery in acute traumatic spinal cord injury after transplantation of human umbilical cord mesenchymal stem cells. *Crit. Care Med.* **2010**, *38*, 2181–2189. [[CrossRef](#)] [[PubMed](#)]
36. Li, H.; Wen, Y.; Luo, Y.; Lan, X.; Wang, D.; Sun, Z.; Hu, L. Transplantation of bone marrow mesenchymal stem cells into spinal cord injury: A comparison of delivery different times. *Zhongguo Xiu Fu Chong Jian Wai Ke Za Zhi* **2010**, *24*, 180–184. [[PubMed](#)]
37. Bollini, S.; Gentili, C.; Tasso, R.; Cancedda, R. The regenerative role of the fetal and adult stem cell secretome. *J. Clin. Med.* **2013**, *2*, 302–327. [[CrossRef](#)] [[PubMed](#)]
38. Balasubramanian, S.; Thej, C.; Venugopal, P.; Priya, N.; Zakaria, Z.; Sundarraj, S.; Majumdar, A.S. Higher propensity of wharton’s jelly derived mesenchymal stromal cells towards neuronal lineage in comparison to those derived from adipose and bone marrow. *Cell Biol. Int.* **2013**, *37*, 507–515. [[CrossRef](#)] [[PubMed](#)]
39. Hsieh, J.Y.; Wang, H.W.; Chang, S.J.; Liao, K.H.; Lee, I.H.; Lin, W.S.; Wu, C.H.; Lin, W.Y.; Cheng, S.M. Mesenchymal stem cells from human umbilical cord express preferentially secreted factors related to neuroprotection, neurogenesis, and angiogenesis. *PLoS ONE* **2013**, *8*, e72604. [[CrossRef](#)] [[PubMed](#)]
40. Drela, K.; Lech, W.; Figiel-Dabrowska, A.; Zychowicz, M.; Mikula, M.; Sarnowska, A.; Domanska-Janik, K. Enhanced neuro-therapeutic potential of wharton’s jelly-derived mesenchymal stem cells in comparison with bone marrow mesenchymal stem cells culture. *Cytotherapy* **2016**, *18*, 497–509. [[CrossRef](#)] [[PubMed](#)]
41. Shi, C. Recent progress toward understanding the physiological function of bone marrow mesenchymal stem cells. *Immunology* **2012**, *136*, 133–138. [[CrossRef](#)] [[PubMed](#)]
42. Li, X.; Bai, J.; Ji, X.; Li, R.; Xuan, Y.; Wang, Y. Comprehensive characterization of four different populations of human mesenchymal stem cells as regards their immune properties, proliferation and differentiation. *Int. J. Mol. Med.* **2014**, *34*, 695–704. [[CrossRef](#)] [[PubMed](#)]
43. Li, C.; Chen, X.; Qiao, S.; Liu, X.; Liu, C.; Zhu, D.; Su, J.; Wang, Z. Effects of wharton’s jelly cells of the human umbilical cord on acute spinal cord injury in rats, and expression of interleukin-1beta and nerve growth factor in spinal cord tissues. *Artif. Cells Nanomed. Biotechnol.* **2016**, *44*, 1254–1258. [[CrossRef](#)] [[PubMed](#)]



44. Lee, K.H.; Suh-Kim, H.; Choi, J.S.; Jeun, S.S.; Kim, E.J.; Kim, S.S.; Yoon, D.H.; Lee, B.H. Human mesenchymal stem cell transplantation promotes functional recovery following acute spinal cord injury in rats. *Acta Neurobiol. Exp.* **2007**, *67*, 13–22.
45. Nakajima, H.; Uchida, K.; Guerrero, A.R.; Watanabe, S.; Sugita, D.; Takeura, N.; Yoshida, A.; Long, G.; Wright, K.T.; Johnson, W.E.; et al. Transplantation of mesenchymal stem cells promotes an alternative pathway of macrophage activation and functional recovery after spinal cord injury. *J. Neurotrauma* **2012**, *29*, 1614–1625. [[CrossRef](#)] [[PubMed](#)]
46. Oh, J.S.; Park, I.S.; Kim, K.N.; Yoon, D.H.; Kim, S.H.; Ha, Y. Transplantation of an adipose stem cell cluster in a spinal cord injury. *Neuroreport* **2012**, *23*, 277–282. [[CrossRef](#)] [[PubMed](#)]
47. Park, S.I.; Lim, J.Y.; Jeong, C.H.; Kim, S.M.; Jun, J.A.; Jeun, S.S.; Oh, W.I. Human umbilical cord blood-derived mesenchymal stem cell therapy promotes functional recovery of contused rat spinal cord through enhancement of endogenous cell proliferation and oligogenesis. *J. Biomed. Biotechnol.* **2012**, *2012*, 362473. [[CrossRef](#)] [[PubMed](#)]
48. Shang, A.J.; Hong, S.Q.; Xu, Q.; Wang, H.Y.; Yang, Y.; Wang, Z.F.; Xu, B.N.; Jiang, X.D.; Xu, R.X. Nt-3-secreting human umbilical cord mesenchymal stromal cell transplantation for the treatment of acute spinal cord injury in rats. *Brain Res.* **2011**, *1391*, 102–113. [[CrossRef](#)] [[PubMed](#)]
49. Matyas, J.J.; Stewart, A.N.; Goldsmith, A.; Nan, Z.; Skeel, R.L.; Rossignol, J.; Dunbar, G.L. Effects of bone-marrow-derived msc transplantation on functional recovery in a rat model of spinal cord injury: Comparisons of transplant locations and cell concentrations. *Cell Transplant.* **2017**, *26*, 1472–1482. [[CrossRef](#)] [[PubMed](#)]
50. Gabr, H.; El-Kheir, W.A.; Farghali, H.A.; Ismail, Z.M.; Zickri, M.B.; El Maadawi, Z.M.; Kishk, N.A.; Sabaawy, H.E. Intrathecal transplantation of autologous adherent bone marrow cells induces functional neurological recovery in a canine model of spinal cord injury. *Cell Transplant.* **2015**, *24*, 1813–1827. [[CrossRef](#)] [[PubMed](#)]
51. Ryu, H.H.; Kang, B.J.; Park, S.S.; Kim, Y.; Sung, G.J.; Woo, H.M.; Kim, W.H.; Kweon, O.K. Comparison of mesenchymal stem cells derived from fat, bone marrow, wharton’s jelly, and umbilical cord blood for treating spinal cord injuries in dogs. *J. Vet. Med. Sci.* **2012**, *74*, 1617–1630. [[CrossRef](#)] [[PubMed](#)]
52. Satti, H.S.; Waheed, A.; Ahmed, P.; Ahmed, K.; Akram, Z.; Aziz, T.; Satti, T.M.; Shahbaz, N.; Khan, M.A.; Malik, S.A. Autologous mesenchymal stromal cell transplantation for spinal cord injury: A phase I pilot study. *Cytotherapy* **2016**, *18*, 518–522. [[CrossRef](#)] [[PubMed](#)]
53. Mendonca, M.V.; Larocca, T.F.; de Freitas Souza, B.S.; Villarreal, C.F.; Silva, L.F.; Matos, A.C.; Novaes, M.A.; Bahia, C.M.; de Oliveira Melo Martinez, A.C.; Kaneto, C.M.; et al. Safety and neurological assessments after autologous transplantation of bone marrow mesenchymal stem cells in subjects with chronic spinal cord injury. *Stem Cell Res. Ther.* **2014**, *5*, 126. [[CrossRef](#)] [[PubMed](#)]
54. Koci, Z.; Vyborny, K.; Dubisova, J.; Vackova, I.; Jager, A.; Lunov, O.; Jirakova, K.; Kubinova, S. Extracellular matrix hydrogel derived from human umbilical cord as a scaffold for neural tissue repair and its comparison with extracellular matrix from porcine tissues. *Tissue Eng. Part C Methods* **2017**, *23*, 333–345. [[CrossRef](#)] [[PubMed](#)]
55. Parr, A.M.; Kulbatski, I.; Zahir, T.; Wang, X.; Yue, C.; Keating, A.; Tator, C.H. Transplanted adult spinal cord-derived neural stem/progenitor cells promote early functional recovery after rat spinal cord injury. *Neuroscience* **2008**, *155*, 760–770. [[CrossRef](#)] [[PubMed](#)]
56. Yang, J.R.; Liao, C.H.; Pang, C.Y.; Huang, L.L.; Chen, Y.L.; Shiue, Y.L.; Chen, L.R. Transplantation of porcine embryonic stem cells and their derived neuronal progenitors in a spinal cord injury rat model. *Cytotherapy* **2013**, *15*, 201–208. [[CrossRef](#)] [[PubMed](#)]
57. Dunham, N.W.; Miya, T.S. A note on a simple apparatus for detecting neurological deficit in rats and mice. *J. Am. Pharm. Assoc.* **1957**, *46*, 208–209. [[CrossRef](#)]
58. Metz, G.A.; Whishaw, I.Q. The ladder rung walking task: A scoring system and its practical application. *J. Vis. Exp.* **2009**. [[CrossRef](#)] [[PubMed](#)]

